

¹ Search for Double Beta Decay to Excited States

² I. Guinn

³ *University of North Carolina at Chapel Hill, NC,
4 USA*

⁵ CONTENTS

⁶ I. Introduction	²
⁷ II. Simulation of Excited State Decays	²
A. Comparing DECAY0 to the Kotila and Iachello generator	³
⁹ III. Background Model Simulation	⁴
¹⁰ IV. ^{56}Co Simulation	⁵
¹¹ V. Simulation Skimming	⁵
¹² VI. Selection of Multi-Detector Events	⁸
A. Variation in Detector Configuration	⁸
B. Dead Layer Effects	⁹
C. Dead Time Effects	⁹
D. Simulation Validation and Errors	⁹
¹⁷ VII. Region of Interest Selection	¹²
A. Signal ROI Optimization	¹⁴
B. Background ROI Selection	¹⁵
C. ROI Detection Efficiency and Uncertainty	¹⁵
D. Detector Crosstalk	¹⁶
²² VIII. Background Cuts	¹⁸
A. Enriched Source Detector Cut	¹⁸
B. Coincident and Sum Energy Cuts	¹⁸
C. Muon Veto Cut	²⁰
²⁶ IX. Combined Detection Efficiency for $\beta\beta$ E.S.	²⁰
²⁷ X. Double Beta Decay to Excited States Results	²¹
²⁸ XI. Validation	²¹
A. Data Rate	²¹
B. Background Cut Evaluation	²²
³¹ XII. Results	²²
A. Statistical Methods	²²
B. Limits and Sensitivities	²⁴
³⁴ XIII. Unblinding Plan	²⁵
³⁵ References	²⁶
³⁶ A. Detailed Results for All Decay Modes	²⁶
³⁷ B. $2\nu\beta\beta$ to 0_1^+	²⁶
³⁸ C. $2\nu\beta\beta$ to 2_1^+	⁴²
³⁹ D. $2\nu\beta\beta$ to 2_2^+	⁴⁹
1. 559 keV peak	⁴⁹
2. 657 keV peak	⁵⁶
3. 1216 keV peak	⁶²
⁴³ E. $0\nu\beta\beta$ to 0_1^+	⁶⁸
⁴⁴ F. $0\nu\beta\beta$ to 2_1^+	⁷⁵
⁴⁵ G. $0\nu\beta\beta$ to 2_2^+	⁸²
1. 559 keV peak	⁸²

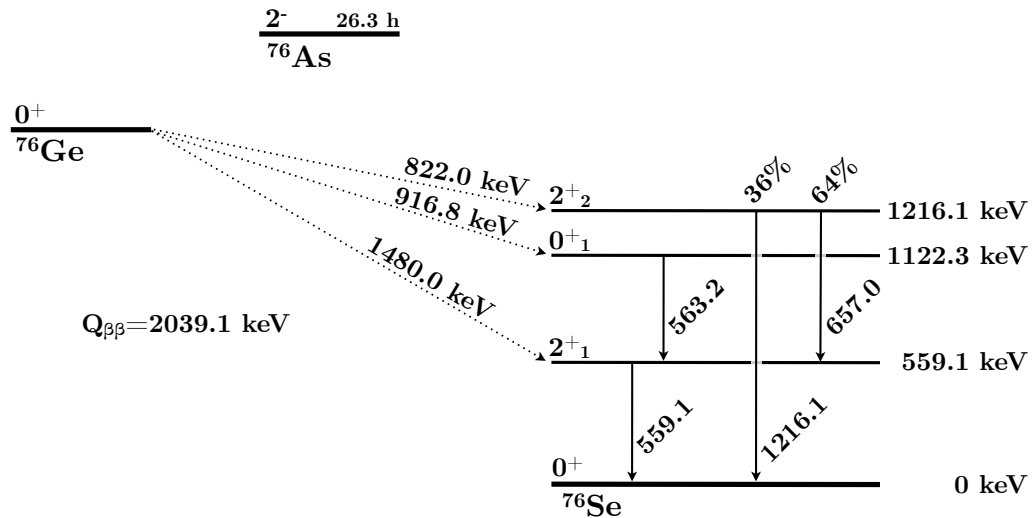


47	2. 657 keV peak	89
48	3. 1216 keV peak	95
49	H. Sensitivity and Discovery Potential	101

50 I. INTRODUCTION

51 ^{76}Se has 3 excited states that ^{76}Ge can decay into in addition to the ground state, as shown in figure 15. While
 52 the ground state decay has been observed, none of the decays to excited states have been yet. Each excited state
 53 decay will have a $\beta\beta$ -decay with a reduced Q -value compared to the ground state decay. The excited state decays will
 54 also promptly produce one or two γ -rays at known energies. These γ s will typically travel several centimeters before
 55 absorption and will often hit a different detector from the $\beta\beta$ -decay site, meaning that we can search for peaks at
 56 these energies.

57



58 FIG. 1 Energy level diagram for $\beta\beta$ -decay of ^{76}Ge to ^{76}Se , including excited states. The Q -values for each decay branch and
 59 the energies and branching ratios for the deexcitation γ s are shown next to their corresponding lines.

60 Furthermore, since these γ s hit separate detectors, this signal is inherently multi-site event. As shown in figure 2,
 61 by searching for the peak only in events with high hit multiplicity, i.e. events that involve 2 or more detectors hit,
 62 $\sim 85\%$ of backgrounds can be cut, while only sacrificing $\sim 25\%$ of the signal. Furthermore, the coincident detector
 63 hit(s) can provide additional observables that can be used to further discriminate excited state signals from multi-site
 64 backgrounds. This chapter will describe the various background reduction data cuts and how they are implemented.
 65 It will also evaluate the detection efficiency and systematic error associated with each cut based on simulations of the
 66 MAJORANA DEMONSTRATOR.

67 II. SIMULATION OF EXCITED STATE DECAYS

68 Simulations of the ^{76}Ge decay to excited states of ^{76}Se are used to evaluate the detection efficiency of the analysis
 69 presented in this document. Two different event generators are used to generate ^{76}Ge $\beta\beta$ -decay within MAGE. The
 70 first generator uses calculations of the phase space factors from J. Kotila and F. Iachello[1]. It is implemented in the
 71 mage class `MGGeneratorDoubleBeta` using data tables with the distribution of both electron energies and angular
 72 correlations. These data tables are provided for the $2\nu\beta\beta$ and $0\nu\beta\beta$ decays to the ground state of ^{76}Se , but not for the
 73 decays to any excited state of ^{76}Se . This calculation is an improvement over other phase space calculations thanks to
 74 an exact evaluation of the Dirac wave functions of the electrons involving a finite nuclear size and electron screening.

75 A second event generator packaged with MAGE is `DECAY0`[2], a FORTRAN program that generates a wide variety
 76 of $\beta\beta$ - and β -decays. `DECAY0` is capable of generating $2\nu\beta\beta$ and $0\nu\beta\beta$ for ^{76}Ge to 0^+ and 2^+ excited states of ^{76}Se
 77 using a variety of physics mechanisms. For the excited state decays, the deexcitation γ s and conversion electrons are

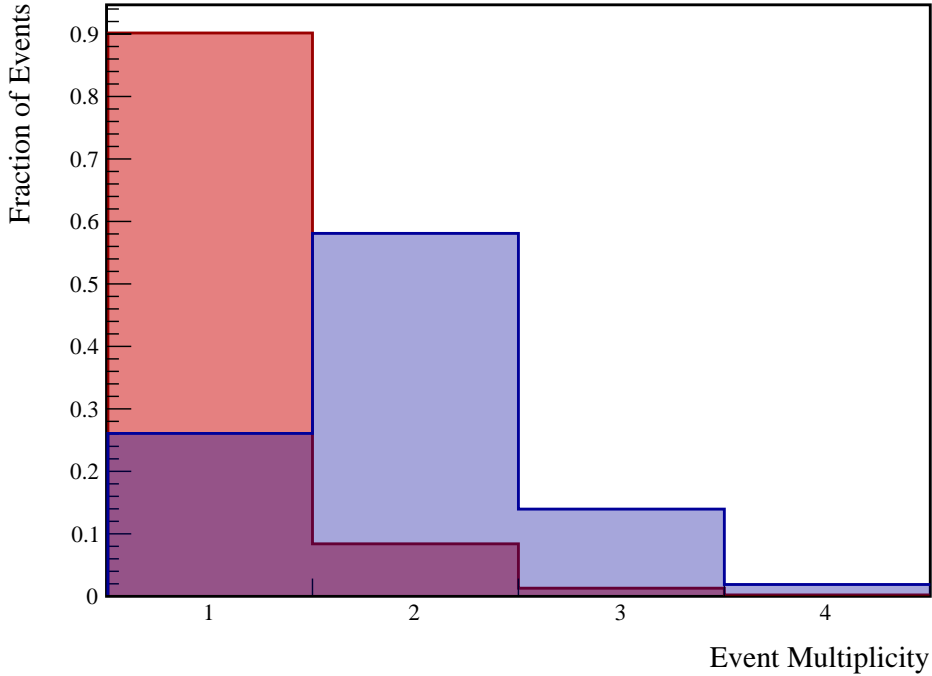


FIG. 2 The simulated distribution of ROI event multiplicities in the background model (red) and $\beta\beta$ E.S. (blue) to 0_1^+ decay. These simulations use the DS6 detector configuration.

also generated. Several modifications were made to DECAY0 for this analysis. First, the precision of the excited state deexcitation energies was increased from 1 keV to 0.001 keV (The γ energies changed from 559 to 559.101 keV, from 563 to 563.178 keV, from 657 to 657.041 keV, and from 1216 to 1216.104 keV). Second, angular correlations were added for the $2_2^+-2_1^+-0_{g.s.}^+$ deexcitation γ cascade which involves a 657 keV γ with multipolarity E2+M1 and mixing ratio of +5.2 followed by a 559 keV γ with multipolarity E2[3]. The angular distribution between the γ s is[4]

$$P(\theta) \propto 1 - 0.372 \cdot \cos^2(\theta) + 0.0439 \cdot \cos^4(\theta) \quad (1)$$

The angular correlation for the $0_1^+-2_1^+-0_{g.s.}^+$ deexcitation was already correctly included in DECAY0, and is represented by the angular distribution[3; 4]

$$P(\theta) \propto 1 - 3 \cdot \cos^2(\theta) + 4 \cdot \cos^4(\theta) \quad (2)$$

Running DECAY0 produces data files with the initial momenta of the generated particles. The MAGE class MGGeneratorDecay0 reads these datafiles and generates initial positions for these events.

Simulations were run for ${}^{76}\text{Ge}$ $2\nu\beta\beta$ and $0\nu\beta\beta$ to the 0_1^+ , 2_1^+ and 2_2^+ excited states of ${}^{76}\text{Se}$ using the DECAY0 generator. For each decay mode, 5,000,000 event primaries were generated in the bulk of the enriched detectors and 500,000 primaries were generated in the bulk of the natural detectors. These events were skimmed with the relative activities set equal to the total isotopic mass in each set of detectors: 26.2538 kg in enriched detectors, and 1.1232 kg in natural detectors. These simulations were additionally post-processed and skim files were produced both with and without a dead layer, and with and without dead times. Figure 3 shows an energy spectrum of multiplicity 2 events produced by the simulation of the ${}^{76}\text{Ge}$ decay to the 0_1^+ excited state of ${}^{76}\text{Se}$.

94 A. Comparing DECAY0 to the Kotila and Iachello generator

95 The Kotila and Iachello generator performs a more accurate calculation of phase space than DECAY0 and is used
96 for the MAJORANA DEMONSTRATOR's measurement of $2\nu\beta\beta$ and $0\nu\beta\beta$ to the ground state. Because Kotila and

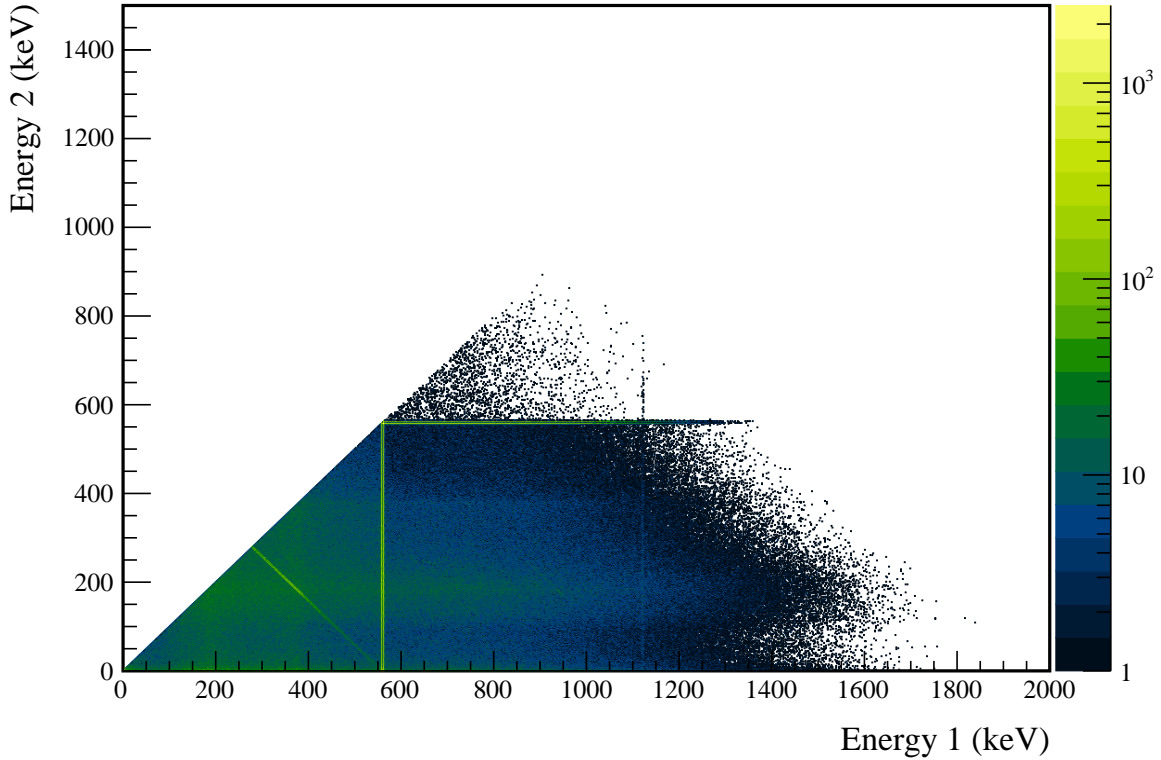


FIG. 3 Multiplicity 2 energy spectrum produced by a DECAY0 simulation of $2\nu\beta\beta$ of ^{76}Ge to the 0_1^+ state of ^{76}Se .

Iachello present only the phase space integral for the excited state decays, and do not include the energy and angular distributions, DECAY0 is used for this analysis. To evaluate the accuracy of DECAY0, we can compare the spectrum of the $2\nu\beta\beta$ to the ground state it generates to that of Kotila and Iachello; this comparison will reflect the error with respect to the true value if we assume that the errors corrected by Kotila and Iachello are the dominant errors in DECAY0. This comparison is performed using a Kolmogorov-Smirnov (KS) test. The KS test statistic is the maximum difference between the CDF of each normalized energy spectrum. As we will see in Section VIII.B, this test is useful in evaluating the uncertainties in the measurement presented in this document. The CDF difference is shown in Figure 4, with a KS statistic of 0.00081. While this error is statistically significant at a level of 97%, we will see that the systematic error generated is subdominant.

III. BACKGROUND MODEL SIMULATION

A simulation of the background spectrum measured by the MAJORANA DEMONSTRATOR will be used to optimize the search for $\beta\beta$ E.S.. MAGE simulations of a variety of decay chains, including ^{232}Th , ^{238}U , ^{40}K , ^{60}Co , ^{222}Rn and ^{68}Ge , have been run using event generators internal to GEANT4. A large number of component groups have been defined, encompassing one or more physical components of the experiment (e.g. all signal electronic connectors are a single component group). The event generators use the combined geometries of these groups to generate start positions, which can be in either the bulk of a component group, or on the surface. The activity of each isotope from each component group is determined by fitting a linear combination of the simulated energy spectra to the measured background spectrum. An incomplete version of this fit is used for this document, producing the spectra in Figures 5 and 6[5]. ^{68}Ge decays with a half-life of 271 days, so its activity is scaled to represent the exposure-weighted activity of each major dataset. ^{210}Pb in the lead shield is simulated using a special generator that samples bremsstrahlung x-rays emitted from the surface of a thick lead shield [6].

The background model used for this analysis is known to be inaccurate. Since it is only used for optimizing the

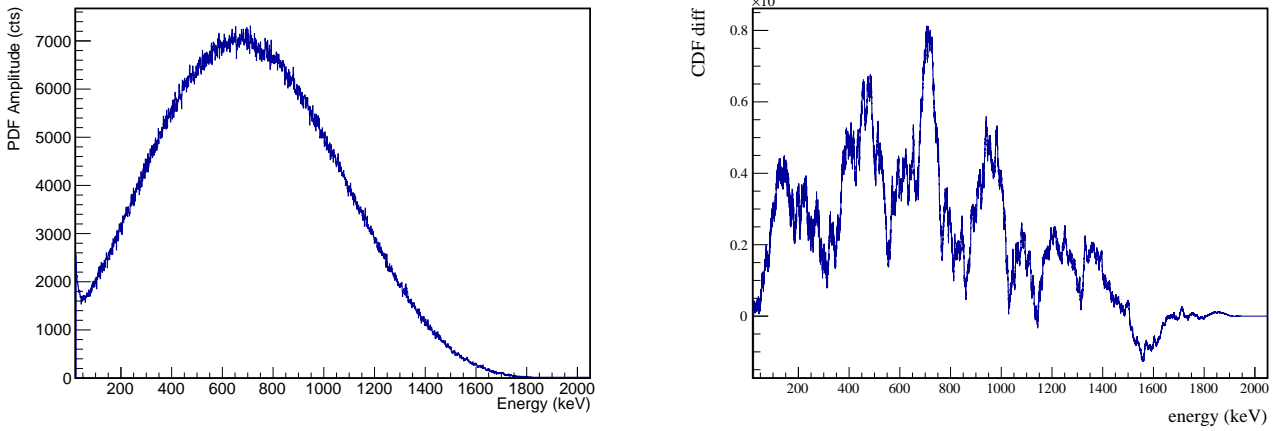


FIG. 4 A KS test is performed comparing the DECAYO $2\nu\beta\beta$ to the ground state energy spectrum to that of Kotila and Iachello. The `decay0` spectrum is shown, along with the difference between the CDF of each spectrum.

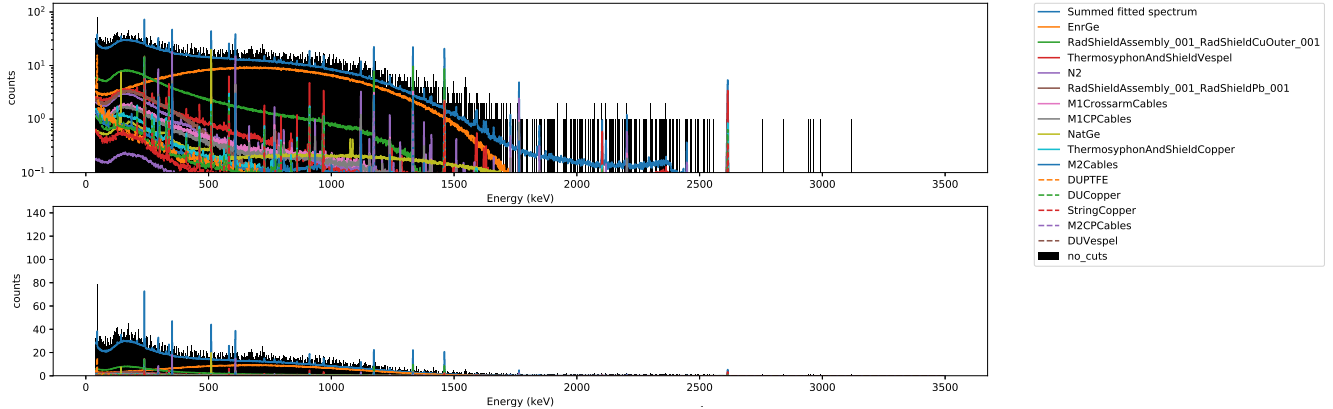


FIG. 5 Energy spectrum of observed multiplicity 1 events produced from a simulation of the preliminary background model, with the highest contributing components labelled.

119 search for $\beta\beta$ E.S. and is not important for the detection efficiency calculation, this does not affect the accuracy of
 120 the result presented. For future versions of this analysis, a complete and more accurate background model will be
 121 used, which should result in small improvements to the cut optimization.

122 IV. ^{56}CO SIMULATION

123 Calibration of the MAJORANA DEMONSTRATOR is performed for each module using a line source that is injected
 124 by motor into a spiral track that winds around the module. Simulations of the ^{56}Co calibration sources are performed
 125 using the GEANT4 generators for these isotopes, and a spiral position sampler written in MAGE. The detection
 126 efficiency test described in Section VI.D uses the ^{56}Co source simulation. The simulated spectra for the ^{56}Co source
 127 can be seen in Figures 7 and 8

129 V. SIMULATION SKIMMING

130 Skim files are produced containing parameters of interest from the post-processed files using the software
 131 `es_skimsims`. Skim files can also mix postprocessed files from multiple sources in ratios corresponding to the
 132 various activities of the sources. `es_skimsims` accepts as input a JSON file listing the simulated sources, the de-

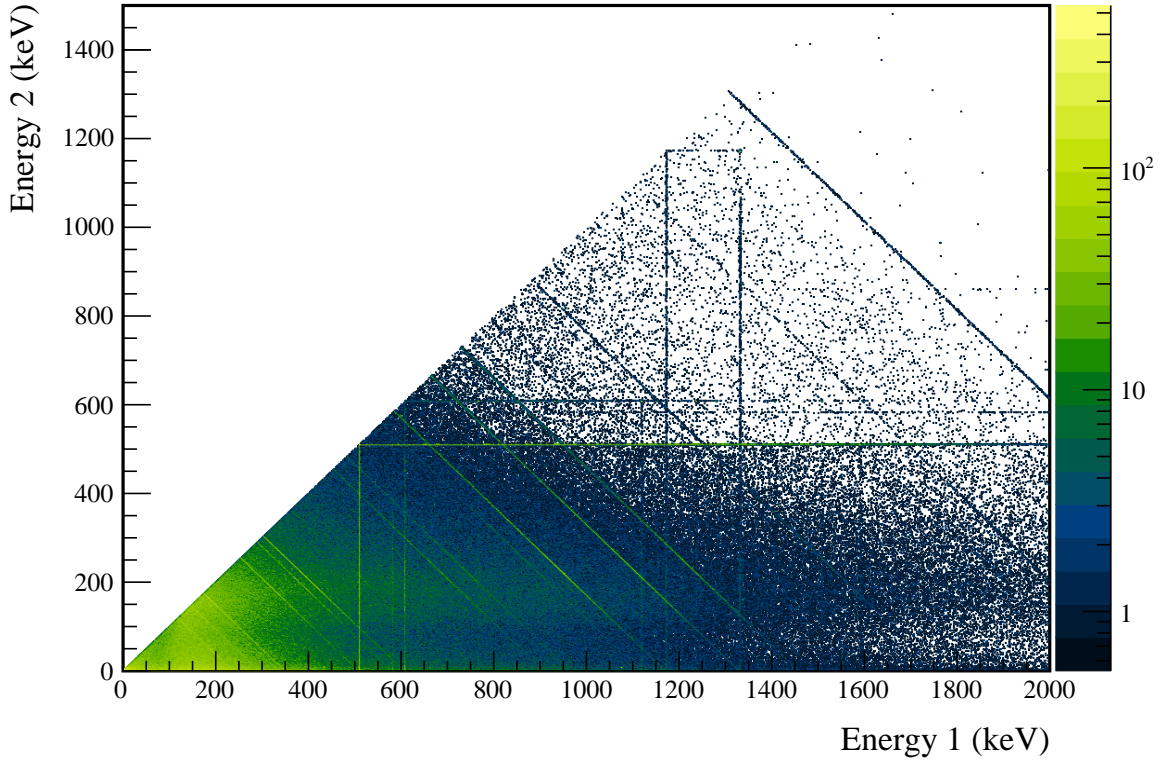


FIG. 6 Multiplicity 2 energy spectrum produced by a simulation of a preliminary version of the MAJORANA DEMONSTRATOR background model.

sired activity of each source, and the number of available event primaries. From this, it calculates the number of primaries to accept from each source by maximizing the total number of events used while maintaining the correct ratio according to the activities. Once this is done, it goes through each source sequentially and saves parameters of interest, including energy and detector position, to a `TTree`[7]. As will be discussed in future chapters, single detector events are of little interest to this analysis, so only multi-detector events are recorded in order to maintain a small file size. Multiplicity 1 events are recorded separately to a histogram according only to energy. The skimming process also accounts for which sets of detectors are enabled. Another input of `es_skimsims` is a JSON file containing a list of detector configurations, containing a bitmask describing which detectors are and are not enabled. The detector configurations will be discussed further in Section VI.A. When the skimmer encounters a disabled detector in an event, it ignores that detector, and does not count it towards the event multiplicity.

Each detector spends some portion of operating time dead, due to the finite rate at which the digitizers can retrigger, which typically cause $< 0.1\%$ of HPGe hits to fail to read. However, during early datasets, some detector channels were effected by a bug in the Gretina cards that caused a high rate of triggers on negative-energy noise pulses, resulting in much higher dead time fractions. This effect is assumed to be random and uncorrelated between detectors. The dead time of each detector is measured by counting the number of pulser events in each detector for each run. Because the pulses occur at a fixed rate, we can predict the number of pulser events that should occur in any given run; the fraction of pulser events missed is assumed to represent the dead time fraction. The JSON detector configuration file contains the dead time fraction and the statistical uncertainty (assuming binomial statistics with respect to the total number of expected pulser events) on that fraction for each active detector. For each simulated detector hit, the data skimmer randomly throws out hits according to the probability represented by the dead fraction, treating that detector as inactive for that event.

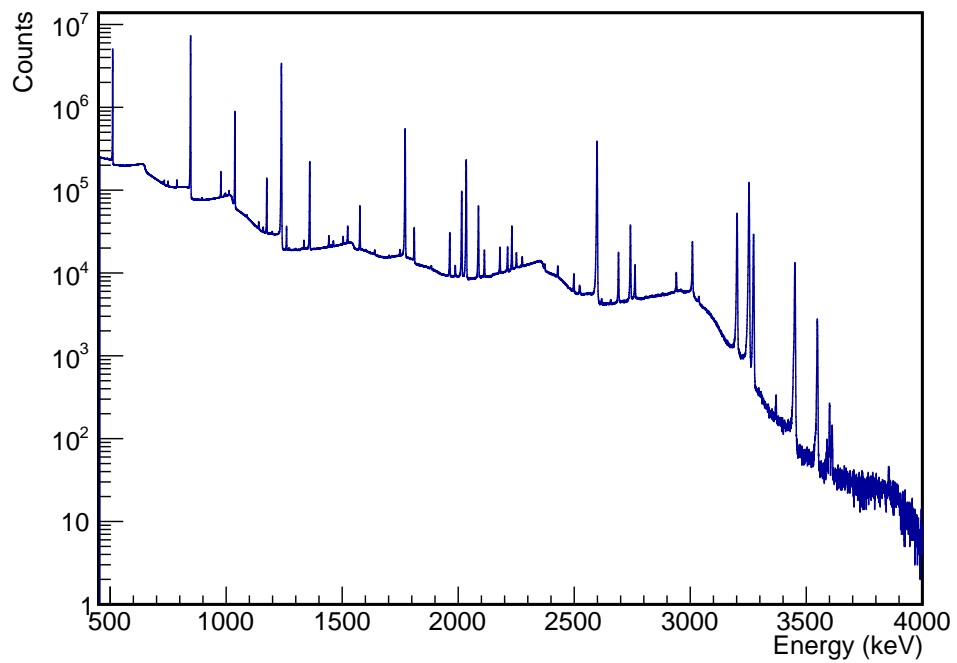


FIG. 7 Energy spectrum of multiplicity 1 events produced from a simulation of the ^{56}Co line source inserted into the module 1 calibration track.

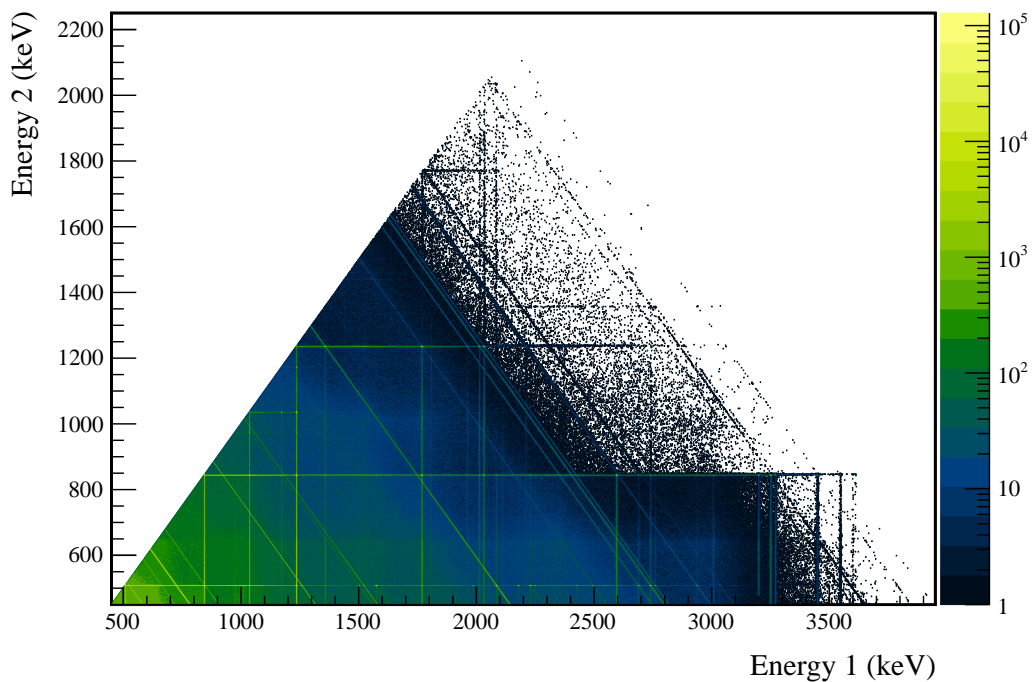


FIG. 8 Multiplicity 2 energy spectrum produced by a simulation of the ^{56}Co line source inserted into the module 1 calibration track.

154 **VI. SELECTION OF MULTI-DETECTOR EVENTS**

155 Simultaneous detector hits are combined into events by the event builder. Events are combined in a $4 \mu\text{s}$ rolling
156 window. This window is expected to accept virtually all true coincidence events (see Figure 9). In a small number of
157 runs, clocks between different Gretina cards were desynchronized. For these runs, the clocks were resynchronized by
158 applying a timing offset during event building that is measured by seeking the time offset that aligns pulser events.
159 With a typical overall rate between both modules of $< 1 \text{ Hz}$, $< 0.4\%$ of all multi-site events are expected to originate
160 from accidental coincidences, making this a negligible background. Once all the data has gone through the standard
161 MAJORANA DEMONSTRATOR processing chain, the skim files from all good open runs in datasets 16a are collected
162 into a single skim file containing a `TTree` with only multi-site events by the program `es_skimdata`.

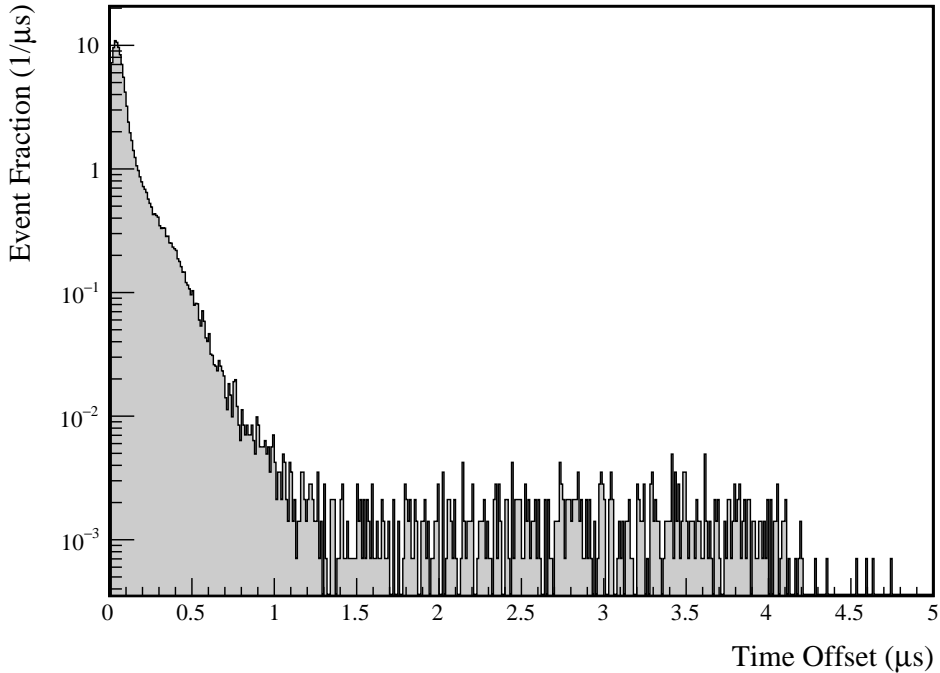


FIG. 9 Distribution of time interval between individual hits within a multi-detector event during a ^{228}Th calibration run. Offsets of greater than $\sim 1.5 \mu\text{s}$ are due to pileup, which is significant due to the high data rate of calibration runs. Offsets greater than $\sim 4 \mu\text{s}$ must involve events with more than two hits, due to the event builder time window.

163 **A. Variation in Detector Configuration**

164 Throughout the runtime of the MAJORANA DEMONSTRATOR, not all detectors were simultaneously active, and
165 within each dataset, the set of active detectors varied significantly. Because we are looking at multi-site event events,
166 the detection efficiency for $\beta\beta$ E.S. events in any detector depends on which other detectors are enabled. For this
167 reason, detection efficiency is computed for each module in its entirety rather than for individual detectors. To account
168 for changes in detector configuration, each dataset is divided into subdatasets based on which detectors are active.
169 The subdatasets are described by a pair of 64-bit masks, one for each module, with each bit representing a single
170 detector's state. To decode the bitmask, the b 'th least significant bit represents string position P , detector position
171 D if

$$b = 8 \cdot P + D \quad (3)$$

172 The set of runs and active channels for each run were determined by the run selection and data cleaning committee,
173 and the procedures are outlined in [8]. The program `es_getdatasets` uses these selections to sort each run into a
174 subdataset.



The detection efficiency is defined as the probability of a signal event in any detector, including inactive detectors. Detection efficiency is calculated individually for each subdataset and for each module by creating a separate skim file for each subdataset as outlined in Section V. The final efficiency is then computed as an isotopic exposure weighted average of the efficiency within each subdataset. Any efficiency uncertainties are assumed to be totally correlated between subdatasets. The livetime of each subdataset is calculated by the program `es_livetimes` by totalling the run time in each run, and subtracting any dead time that affects the entire module, including dead time caused by the muon veto system and by liquid nitrogen fills. Additional sources of dead time that affect individual detectors are calculated as inefficiencies rather than being subtracted from the livetime, as discussed in Section V. This is done because dead time in any individual detector affects the detection efficiency of all other detectors. The isotopic exposure is computed by multiplying the livetime of each module by the total isotopic mass in each module. Since this includes mass in inactive detectors and dead layers, the isotopic exposure for this analysis will differ from that presented in the $0\nu\beta\beta$ analysis. Table I lists each subdataset along with its livetime and exposure.

B. Dead Layer Effects

For multi-detector events, each individual hit may be degraded by the dead layer, so the loss of sensitivity from dead layers is larger for this search than for searches for single-site events. For this reason, dead layer effects are treated as a loss of detection efficiency instead of a loss of exposure (as in the $0\nu\beta\beta$ analysis). Dead layers are included in the simulations as a part of simulation post-processing. To account for uncertainty in the thickness of the dead layer, two separate simulations are run, with and without dead layers. By comparing the efficiency measurement from each simulation, we measure the size of the dead layer effect. The percent uncertainty in the efficiency loss from dead layers is assumed to be the same as the percent uncertainty in the dead layer thickness. Typical loss of efficiency for multi-site peaks is 25-35%; for the $2\nu\beta\beta$ to the 0_1^+ decay, the losses are 26% for module 1 and 34% for module 2. The uncertainty in the dead layer tends to be one of the dominant uncertainties in measuring the detection efficiency. This is much larger than the $\sim 10\%$ loss seen in the $0\nu\beta\beta$ analysis for two reasons. First, for multi-detector events, there are multiple hits that could possibly be lost to the dead layer. Second, γ hits will be more concentrated at the surface of the detectors, near the dead layers, than $\beta\beta$ sites. The effect of dead layers on detection efficiency can be seen in Figure 10.

C. Dead Time Effects

Detector dead times, which affect only a single detector at a time, reduce the detection efficiency for events that occur in all detectors in the module. For this reason, instead of subtracting these dead times from the livetime, the dead times are incorporated into the detection efficiency. Detector dead times are measured individually for each run by counting pulser events and comparing to the number of expected pulser events for each detector. The program `es_livetime` collects the detector dead times that are measured in this way and finds the average detector dead time for each subdataset. These dead times are then applied to the simulation skimming process as described in Section V. Similar to the dead layers, simulation files are produced with and without dead times in order to measure the size of the effect. Uncertainties in the detector dead times are measured as the statistical uncertainties from pulser counts. The percent uncertainty in efficiency loss from detector dead times is assumed to be the same as the average percent uncertainty in the detector dead time. Typical loss of efficiency from detector dead times range from 1-3%. For the $2\nu\beta\beta$ to the 0_1^+ decay, the losses are 2.5% for module 1 and 1.9% for module 2. The effects of detector dead times can be seen in Figure 10.

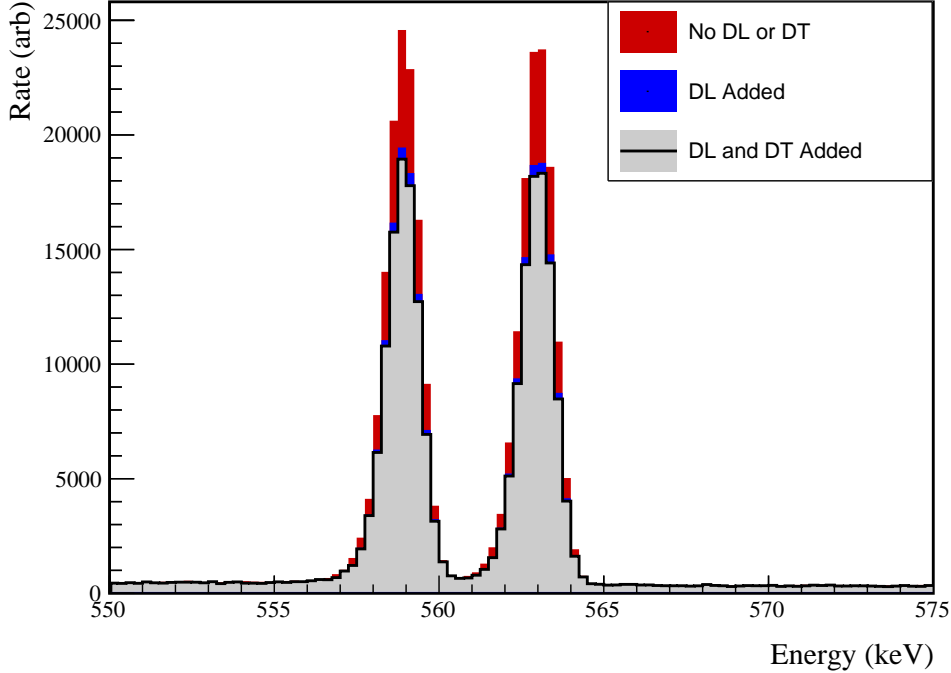
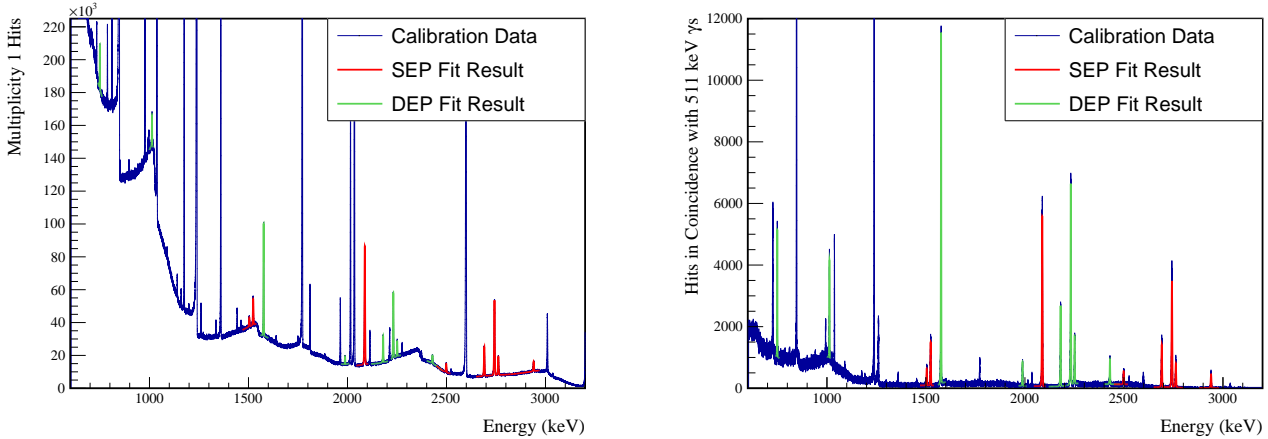
D. Simulation Validation and Errors

In addition to dead layer and dead time effects that can be explicitly accounted for, other possible sources of systematic uncertainty from the simulation exist, such as inaccuracies in the simulation geometry. To account for these, we use pair production events from calibration runs as a proxy for $\beta\beta$ E.S. events. In pair production events, an electron-positron pair is produced in the bulk of a detector, followed promptly by two 511 keV γ s from the annihilation of the positron. Because these events involve a single pair production site and the prompt emission of gamma rays which may be absorbed in a separate detector, they make a good proxy for $\beta\beta$ E.S. events. In single-escape peak (SEP) events, one gamma is absorbed in the detector containing the pair-production, while the other escapes, resulting in a source detector hit with energy equal to the γ energy minus 511 keV. In double-escape peak (DEP) events, both



TABLE I List of each subdataset, labelled by the bitmasks defined in equation 3, with its livetime, detection efficiency measured for the $\beta\beta$ E.S. to 0^+_1 decay, and total isotopic exposure. Note the large amount of variance in the detection efficiency.

DS	M1 Detector Mask	M2 Detector Mask	Run Time (days)	M1 L.T. (days)	M1 Eff.	M2 L.T. (days)	M2 Eff.	Exposure (kg.y)
DS1	061a08001e0e1c00	0000000000000000	2.64	2.60	1.693%	0.00	0.000%	0.109
DS1	161a08341e0e1c00	0000000000000000	0.02	0.02	1.978%	0.00	0.000%	0.001
DS1	161a0c341e0e1c00	0000000000000000	4.51	4.48	1.915%	0.00	0.000%	0.188
DS1	161a0c361e0e1c00	0000000000000000	3.49	3.48	1.449%	0.00	0.000%	0.146
DS1	1e1a0001e0e1c00	0000000000000000	7.82	7.73	2.015%	0.00	0.000%	0.324
DS1	1e1a08001e0e1c00	0000000000000000	25.49	25.19	2.202%	0.00	0.000%	1.057
DS1	1e1a08041e0e1c00	0000000000000000	2.95	2.93	2.277%	0.00	0.000%	0.123
DS1	1e1a08141e0e1c00	0000000000000000	0.26	0.25	2.297%	0.00	0.000%	0.011
DS1	1e1a08301e0e1c00	0000000000000000	1.40	1.37	2.305%	0.00	0.000%	0.057
DS1	1e1a08341e0e1c00	0000000000000000	7.58	7.50	2.095%	0.00	0.000%	0.315
DS1	1e1a0c001e0e1c00	0000000000000000	1.96	1.93	2.226%	0.00	0.000%	0.081
DS1	1e1a0c341e0e1c00	0000000000000000	0.67	0.67	2.296%	0.00	0.000%	0.028
DS2	1e1a08001e0e1c00	0000000000000000	9.58	9.51	2.248%	0.00	0.000%	0.399
DS3	1e1a0c3e1e0e1c00	0000000000000000	29.88	29.67	2.566%	0.00	0.000%	1.245
DS4	0000000000000000	1c061a16060e1e00	19.15	0.00	0.000%	18.85	1.811%	0.622
DS5a	08000020040e1c00	18060a02040e1e00	1.49	1.48	0.703%	1.46	1.111%	0.110
DS5a	08080020040e1c00	18060a16060e1e00	2.51	2.49	0.842%	2.47	1.484%	0.186
DS5a	08080030040e1c00	18060a02040e1e00	0.01	0.01	0.888%	0.01	1.094%	0.001
DS5a	0e1a04321e0e1c00	08020a16060e1e00	2.69	2.71	2.265%	2.66	1.165%	0.201
DS5a	0e1a0c321e0e1c00	0000000000000000	0.65	0.63	2.522%	0.00	0.000%	0.026
DS5a	0e1a0c321e0e1c00	08060a16060e1e00	1.24	1.24	2.513%	1.21	1.451%	0.092
DS5a	0e1a0c321e0e1c00	18060a02040e1e00	2.94	2.92	2.288%	2.89	1.098%	0.218
DS5a	0e1a0c321e0e1c00	18060a1406061600	0.04	0.04	2.487%	0.04	0.906%	0.003
DS5a	0e1a0c321e0e1c00	18060a1606060600	3.19	3.15	2.452%	3.16	0.774%	0.237
DS5a	0e1a0c321e0e1c00	18060a16060e0600	3.30	3.28	2.458%	3.29	0.793%	0.246
DS5a	0e1a0c3e1e0e1c00	1806020606081800	1.75	1.73	2.703%	1.73	0.726%	0.129
DS5a	0e1a0c3e1e0e1c00	18060216060c1e00	6.84	6.77	2.698%	6.74	1.068%	0.507
DS5a	0e1a0c3e1e0e1c00	18060216060e1e00	13.48	13.30	2.677%	13.27	1.189%	0.996
DS5a	0e1a0c3e1e0e1c00	18060816060e1c00	0.05	0.05	2.502%	0.05	1.247%	0.004
DS5a	0e1a0c3e1e0e1c00	18060a060606000	2.16	2.12	2.670%	2.12	0.982%	0.159
DS5a	0e1a0c3e1e0e1c00	18060a16040e1e00	0.76	0.76	2.668%	0.74	1.222%	0.056
DS5a	0e1a0c3e1e0e1c00	18060a160606000	0.25	0.25	2.682%	0.25	1.060%	0.019
DS5a	0e1a0c3e1e0e1c00	18060a1606061800	1.88	1.86	2.686%	1.86	0.998%	0.140
DS5a	0e1a0c3e1e0e1c00	18060a1606061c00	9.20	9.13	2.657%	9.06	1.353%	0.682
DS5a	0e1a0c3e1e0e1c00	18060a16060c1e00	7.89	7.79	2.688%	7.79	1.350%	0.584
DS5a	0e1a0c3e1e0e1c00	18060a16060e1c00	11.68	11.53	2.340%	11.51	1.357%	0.864
DS5a	0e1a0c3e1e0e1c00	18060a16060e1e00	5.21	5.15	2.665%	5.13	1.486%	0.386
DS5a	0e1a0c3e1e0e1c00	18061216060e1e00	2.39	2.37	2.676%	2.37	1.266%	0.178
DS5b	1e1a0c3e1e0c1c00	18061216060e1e00	24.46	24.09	2.672%	24.06	1.268%	1.805
DS5b	1e1a0c3e1e0c1c00	18061a16060e1e00	0.75	0.75	2.670%	0.75	1.654%	0.056
DS5b	1e1a0c3e1e0e1c00	18061216060e1e00	14.28	14.12	2.766%	14.07	1.169%	1.057
DS5c	1e1a0c3e1e0c1c00	00060216060e0e00	0.00	0.00	2.567%	0.00	0.787%	0.000
DS5c	1e1a0c3e1e0c1c00	00060a16060e0e00	0.91	0.89	2.664%	0.91	1.016%	0.067
DS5c	1e1a0c3e1e0c1c00	00061216060e0e00	10.22	10.15	2.645%	10.03	0.857%	0.757
DS6a	120000000000c0800	1002020006040600	1.33	1.31	0.160%	1.31	0.230%	0.099
DS6a	12000c2000001c000	18061216060c1e00	6.93	6.84	0.756%	6.86	0.679%	0.514
DS6a	12020000040c0800	1802020006040600	1.30	1.28	0.284%	1.28	0.275%	0.096
DS6a	12020c00040c1800	1802020006040600	2.37	2.33	0.676%	2.33	0.275%	0.175
DS6a	12080c2000001c000	18061216060c1e00	3.38	3.34	0.931%	3.34	0.677%	0.251
DS6a	12120c3e1c0c1c00	18061216060c1e00	0.56	0.54	1.847%	0.56	0.676%	0.041
DS6a	16020c10040c1800	1806020006060600	3.23	3.20	0.883%	3.19	0.416%	0.239
DS6a	160a0c321c0c1c00	1806021006061600	1.98	1.95	2.022%	1.97	0.521%	0.147
DS6a	1e0a0c321c0c1c00	1806020006040200	2.62	2.59	2.275%	2.59	0.260%	0.194
DS6a	1e0a0c321c0c1c00	1806020006040600	1.31	1.29	2.275%	1.29	0.390%	0.097
DS6a	1e0a0c321c0c1c00	1806020006041600	1.30	1.28	2.275%	1.26	0.459%	0.096
DS6a	1e0a0c321c0c1c00	1806021006061600	1.61	1.59	2.275%	1.59	0.521%	0.119
DS6a	1e120c3e1c0c1c00	18061216060c1e00	0.95	0.93	2.284%	0.93	0.676%	0.070
DS6a	1e1a0c321c0c1c00	1806020006060600	1.30	1.28	2.457%	1.28	0.416%	0.096
DS6a	1e1a0c321c0c1c00	1806021006040600	3.91	3.88	2.457%	3.87	0.415%	0.291
DS6a	1e1a0c321c0c1c00	1806021006041600	2.92	2.90	2.457%	2.90	0.495%	0.217
DS6a	1e1a0c321c0c1c00	1806021006060600	1.31	1.30	2.455%	1.30	0.436%	0.097
DS6a	1e1a0c3a1c0c1c00	1806020006040600	2.32	2.31	2.553%	2.32	0.390%	0.174
DS6a	1e1a0c3a1c0c1c00	1806021006040600	1.77	1.77	2.552%	1.75	0.415%	0.132
DS6a	1e1a0c3a1c0c1c00	1806021006041600	0.67	0.67	2.553%	0.67	0.494%	0.050
DS6a	1e1a0c3e1c0c1c00	1806000006040600	2.22	2.18	2.631%	2.16	0.360%	0.163
DS6a	1e1a0c3e1c0c1c00	1806020006041600	1.32	1.30	2.630%	1.30	0.458%	0.097
DS6a	1e1a0c3e1c0c1c00	1806021006041600	1.30	1.28	2.630%	1.28	0.494%	0.096
DS6a	1e1a0c3e1c0c1c00	18060210060c1e00	4.63	4.58	2.629%	4.55	0.533%	0.342
DS6a	1e1a0c3e1c0c1c00	1806021206041600	2.61	2.56	2.628%	2.57	0.515%	0.192
DS6a	1e1a0c3e1c0c1c00	18060214060c0600	1.70	1.70	2.628%	1.68	0.492%	0.127
DS6a	1e1a0c3e1c0c1c00	18060214060c1e00	1.38	1.36	2.627%	1.36	0.576%	0.102
DS6a	1e1a0c3e1c0c1c00	18060214060e1e00	23.42	23.19	2.601%	23.12	0.555%	1.736
DS6a	1e1a0c3e1c0c1c00	18061212060c1e00	2.93	2.89	2.628%	2.90	0.644%	0.217
DS6a	1e1a0c3e1c0c1c00	18061216060c1e00	6.59	6.51	2.628%	6.51	0.690%	0.488
DSTotal	-	-	321.60	318.26	2.354%	238.53	0.987%	21.228

FIG. 10 Effect of dead layers and dead times on peak amplitudes for $2\nu\beta\beta$ to the 0_1^+ peaks in multi-site event events.FIG. 11 Spectra are shown of multiplicity 1 ^{56}Co events (left) and multiplicity 2 ^{56}Co events in coincidence with an annihilation gamma. The results of the simultaneous peak fits are drawn in red (SEP fit) and green (DEP fit).

223 gammas escape the detector, resulting in a source detector hit with energy equal to the γ energy minus 1022 keV. Both
 224 SEP and DEP events present the possibility for a second 511 keV detector hit. By comparing the rate of multiplicity-1
 225 events in the SEPs and DEPs to the rate of multiplicity-2 events in which one hit falls into one of these peaks and
 226 the other falls into the 511 keV peak, we can measure a proxy for the detection efficiency of our multi-site event
 227 signature. By comparing this measurement to simulation, we can estimate the size of any unknown uncertainties in
 228 our simulation-based efficiency estimate.

229 To achieve this, we will use a ^{56}Co calibration source. ^{56}Co presents the advantage of a large number of γ s at
 230 energies high enough to cause pair production, which allows for a comparison of many peaks to our simulation. A



231 ^{56}Co line source was inserted into the module 1 calibration track on January 15, 2019 and 168.1 h of data were
 232 recorded, until January 22, 2019. Immediately after this, the source was inserted into the module 2 calibration track
 233 and 167.1 h of data were recorded until January 29, 2019. The source had a nominal activity of 6 kHz, resulting in a
 234 high enough data rate that the energy threshold for each channel was raised to ~ 400 keV. As discussed in Section IV,
 235 3 billion event primaries were simulated for the ^{56}Co source in each module's source track in order to achieve similar
 236 events statistics for both the simulations and data. Simulations were run with and without dead layers.

237 8 SEPs and 7 DEPs were selected as proxies for the $\beta\beta$ E.S. signal; these peaks were selected because of their
 238 prominence above the Compton continuum and the absence of nearby peaks that would interfere with a peak-height
 239 measurement. A simultaneous fit, using the multipeak fitter, of all SEPs as single-detector events and as two-detector
 240 events in coincidence with a 511 keV peak event was performed in the calibration data and in the simulations both with
 241 and without dead layers. SEPs and DEPs have abnormal peakshapes due to in-flight annihilation of the positrons,
 242 which results in Doppler broadening of the peaks. For this reason, a high energy tail is added to the typical peak
 243 shape function. The peak height ratios and uncertainties for peak k are determined as follows:

$$\epsilon_k = \frac{A_{k,m2}}{A_{k,m1}} \quad (4)$$

244

$$\sigma_{stat,k} = \epsilon_k \sqrt{\frac{\Sigma_{A,k,m1;A,k,m1}}{A_{k,m1}^2} - 2 \frac{\Sigma_{A,k,m1;A,k,m2}}{A_{k,m1} A_{k,m2}} + \frac{\Sigma_{A,k,m2;A,k,m2}}{A_{k,m2}^2}} \quad (5)$$

245 where $A_{k,m1/2}$ are the fitted amplitudes of peak k with multiplicity 1 and multiplicity 2 respectively, and $\Sigma_{A,k,m1/2;A,k,m1/2}$
 246 is the fitted covariance matrix element for these amplitudes. The same process of simultaneously fitting DEPs is
 247 followed to extract the DEP peak-height ratios. The measured data spectra and fit results are shown in Figure 11.

248 Figure 12 shows an overall offset that cannot be explained by statistical errors; this discrepancy is measured and
 249 treated as a systematic error which will be applied to the $\beta\beta$ E.S. measurement. Since some of this discrepancy can be
 250 explained by the dead layer uncertainty, the difference between the simulated peak-height ratios with and without the
 251 dead layer is multiplied by the percent uncertainty in the dead layer thickness in order to measure the systematic error
 252 caused by the dead layer. Finally, a χ^2 value is computed for the comparison between the simulated and measured
 253 peak-heights using the statistical and dead layer uncertainties.

$$\chi^2(\mu, \delta_{DL}) = \sum_{k=1}^N \frac{(\epsilon_{k,meas} - \epsilon_{k,sim} - \delta_{DL} \cdot \sigma_{DL,k} - \mu)^2}{\sigma_{stat,dat,k}^2 + \sigma_{stat,sim,k}^2} + \delta_{DL}^2 \quad (6)$$

254 where $\sigma_{DL,k}$ is the uncertainty from dead layers, δ_{DL} is the measured error from dead layers (correlated across all
 255 peaks with a prior of 1 σ), and μ is the mean error that remains. This χ^2 function is minimized with respect to μ
 256 and δ_{DL} and the profile likelihood is used to compute the uncertainty on μ , using MINUIT[9]. The systematic error
 257 is taken to be

$$\sigma_{sim}^2 = \mu^2 + \sigma_\mu^2 \quad (7)$$

258 Tables II and III list the peak height ratios and uncertainties for each peak for module 1 and module 2, respectively.
 259 The final fractional uncertainties measured are $\sigma_{sim,M1} = 0.0020$ and $\sigma_{sim,M2} = 0.0047$. This uncertainty is applied
 260 directly to the detection efficiency measured before applying any other effects such as dead layers, dead times and
 261 cuts, without any scaling. This uncertainty is one of the dominant uncertainties on the detection efficiency along with
 262 the dead layer uncertainty; while the absolute uncertainty is small, because it is applied to the detection efficiency,
 263 which tends to be $\sim 5\%$, directly rather than to the loss from an individual effect, the fractional uncertainty is on the
 264 order of 10%. In cases where the detection efficiency is very low, such as the 1216 keV peak in module 2 from decays
 265 to the 2_2^+ state, this uncertainty can completely overwhelm the detection efficiency. Figure 12 plots the peak height
 266 ratios for simulated and measured data for both modules 1 and 2.

267 VII. REGION OF INTEREST SELECTION

268 Once the multi-site events have been collected, we want to search for detector hits with the energies of the γ s
 269 emitted in each $\beta\beta$ E.S. decay mode. To do this, a signal region of interest (ROI) must be identified. To estimate
 270 the number of background events in the signal ROI, a background ROI must also be selected near the signal ROI.

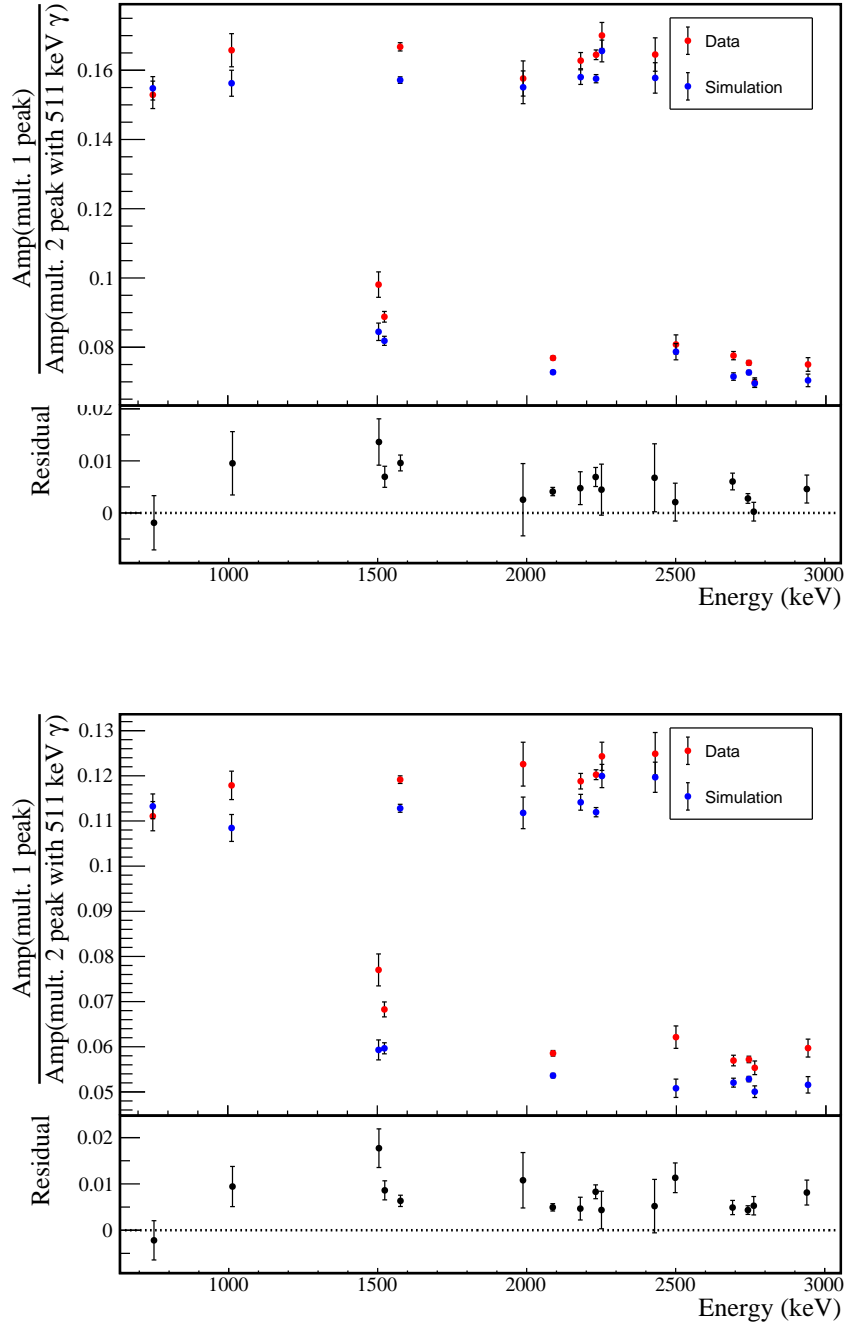


FIG. 12 Measurement of peak height ratios between multiplicity 1 events and multiplicity 2 events containing a 511 keV annihilation γ for both simulated and measured ^{56}Co spectra. Only statistical error bars are drawn. These ratios are listed in tables II and III.

271 This section will describe the selection of the signal and background ROIs and the calculation of the efficiency and
 272 uncertainties on the efficiency due to the ROI selection.

273 For each dataset, a simultaneous fit of many peaks is performed to a combined spectrum of all detectors and all
 274 calibration runs, ensuring that any variation in gain or energy nonlinearity between detectors is accounted for. From
 275 each fit result, a set of parameters describing a single peak at the energy of the signal ROI can be extracted, along
 276 with a covariance matrix for those parameters. From these fit results, we can compute the optimal ROI, detection
 277 efficiency and uncertainty for each data set. An example of a calibration spectrum with the FWHM curve fit to it is



TABLE II Table of measured peak height ratios between multiplicity 1 events and multiplicity 2 events containing a 511 keV annihilation γ in module 1 for both simulated and measured ^{56}Co spectra, with uncertainties. A plot of these numbers is shown in Figure 12

Peak	$\frac{A_{m2,\text{dat}}}{A_{m1,\text{dat}}}$	$\frac{A_{m2,\text{sim}}}{A_{m1,\text{sim}}}$	$\frac{A_{m2,\text{noDL}}}{A_{m1,\text{noDL}}}$	$\sigma_{\text{dat,stat}}$	$\sigma_{\text{sim,stat}}$	$\sigma_{\text{sim,DL}}$	Residual	σ_{resid}
1504 keV (SEP)	0.098	0.084	0.110	0.004	0.003	0.004	0.014	0.004
1524 keV (SEP)	0.089	0.082	0.109	0.002	0.001	0.005	0.007	0.002
2088 keV (SEP)	0.077	0.073	0.098	0.001	0.001	0.004	0.004	0.001
2499 keV (SEP)	0.081	0.079	0.108	0.003	0.002	0.005	0.002	0.004
2691 keV (SEP)	0.078	0.072	0.099	0.001	0.001	0.005	0.006	0.002
2743 keV (SEP)	0.075	0.073	0.101	0.001	0.001	0.005	0.003	0.001
2762 keV (SEP)	0.070	0.070	0.096	0.001	0.001	0.004	0.000	0.002
2940 keV (SEP)	0.075	0.070	0.100	0.002	0.002	0.005	0.005	0.003
749 keV (DEP)	0.153	0.155	0.225	0.004	0.003	0.012	-0.002	0.005
1013 keV (DEP)	0.166	0.156	0.229	0.005	0.004	0.012	0.010	0.006
1577 keV (DEP)	0.167	0.157	0.224	0.001	0.001	0.011	0.010	0.002
1988 keV (DEP)	0.158	0.155	0.222	0.005	0.005	0.011	0.003	0.007
2180 keV (DEP)	0.163	0.158	0.225	0.002	0.002	0.011	0.005	0.003
2232 keV (DEP)	0.164	0.158	0.225	0.001	0.001	0.012	0.007	0.002
2251 keV (DEP)	0.170	0.166	0.233	0.004	0.003	0.011	0.004	0.005
2429 keV (DEP)	0.165	0.158	0.230	0.005	0.004	0.012	0.007	0.007

TABLE III Table of measured peak height ratios between multiplicity 1 events and multiplicity 2 events containing a 511 keV annihilation γ in module 2 for both simulated and measured ^{56}Co spectra, with uncertainties. A plot of these numbers is shown in Figure 12

Peak	$\frac{A_{m2,\text{dat}}}{A_{m1,\text{dat}}}$	$\frac{A_{m2,\text{sim}}}{A_{m1,\text{sim}}}$	$\frac{A_{m2,\text{noDL}}}{A_{m1,\text{noDL}}}$	$\sigma_{\text{dat,stat}}$	$\sigma_{\text{sim,stat}}$	$\sigma_{\text{sim,DL}}$	Residual	σ_{resid}
1504 keV (SEP)	0.077	0.059	0.082	0.004	0.002	0.004	0.018	0.004
1524 keV (SEP)	0.068	0.060	0.081	0.002	0.001	0.004	0.009	0.002
2088 keV (SEP)	0.059	0.054	0.074	0.001	0.000	0.003	0.005	0.001
2499 keV (SEP)	0.062	0.051	0.073	0.002	0.002	0.004	0.011	0.003
2691 keV (SEP)	0.057	0.052	0.074	0.001	0.001	0.004	0.005	0.002
2743 keV (SEP)	0.057	0.053	0.075	0.001	0.001	0.004	0.004	0.001
2762 keV (SEP)	0.055	0.050	0.071	0.002	0.001	0.004	0.005	0.002
2940 keV (SEP)	0.060	0.052	0.072	0.002	0.002	0.003	0.008	0.003
749 keV (DEP)	0.111	0.113	0.155	0.003	0.003	0.007	-0.002	0.004
1013 keV (DEP)	0.118	0.108	0.156	0.003	0.003	0.008	0.009	0.004
1577 keV (DEP)	0.119	0.113	0.161	0.001	0.001	0.008	0.006	0.001
1988 keV (DEP)	0.123	0.112	0.153	0.005	0.003	0.007	0.011	0.006
2180 keV (DEP)	0.119	0.114	0.164	0.002	0.002	0.008	0.005	0.002
2232 keV (DEP)	0.120	0.112	0.160	0.001	0.001	0.008	0.008	0.001
2251 keV (DEP)	0.124	0.120	0.170	0.003	0.003	0.008	0.004	0.004
2429 keV (DEP)	0.125	0.120	0.159	0.005	0.003	0.007	0.005	0.006

279 shown in Figure 13.

280 A. Signal ROI Optimization

281 The signal region of interest around each peak is optimized based on the peak shape functions as fit for each data
282 set. The optimization follows the procedure laid out in Appendix H and maximizes the rate sensitivity with respect
283 to the region of interest upper and lower boundaries, E_{low} and E_{high} respectively:

$$\hat{\Gamma}(E_{low}, E_{high}, \bar{B}) \propto \frac{\text{DP}(\bar{B}(E_{high} - E_{low}))}{\epsilon_{ROI}(E_{low}, E_{high})} \quad (8)$$

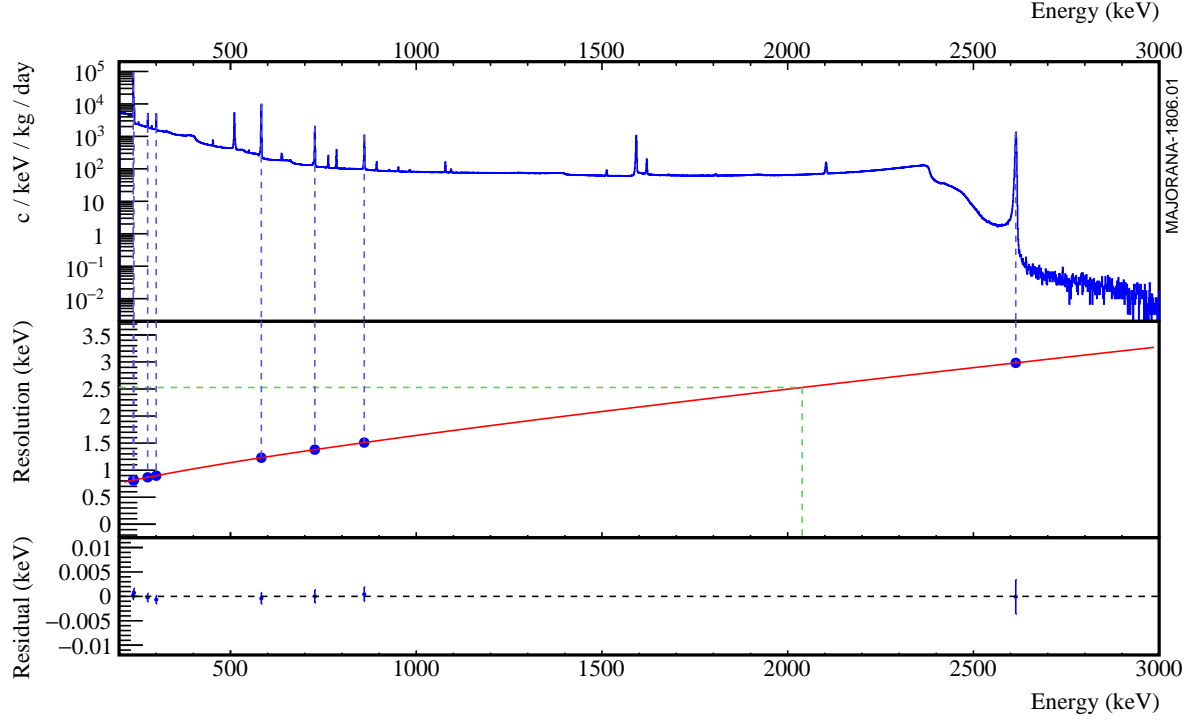


FIG. 13 A ^{228}Th calibration run with the FWHM fit curve and individual uncertainties at several peaks. This curve is used to compute the FWHM for a peak at a given energy. The statistical uncertainties are extracted from the fit result. An additional systematic uncertainty is added to account for the residuals.

where DP is the discovery potential as defined in Appendix H, and a flat background with background index \bar{B} measured from data is assumed. The efficiency is defined by the CDF of the Gaussian and LE tail components

$$\epsilon_{ROI}(E_{low}, E_{high}; \mu, \sigma, f_{tail}, \tau) = \frac{1}{2} \left(\operatorname{erfc} \left(\frac{E_{low} - \mu}{\sqrt{2}\sigma} \right) - \operatorname{erfc} \left(\frac{E_{high} - \mu}{\sqrt{2}\sigma} \right) \right) + f_{tail}\tau \left(\operatorname{ExGaus}(E_{high}; \mu, \sigma, \tau) - \operatorname{ExGaus}(E_{low}; \mu, \sigma, \tau) \right) \quad (9)$$

The optimal ROI is numerically calculated by minimizing $\frac{1}{\Gamma(E_{low}, E_{high}, \bar{B})}$ with respect to E_{low} and E_{high} using MINUIT[9].

B. Background ROI Selection

For each peak, a background ROI of width 50 – 100 keV surrounding the peak is selected. The ROI is selected to avoid any known background peaks and exclude them with at least 99.9% efficiency. A 99.9% exclusion region calculated from the peakshape function is selected around the peak and removed from the background ROI.

C. ROI Detection Efficiency and Uncertainty

The ROI detection efficiency is calculated from the CDF defined in Equation 9. The covariance matrix of the peak shape parameters obtained from the fit result is used to calculate the statistical uncertainty of the efficiency. Several additional systematic effects must also be accounted for:

- **Gain drift:** ^{228}Th energy calibrations are taken once per week, for 90 minutes each. In between these calibration runs, the energy calibration parameters undergo small adjustments that result in energy inaccuracies for background runs taken in between. This gain drift results in an increase in the width of the peak, which is accounted for by adding in quadrature σ_{drift} to the value of σ obtained from the fit. This also results in the dominant systematic uncertainty on the peak width, $\delta_{fwhm,drift}$. The gain drift also results in a small



systematic error in the measured energy of the peak $\delta_{\mu,drift}$. A detailed description of the measurement of this systematic effect is contained in Reference [10].

• **Energy nonlinearity:** While the energy response for HPGe detectors is ostensibly linear, several factors result in small nonlinearities. Local nonlinearities that are correlated over small energy scales of arise from the response of the Gretina digitizers. While these nonlinearities are corrected for, a residual nonlinearity of ~ 0.1 keV with a period of ~ 300 keV remains. Global nonlinearities result from systematic uncertainties in the energy estimation. One source of global nonlinearity arises from uncertainty in the start time of the waveform, which is energy dependant. Another is a small quadratic term resulting from charge recombination. Because calibrations are performed on peaks with energies ranging from 238 keV to 2614 keV, energy shifts due to global nonlinearities are very small in this range and local energy nonlinearities dominate. At smaller and larger energies, the shifts can be as large as ~ 0.5 keV in some detectors. In addition to this bias, energy nonlinearities result in an increase in σ as a result of the combining of peaks from different detectors with different shifts; however, since the energy calibrations include all detectors, this shift is already included in the fit result, so no action is required. Energy nonlinearities also have a significant affect on the uncertainty in the measured peak energy, $\delta_{\mu,NL}$, which is a dominant uncertainty. A detailed description of the measurement of each of these systematic effects is contained in Reference [10].

• **Detector Crosstalk:** Because we are searching for peaks in coincidence events, the possibility for a distortion in the energy measurement due to crosstalk between the involved events exists. This effect is measured in Section VII.D to be small enough that no energy correction or peakshape correction is required. However, this effect does contribute to small uncertainties in the peak position, $\delta_{\mu,xtalk}$ and peak width, $\delta_{fwhm,xtalk}$.

Once these uncertainties have been measured, they must be propagated into the detection efficiency. The statistical and systematic uncertainties on μ and the FWHM are added in quadrature to obtain δ_μ and δ_{fwhm} . The uncertainty on the FWHM is used to calculate a width scale uncertainty, δ_α , which is simply the fractional uncertainty on the FWHM. To compute the uncertainty on the efficiency, the efficiency is computed after modifying the peakshape parameters by one-sigma in either direction. For the uncertainty from the width, we take:

$$\sigma_{\epsilon_{ROI,fwhm}} = \frac{1}{2} (\epsilon_{ROI}(E_{low}, E_{high}; \mu, \sigma(1 + \delta_\alpha), f_{LE}, \tau(1 + \delta_\alpha)) - \epsilon_{ROI}(E_{low}, E_{high}; \mu, \sigma(1 - \delta_\alpha), f_{LE}, \tau(1 - \delta_\alpha))) \quad (10)$$

Because the ROI is optimized around μ , shifts in the peak in either direction will cause a reduction in efficiency. For this reason, we must perform a second order propagation of uncertainties with respect to δ_μ . The result is a slight degradation in the efficiency, so that

$$\epsilon_{ROI} = \frac{\epsilon_{ROI}(E_{low}, E_{high}; \mu + \delta_\mu, \sigma, f_{LE}, \tau) + \epsilon_{ROI}(E_{low}, E_{high}; \mu - \delta_\mu, \sigma, f_{LE}, \tau)}{2} \quad (11)$$

and

$$\sigma_{\epsilon_{ROI,\mu}} = \epsilon_{ROI}(E_{low}, E_{high}; \mu, \sigma, f_{LE}, \tau) - \epsilon_{ROI} \quad (12)$$

These uncertainties are taken to be uncorrelated and added in quadrature to obtain the final uncertainty on the ROI efficiency. Table XXVI contains a full summary of all of the energy uncertainties, the ROIs, and the ROI efficiencies and uncertainties.

D. Detector Crosstalk

Detector crosstalk is caused when a true signal in one detector channel induces a small signal in another channel. This is not a large enough effect to trigger events in a separate channel, meaning that it does not effect single-detector events. However, it could produce an energy estimation error in multi-detector events since coincident pulses could induce signals that interfere either constructively or destructively, shifting the measured energies. In practice, this could produce both a shift and additional uncertainty in both the measured energy of the peak and in the width of the peak. To check for this effect, we can look at multi-detector events in ^{228}Th calibration data. In particular, we will compare the centroid and FWHM for several peaks in both single-detector events and multi-detector events.

5 peaks were selected from the ^{208}Tl γ cascade, at 277, 583, 763, 860 and 2614 keV, and one additional peak was selected from the ^{212}Bi cascade, at 785 keV. These peaks were selected based on their prominence in the high



TABLE IV Table of energy estimation uncertainties, regions of interest, and efficiencies

DS	E_{peak} (keV)	σ_{fit} (keV)	σ_{drift} (keV)	σ (keV)	$f_{t,fit}$ (keV)	τ_{fit} (keV)	$\delta_{\mu,fit}$ (keV)	$\delta_{\mu,NL}$ (keV)	$\delta_{\mu,drift}$ (keV)	$\delta_{\mu,peak}$ (keV)	δ_u (keV)	FWHM (keV)	$\delta_{fwhm,drift}$ (keV)	$\delta_{fwhm,fit}$ (keV)	$\delta_{fwhm,xtalk}$ (keV)	δ_{FWHM} (keV)	δ_α	$E_{ROI,1}$ (keV)	$E_{ROI,2}$ (keV)	ϵ_{ROI}	$\sigma_{\epsilon_{ROI}}$	
DS1	559.101	0.460	0.063	0.464	0.230	0.515	0.001	0.104	0.002	0.012	0.005	0.105	1.152	0.001	0.039	0.011	0.040	0.035	558.199	559.847	0.871	0.015
DS2	559.101	0.461	0.055	0.464	0.249	0.515	0.002	0.067	0.004	0.012	0.005	0.068	1.158	0.001	0.107	0.011	0.108	0.093	558.186	559.845	0.874	0.031
DS3	559.101	0.470	0.066	0.474	0.224	0.505	0.001	0.026	0.024	0.012	0.005	0.038	1.174	0.001	0.073	0.011	0.074	0.063	558.187	559.863	0.879	0.021
DS4	559.101	0.455	0.077	0.461	0.108	0.445	0.002	0.076	0.010	0.012	0.005	0.078	1.111	0.001	0.106	0.011	0.107	0.096	558.283	559.856	0.888	0.032
DS5a	559.101	0.560	0.085	0.567	0.106	0.855	0.002	0.079	0.005	0.012	0.005	0.080	1.367	0.002	0.055	0.011	0.056	0.041	558.098	560.022	0.875	0.014
DS5b	559.101	0.469	0.074	0.475	0.158	0.491	0.001	0.020	0.011	0.012	0.005	0.026	1.157	0.001	0.125	0.011	0.125	0.108	558.229	559.872	0.885	0.036
DS5c	559.101	0.460	0.085	0.468	0.174	0.489	0.001	0.037	0.030	0.012	0.005	0.050	1.145	0.001	0.162	0.011	0.162	0.142	558.231	559.860	0.883	0.046
DS6a	559.101	0.456	0.044	0.458	0.191	0.463	0.001	0.069	0.025	0.012	0.005	0.075	1.123	0.000	0.041	0.011	0.042	0.038	558.241	559.841	0.881	0.014
DS1	563.178	0.461	0.064	0.466	0.230	0.518	0.001	0.104	0.002	0.012	0.005	0.105	1.156	0.001	0.039	0.011	0.040	0.035	562.273	563.927	0.871	0.015
DS2	563.178	0.463	0.055	0.466	0.249	0.517	0.002	0.067	0.004	0.012	0.005	0.068	1.162	0.001	0.107	0.011	0.108	0.093	562.259	563.924	0.874	0.030
DS3	563.178	0.471	0.066	0.476	0.224	0.508	0.001	0.026	0.024	0.012	0.005	0.038	1.179	0.001	0.073	0.011	0.074	0.063	562.261	563.943	0.879	0.021
DS4	563.178	0.457	0.077	0.463	0.108	0.447	0.002	0.076	0.010	0.012	0.005	0.078	1.115	0.001	0.106	0.011	0.107	0.096	562.357	563.935	0.888	0.032
DS5a	563.178	0.562	0.086	0.569	0.106	0.858	0.002	0.079	0.006	0.012	0.005	0.080	1.372	0.002	0.055	0.011	0.056	0.041	562.172	564.103	0.875	0.014
DS5b	563.178	0.471	0.074	0.477	0.158	0.494	0.001	0.020	0.011	0.012	0.005	0.026	1.162	0.001	0.125	0.011	0.125	0.108	562.303	563.952	0.885	0.035
DS5c	563.178	0.462	0.086	0.470	0.174	0.492	0.001	0.037	0.030	0.012	0.005	0.050	1.449	0.001	0.162	0.011	0.162	0.141	562.305	563.939	0.883	0.046
DS6a	563.178	0.457	0.044	0.459	0.191	0.465	0.001	0.069	0.026	0.012	0.005	0.075	1.127	0.000	0.041	0.011	0.042	0.038	562.315	563.921	0.881	0.013

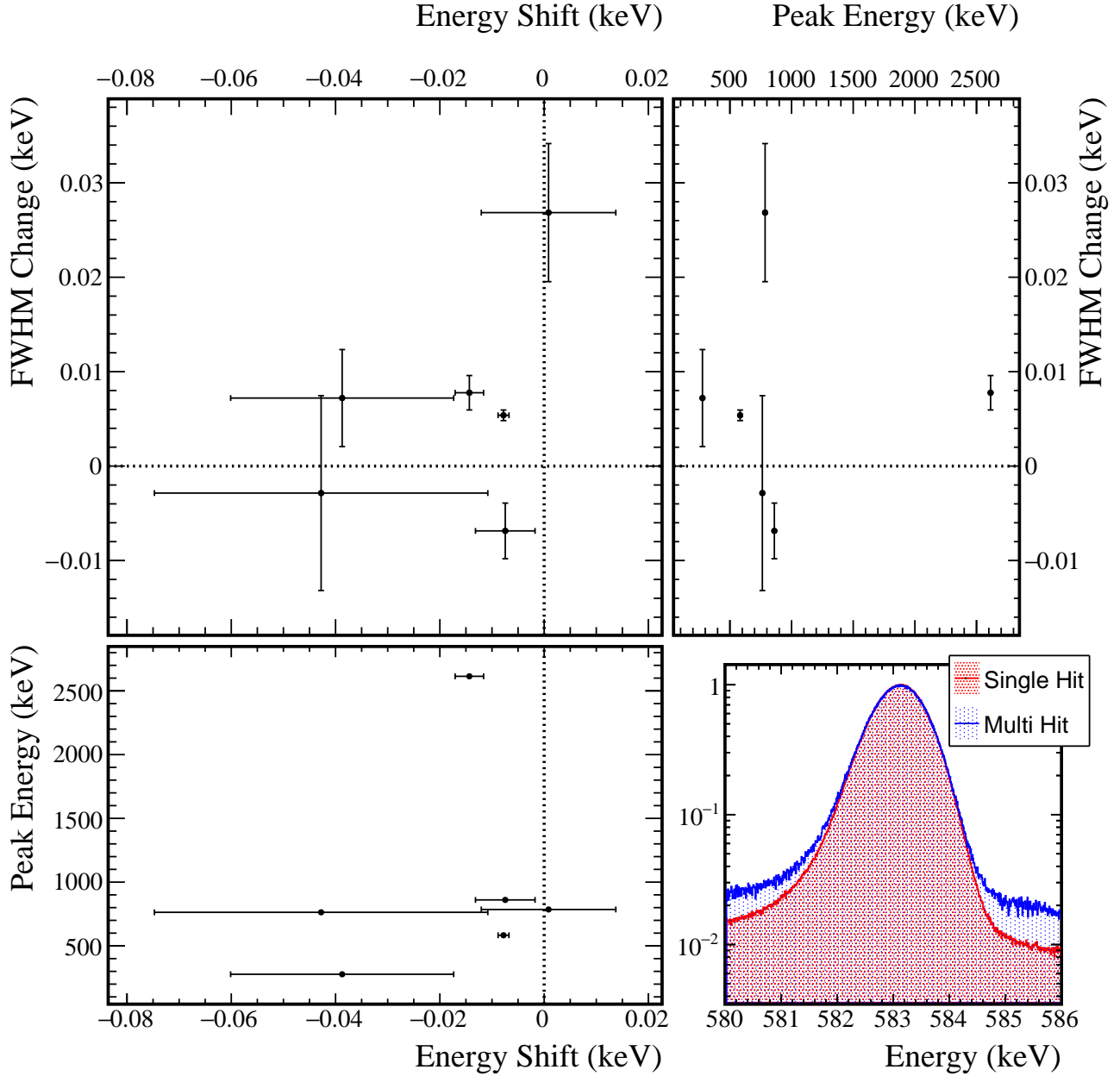


FIG. 14 Difference of the measured centroid and FWHM of several ^{228}Th calibration peaks. Error bars represent the fit errors. Notice on the bottom right, that any difference is not visible to the naked eye.

345 multiplicity hit spectrum. The combined calibration spectra from dataset 6 were used to perform this analysis. These
 346 peaks were fit individually, and the centroid and FWHM were computed for multiplicity 1 and multiplicity 2 events.
 347 Figure 14 shows the results of these measurements. While a very small reduction in peak centroid and increase in
 348 peak width are observed, the shifts are small compared to the existing uncertainties in these parameters. As a result,
 349 we will ignore this shift and instead compute an uncertainty in each parameter caused by crosstalk. We will treat the
 350 systematic error as uncorrelated between the peaks and compute the necessary error needed to make the combined
 351 statistical and systematic errors large enough to make the χ^2 value computed by comparing these peaks equal to 1:

$$\chi^2 = \sum_{k=0}^N \frac{(cen_{k,m1} - cen_{k,m2})^2}{\sigma_{cen,k,m1}^2 + \sigma_{cen,k,m2}^2 + \delta_{\mu,xtalk}^2} \quad (13)$$



$$\chi^2 = \sum_{k=0}^N \frac{(\text{FWHM}_{k,m1} - \text{FWHM}_{k,m2})^2}{\sigma_{fwhm,k,m1}^2 + \sigma_{fwhm,k,m2}^2 + \delta_{fwhm,xtalk}^2} \quad (14)$$

353 Both systematic errors are numerically computed using a Brent minimization algorithm[11]. The results are $\delta_{\mu,xtalk} =$
 354 0.012 keV and $\delta_{fwhm,xtalk} = 0.011 \text{ keV}$, both of which are subdominant uncertainties.

355 VIII. BACKGROUND CUTS

356 By making use of known properties of background events, data cleaning cuts can be designed to selectively reduce
 357 backgrounds while minimizing sacrifice of excited state events. Because of the multi-detector event nature of the event
 358 selection, many of these background cuts are designed to make use of observables from the detector hits in coincidence
 359 with candidate hits.

360 A. Enriched Source Detector Cut

361 Since the $\beta\beta$ E.S. events must originate in ^{76}Ge , events are far likelier to originate in enriched HPGe detectors
 362 than those with natural germanium isotopic abundances. There are 29.8 kg of enriched detectors, with $88.1 \pm 0.7\%$
 363 abundance of ^{76}Ge and 14.4 kg of natural detectors, with $7.83 \pm 0.07\%$ abundance of ^{76}Ge . This means that $95.8 \pm 0.1\%$
 364 of $\beta\beta$ E.S. events will originate in enriched detectors. If we assume that background events will hit all detector mass
 365 at the same rate, then we would expect only 67% of hits from background events involving two detectors to be in
 366 coincidence with a hit in an enriched detector. This means that a significant gain in sensitivity can be achieved by
 367 cutting hits that are not in coincidence with an enriched detector hit. While the detection efficiency of this cut is
 368 expected to be close to 95.8%, the actual efficiency is measured from simulations, and tends to be greater, since a
 369 greater proportion of enriched detectors are active compared to natural detectors.

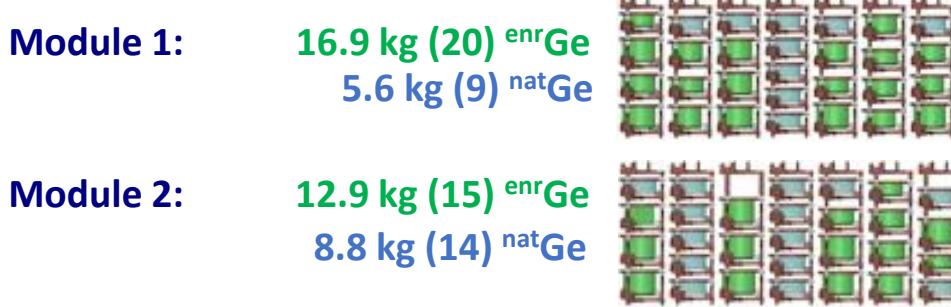


FIG. 15 Diagram showing each detector in each module, arranged by which string and position they are in. Enriched detectors are colored green and natural detectors are colored blue. 95% of ^{76}Ge in the array is contained in the enriched detectors.

370 B. Coincident and Sum Energy Cuts

371 The greatest source of background events is expected to be γ -rays from a handful of known primordial and cos-
 372 mogenic isotopes. Because γ -rays are monoenergetic, they will often present a clear detection signature that can be
 373 targeted. γ -rays will often Compton scatter from one detector into another, depositing their entire energy between
 374 the two. For this reason, events whose total energy is equal to the energy of a known γ can be cut. β -decays will
 375 often result in a cascade of multiple γ s, at least one of which may be fully absorbed in a single detector. These events
 376 can be cut by searching for a coincident detector with energy equal to that of a known γ . Finally, whereas the $\beta\beta$
 377 decay spectrum approaches zero amplitude at low energies and at $Q_{\beta\beta}$, the Compton continuum of γ s has a large
 378 amplitude at low energies. This means that sensitivity can be gained by setting low- and high-energy thresholds on
 379 hits in coincidence with a candidate event. These combined backgrounds can be reduced by cutting events with either



sum energies or coincident hit energies that fall in a set of energy ranges. For $\beta\beta$ E.S. modes with multiple γ s, the optimal energy ranges will differ between natural and enriched detectors, since natural detectors will mostly include hits from one of the γ s, while enriched events will include $\beta\beta$ hits, γ hits, and pileup events including both of these, allowing a much wider energy range. For this reason, a separate set of coincident cut energy ranges are used for natural and enriched detectors.

The energy ranges that are cut can be determined by comparing the background model simulation to simulations of each $\beta\beta$ E.S. decay mode. An algorithm was written that simultaneously selects a set of both sum and coincident energy ranges to cut that optimizes discovery potential, as defined in Appendix H. The algorithm begins by identifying events in the $\beta\beta$ E.S. simulation that include at least one hit consisting of the full absorption of a γ photon and events in the background model simulation that include at least one hit in the background region of interest. These events are then sorted into energy bins for each coincident hit and for the sum energy of the event (a single event will be in multiple bins). For each bin, the algorithm checks the change in discovery potential if the bin was toggled to be either cut or included. Following Equation H10, the discovery potential will be improved by toggling bin k if:

$$\text{DP}'(s \cdot N_{BG}) \frac{s \cdot n_{k,BG}}{\text{DP}(s \cdot N_{BG})} < \frac{n_{k,ES}}{N_{ES}} \quad (15)$$

where N_{ES} and N_{BG} are the total number of events remaining in the simulated $\beta\beta$ E.S. and background spectra, respectively; s is a scaling to estimate the number of background events in the data from the number in the simulation; and $n_{k,ES}$ and $n_{k,BG}$ are the number of simulated $\beta\beta$ E.S. and background events contained in the bin. A χ value is computed representing the normal quantile of the probability that cutting or including the bin will improve the discovery potential. This is done by assuming that the uncertainty on the number of events in the bin is Gaussian distributed, with standard deviations $\sqrt{n_{k,ES}}$ and $\sqrt{n_{k,BG}}$, respectively. In this case, we get:

$$\chi_k = \frac{\frac{n_{k,ES}}{N_{ES}} - \text{DP}'(s \cdot N_{BG}) \frac{s \cdot n_{k,BG}}{\text{DP}(s \cdot N_{BG})}}{\sqrt{\left(\text{DP}'(s \cdot N_{BG}) \frac{s}{\text{DP}(s \cdot N_{BG})}\right)^2 n_{k,BG} + \frac{n_{k,ES}}{N_{ES}^2}}} \quad (16)$$

All events in the bin with highest probability of improving the discovery potential are then either cut or included, and must be cut or included to all other bins that they fall into. Note that a included event will only be included if it is not cut by any other bin. This process is repeated until toggling any bin will have $\chi_k < 0$, meaning there is a $< 50\%$ chance of improving the discovery potential. At this point, the bins are then combined in order to determine the ranges of energies to be cut in sum energy and coincident energies.

Because of limited statistics in the simulations, this cut will be biased to cut events in bins with a downward fluctuation in $\beta\beta$ E.S. rate and accept bins with an upward fluctuation, and vice-versa for the simulated background model. In order to minimize this bias and ensure that energy ranges are selected based on real backgrounds rather than statistical fluctuations, a penalty is applied to the probability calculations if a new range would be added. If cutting or readding a bin would increase the number of energy ranges, a penalty of 3 is added to the χ value, and if it would reduce the number of ranges, a penalty of -3 is added. This corresponds to requiring a 99.8% chance that adding a new energy range will represent an improvement before we conclude that it is not a statistical fluctuation. This is inspired by the Akaike Information Criterion (AIC)[12], which adds a penalty of 1 to a likelihood for each parameter added to a model. In this case, adding an energy range adds two parameters to our cut, so the equivalent penalty is 1.5 per parameter, which is a larger penalty than AIC. This difference can be explained by the fact that the AIC penalty of 1 requires 97.7% that toggling a bin represents an improvement; however, it has been observed that ~ 100 bins exist close enough to the threshold for inclusion or exclusion to accidentally toggle the bin. As a result, using a penalty of 1 will result in multiple accidentally excluded energy regions, on average, while a penalty of 1.5 will not.

To further control limited simulation statistics, a variety of bin widths is used to determine the optimal energy ranges. This is necessary because with a narrow binning, bins do not have enough statistics to overcome the penalty described above, but wider bins produce very imprecise energy ranges. The algorithm starts by optimizing the cut ranges with a bin width of 6.4 keV starting from a prior of cutting no energy ranges. Once this optimization is complete, the bin width is split in half and the algorithm re-optimizes the energy ranges, using the previous ranges as a prior. This halving of bin width is repeated until a final bin width of 0.2 keV is reached. The results of this cut optimization procedure are shown in figures 16 and 17.

The efficiency of each of the sum and coincident energy cuts can be evaluated by computing the ratio of simulated $\beta\beta$ E.S. events that pass the cut to the total number of simulated events. The primary source of uncertainty arises from imperfections in the simulated $\beta\beta$ E.S. spectra produced by DECAYO (see Section II). Additionally uncertainty in

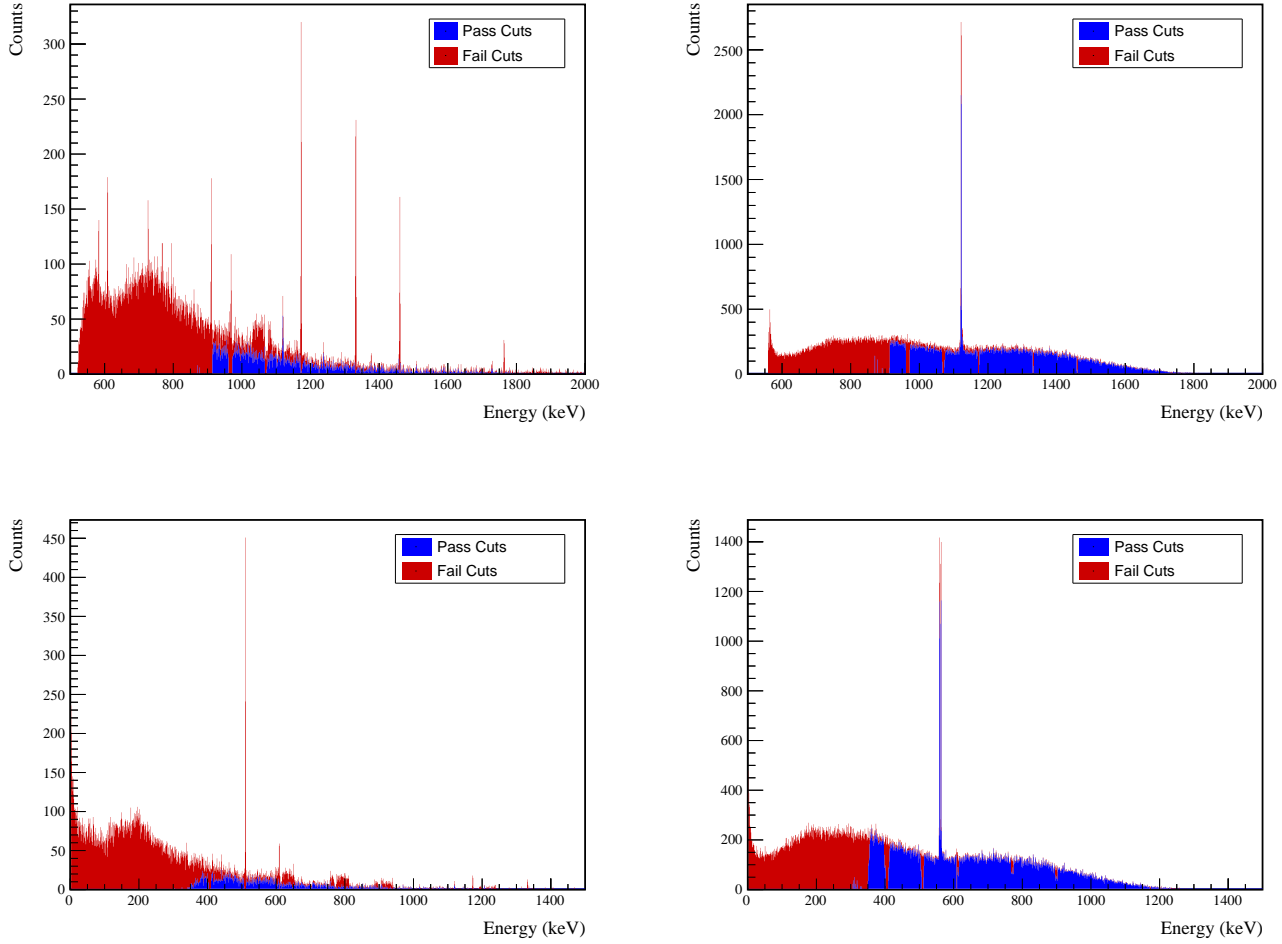


FIG. 16 Top: Simulated sum energy spectra of simulated ES and BG events. The events in red are cut by the sum- or coincident-energy cut. Note that regions around many peaks are cut, as intended.
 Bottom: Simulated energy spectrum of events in coincidence with events in the ROI. Excesses in red are cut by the sum- or coincident-energy cut. Once again, regions around prominent peaks are cut out as intended.

428 the spectral shape arises from energy nonlinearity. Since the efficiency is calculated by integrating over portions of
 429 the coincidence spectrum, an upper limit on the systematic error can be found using the KS statistic of a comparison
 430 between the simulated spectrum and the true spectrum. As discussed in Section II.A, we can perform this comparison
 431 by using the Kotila and Iachello spectrum as a proxy. This relies on the assumption that the Kotila and Iachello
 432 spectrum has corrected the dominant errors in the DECAY0 spectrum; if any errors coexist in both spectra that have a
 433 similar order of magnitude, then this approach will underestimate the uncertainty. To account for energy nonlinearity,
 434 each simulated energy is shifted to represent the effects of digitizer nonlinearity and energy drift. Digitizer nonlinearity
 435 originates from the fact that some digitizer energy bins are slightly wider than others and has an approximately
 436 sawtooth dependency on energy with a period of ~ 600 keV. A correction is applied that reduces the size of this
 437 nonlinearity to ~ 0.1 keV in magnitude and smooths it out significantly, as shown in Figure 18. Digitizer nonlinearity
 438 is included in the simulation by shifting each energy according to a sawtooth function with rms 0.1 keV and period
 439 600 keV:

$$\Delta(E) = \sqrt{3} \cdot (0.1 \text{ keV}) \left(\text{rem}\left(\frac{E - 150 \text{ keV}}{600 \text{ keV}}\right) \right) \quad (17)$$

440 where `rem` is the remainder function as defined in the C++ standard library. An additional shift that is randomly
 441 sampled from a Gaussian distribution with standard deviation $0.00015 \cdot E$ is applied to simulate the effect of gain
 442 drift, based on the drift observed during DS5. After applying both of these alterations to the DECAY0 spectrum, a KS

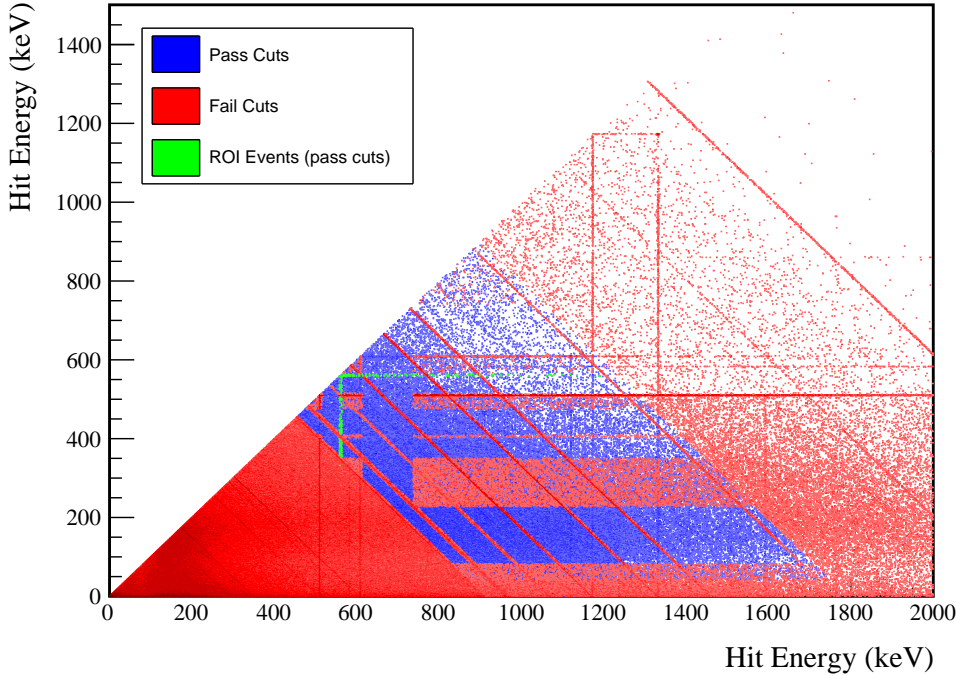


FIG. 17 2D energy spectrum of simulated BG events. Blue bins have at least one hit that passes both the sum- or coincident-energy cuts. For red bins, both hits have failed at least one of these cuts. Green bins have at least one hit in the BG or ES ROI that passes these cuts.

443 test is performed against the Kotila and Iachello spectrum, and a maximum CDF difference of 0.08% is observed, as
 444 shown in Figure 19. This difference is used as an upper limit on the uncertainty from the energy range cuts for $2\nu\beta\beta$
 445 modes.

446 For $0\nu\beta\beta$, the energy ranges selected by this cut surround peaks corresponding to the $Q_{\beta\beta}$ s of the decay modes or
 447 sum peaks of the $Q_{\beta\beta}$ with a deexcitation γ . In this case, since we are no longer integrating over a $\beta\beta$ -spectrum, the
 448 uncertainty in the efficiency will depend on shifts in the peak, similar to the ROI-efficiency. Since the energy regions
 449 selected keep at least 99.9% of these peaks in all cases, we can set an upper limit on the uncertainty by checking
 450 the ROI efficiency uncertainty around the 2039 keV $Q_{\beta\beta}$, assuming an ROI tuned to select 99.9% of the peak. The
 451 uncertainty observed in this case is 0.325%, which is applied to the energy range cuts for $0\nu\beta\beta$ modes. For both $0\nu\beta\beta$
 452 and $2\nu\beta\beta$ modes, this efficiency uncertainty is sub-dominant, so these highly conservative uncertainty estimates will
 453 suffice.
 454

455 C. Muon Veto Cut

456 Cosmic ray muons have the potential to produce particle showers in the MAJORANA DEMONSTRATOR that can
 457 produce multi-site event events and can activate short-lived isotopes that in turn may decay, producing delayed multi-
 458 site event events. Background events caused by muons can be cut using the muon veto system. This analysis follows
 459 the standard MAJORANA DEMONSTRATOR muon cut procedure, for which any HPGe detector events occurring 20 ms
 460 before and 1 s after a tagged muon event are cut. This cut will remove > 99.9% of events induced by the muon shower,
 461 based on simulations[13]. In reality, the cut efficiency is slightly lower due to periods of time where the muon veto
 462 system clock became desynchronized with the Germanium detector clock. The impact of this cut is to reduce the
 463 total livetime in each module by < 40 s per day[13].

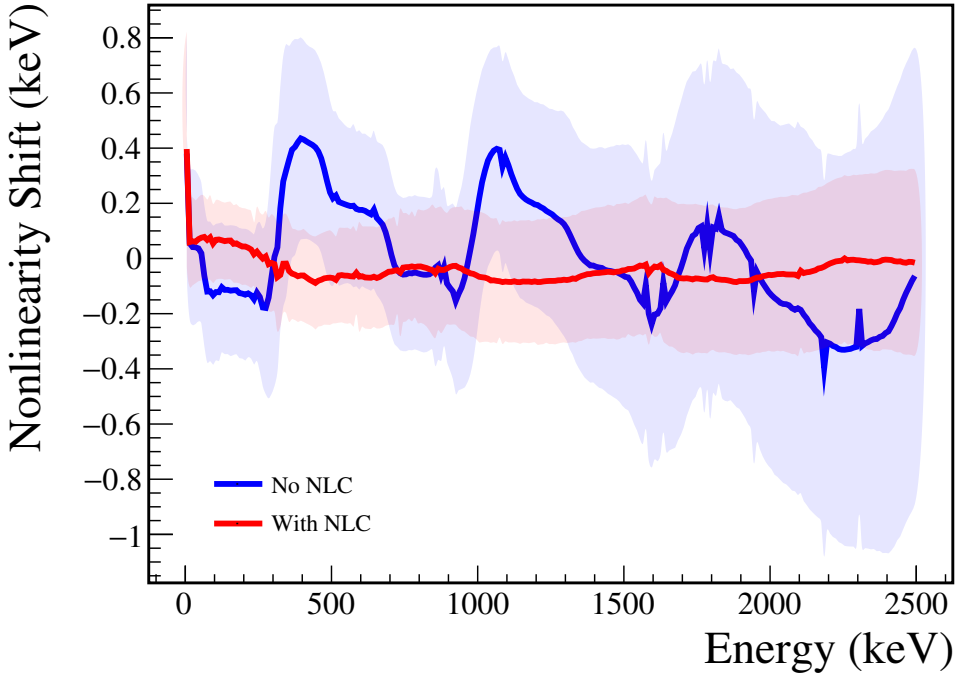


FIG. 18 Digitizer nonlinearity before (red) and after (blue) being corrected. This nonlinearity is measured by comparing the energy measured in the high gain channel to that of the low gain channel.

464 IX. COMBINED DETECTION EFFICIENCY FOR $\beta\beta$ E.S.

465 The final efficiency measurement combining all of the effects described in this chapter for each $\beta\beta$ E.S. mode is
 466 measured directly from the simulations by computing the ratio of events that survive all cuts and effects to the
 467 total number of generated events. The efficiency used is the exposure-weighted average of the simulated efficiency
 468 for each subdataset. Because each module is an independent measurement, separate efficiencies are measured for
 469 modules 1 and 2. Because of correlations causing the probability of certain effects causing sacrifice of a $\beta\beta$ E.S. event
 470 to be conditional on other effects, the combined efficiency will differ from simply being the product of the individual
 471 efficiencies. This means that the combined efficiency ϵ_{comb} for each effect k is:

$$\epsilon_{comb} = \prod_{k=0}^N P(\text{event is cut} | \text{cuts } 0 \dots k-1 \text{ are applied}) \quad (18)$$

472 In spite of this, we will assume that the sources of error are uncorrelated and the fractional uncertainty is independent
 473 of what other effects have been applied. The effect of this assumption will be discussed below. This implies that the
 474 uncertainty on the combined efficiency, $\sigma_{\epsilon,comb}$ can be expressed as:

$$\sigma_{\epsilon,comb} = \epsilon_{comb} \sqrt{\sum_{k=0}^N N \left(\frac{\sigma_{\epsilon,k}}{\epsilon_k} \right)^2} \quad (19)$$

475 The values ϵ_k represent the probability of cutting an event assuming no other analysis cuts are applied. Because
 476 of correlations among the cuts (particularly between the sum and coincident energy cuts), this results in a double-
 477 counting of uncertainty, making this a conservative estimate.

478 Table V shows the efficiency for each effect described in this chapter and uncertainty on each efficiency, and the
 479 combined efficiency and uncertainty. Similar tables for each other $\beta\beta$ E.S. peak are shown in Appendix A. In all cases
 480 the dominant uncertainties come from either the dead layer thickness or the simulation uncertainty. Figure 21 shows
 481 the effect of each cut as it is applied sequentially to the $2\nu\beta\beta$ to 0_1^+ peaks.

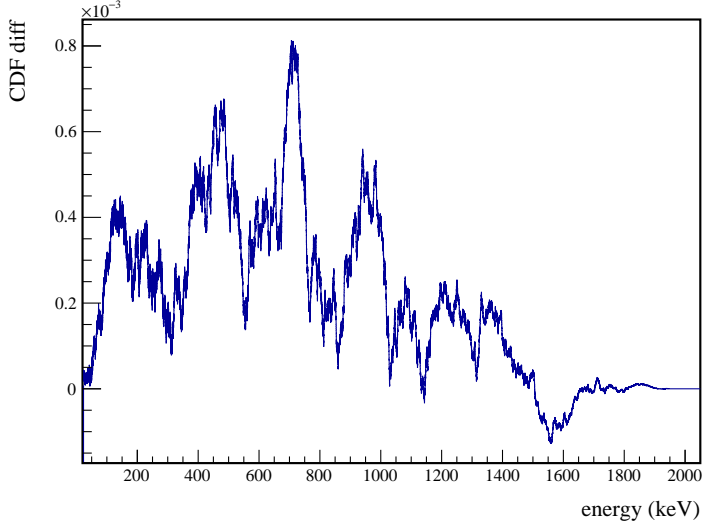


FIG. 19 KS test comparing the CDFs of the simulated DECAY0 $2\nu\beta\beta$ ground state decay with energy nonlinearity modifications applied to the Kotila and Iachello simulated spectrum.

Source	Module 1 efficiency	Module 2 efficiency
Multi-Detector with Full Energy γ	$5.9 \pm 0.2\%$	$3.2 \pm 0.5\%$
Region of Interest	$87.9 \pm 1.4\%$	$87.9 \pm 1.4\%$
Dead Layer	$74.5 \pm 4.3\%$	$65.7 \pm 6.0\%$
Detector Dead Times	$97.5 \pm 1.2\%$	$98.1 \pm 0.9\%$
Enriched Source Detector Cut	$96.8 \pm <0.1\%$	$89.4 \pm <0.1\%$
Coincident Energy Cut	$88.5 \pm 0.5\%$	$84.4 \pm 0.5\%$
Sum Energy Cut	$60.2 \pm 0.5\%$	$54.0 \pm 0.5\%$
Final Efficiency	$2.29 \pm 0.16\%$	$0.97 \pm 0.17\%$

TABLE V Table of detection efficiencies and uncertainties for $2\nu\beta\beta$ of ^{76}Ge to the 0_1^+ state of ^{76}Se . Efficiencies of individual effects are calculated without applying other cuts; because of correlations between cuts (especially the sum and coincident energy cuts), simply multiplying these efficiencies together will underestimate the efficiency. The final efficiency calculated here correctly accounts for such correlations. Note that the efficiencies are the combined efficiency for the 559 and 563 keV peaks.

484 X. DOUBLE BETA DECAY TO EXCITED STATES RESULTS

485 Now that we have found and characterized a specific detection signature for each decay mode, we can apply this
 486 search to data. This result will look at open runs from datasets 1 through 6a that were designated silver or gold in
 487 run quality. The duty cycle and changes that define each data set are shown in Figure 22. These were taken from
 488 January 12, 2016 to April 18, 2018, and contain a total of 13.4 kg y of isotopic exposure for module 1 and 7.9 kg y
 489 for module 2. Approximately half the data in these datasets is blinded, and is not included in this analysis. The
 490 MAJORANA DEMONSTRATOR uses a statistical blinding scheme in which 3/4 of runs are blinded administratively
 491 (i.e. through file access) in cycles of 31 h of unblinded runs followed by 93 h of blinded runs. Unblinding data proceeds
 492 in a staged fashion, where first single-site events, not including any interesting physics regions are unblinded (i.e. no
 493 background ROI, $0\nu\beta\beta$ to the ground state ROI, low energy or multi-site data). This data is used for a variety of
 494 data validation checks prior to unblinding of any other data. The remaining data are separately unblinded after a
 495 collaboration review for individual analyses and users. For this analysis, the multi-site events have been left blinded.

496 In the open multi-site data, 5558 multi-detector events were observed. A histogram of the event multiplicities is
 497 shown in Figure 23, and a spectrum of all multiplicity 2 event energies is shown in Figure 24.

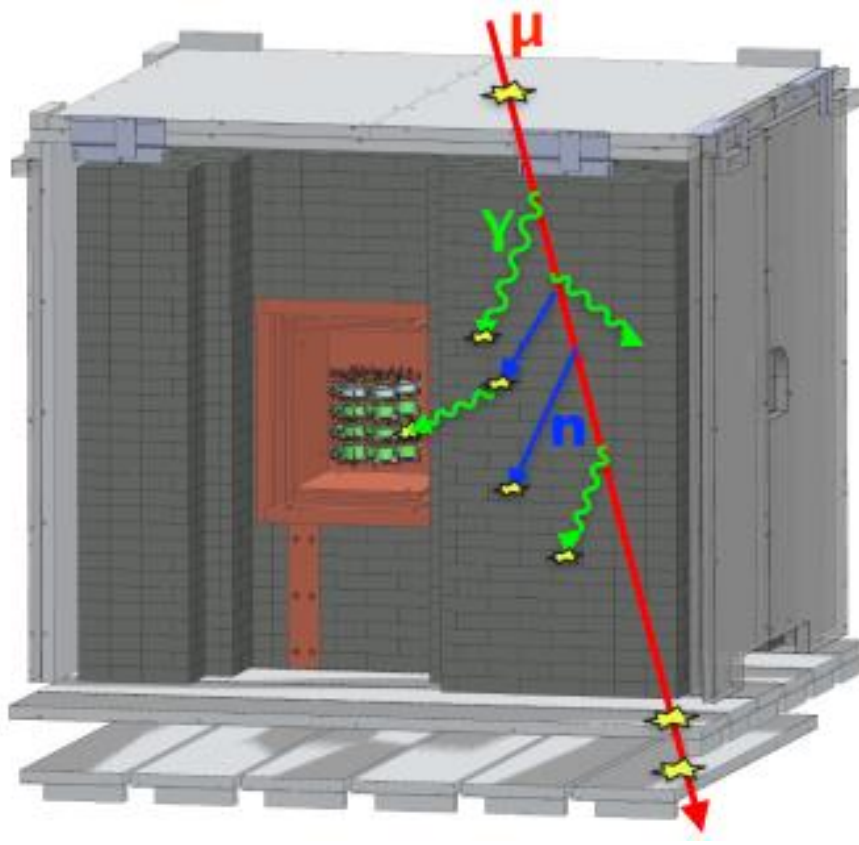


FIG. 20 A cartoon of a particle shower created by a muon event. The particles produced in such a shower can hit multiple detectors, producing multi-detector events.

500 XI. VALIDATION

501 In addition to the basic run selection and data cleaning validation checks that are run on all multiplicity 1 data,
 502 we perform some additional checks on high multiplicity data. As previously, this section will describe these checks
 503 applied to the $2\nu\beta\beta$ to the 0_1^+ state of ^{76}Se . Similar checks are performed on other decay modes in Appendix A.

504 A. Data Rate

505 Any spikes in the rate of multi-site events would potentially indicate problems with run selection or data cleaning.
 506 Significant variation in the data rate is expected due to changes in which detectors are active. For this reason,
 507 the rate of multi-site events with respect to the sensitive exposure, defined as the exposure times the detection
 508 efficiency of $\beta\beta$ E.S. events, is used instead. This quantity is interesting because the rate of observed $\beta\beta$ E.S. events
 509 should be constant with respect to it. The changes in detection efficiency from one subdataset to another for both
 510 backgrounds and $\beta\beta$ E.S. are highly correlated and driven by which detectors are enabled. For this reason, we can
 511 reasonably expect that the backgrounds should also have a nearly constant rate with respect to sensitive exposure,
 512 although differences between background source positions and the distribution of ^{76}Ge in the detectors imply that
 513 some differences should be expected. Figure 25 indeed shows a slow reduction in the overall background rate over
 514 time. One possible explanation for this is that a significant quantity of ^{68}Ge exists in natural HPGe detectors as a
 515 result of cosmogenic activation, and has a half-life of 271 days, which is observable on the timescale of the MAJORANA
 516 DEMONSTRATOR's operation. ^{68}Ga is a β^+ emitter which is a part of the ^{68}Ge decay chain, which produces two
 517 511 keV γ s and has a high probability of producing multi-detector events.

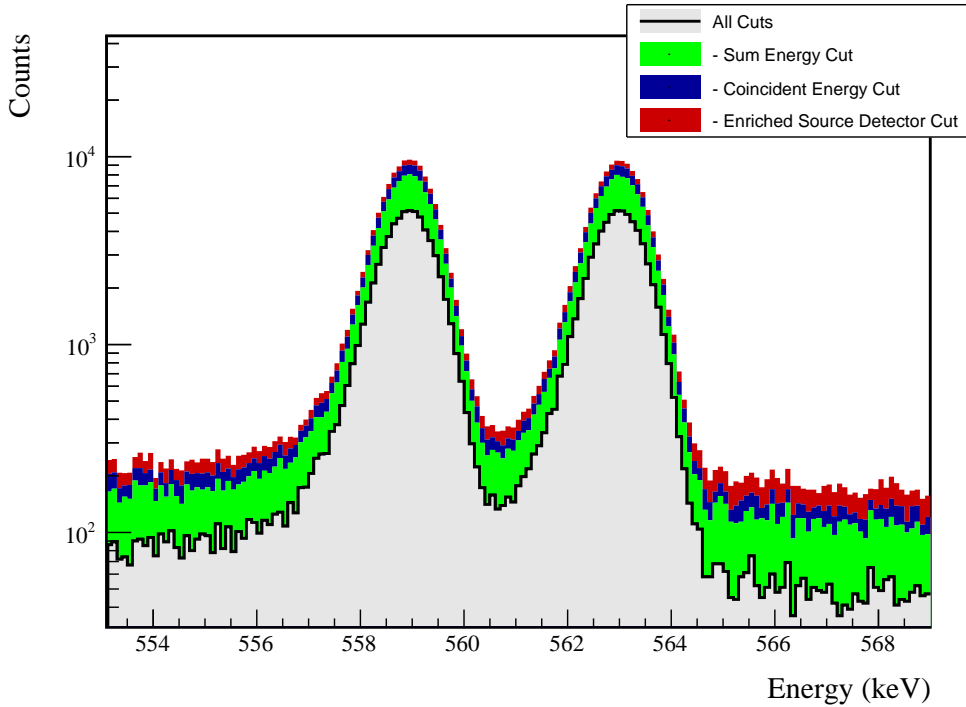


FIG. 21 The 559 and 563 keV peaks from the $2\nu\beta\beta$ decay to the 0_1^+ decay mode, with the effect of all cuts applied sequentially to simulated ES events. The cuts are applied from top to bottom (i.e. red, blue, then green). Many events will be cut by more than one of these; in that case it will be colored by whichever cut is applied first.

519 B. Background Cut Evaluation

520 A second important check to ensure that the cuts applied to each $\beta\beta$ E.S. mode is to compare each cut efficiency to
 521 the expected background cut efficiency. Since the background model used for this analysis uses preliminary results,
 522 disagreement between the expected and measured cut efficiencies could indicate a difference between the background
 523 model and the measured backgrounds rather than a problem with the application of cuts. However, any major
 524 discrepancies could indicate a bug in the analysis. To perform this comparison, the cut efficiencies are measured both
 525 in terms of the total number of events cut, ϵ_{total} and the number of events that are uniquely cut, ϵ_{unique} (i.e. not cut
 526 by any of the others). Table VI lists each cut for the $\beta\beta$ E.S. decay to the 0_1^+ state and the expected and measured
 527 cut efficiencies. The expected background cut efficiencies, $\langle \epsilon \rangle$ represent the fraction of simulated events cut, measured
 528 as an exposure-weighted average across all open datasets. The measured background cut efficiencies, $\hat{\epsilon}$ represent
 529 the measured fraction of events cut. Statistical uncertainties in the expected efficiencies are negligible compared to
 530 the uncertainties in the measured efficiencies, and are not included. The sacrifice is the number of events uniquely
 531 sacrificed by the cut. ΔDP is the expected improvement in discovery potential, defined in Appendix H, as a result
 532 of the cut. Figure 26 shows the effects of data cuts on multiplicity 2 events. Figure 27 shows the effects of cuts on
 533 events in the ROI in both measured and simulated data.

534 XII. RESULTS

535 A. Statistical Methods

536 Neyman confidence intervals are computed for each peak in each $\beta\beta$ E.S. decay mode, and each module. For a
 537 given peak k , the expected number of signal counts is

$$\langle s_k \rangle = \ln 2 \frac{N_A}{m_{76}} \epsilon_k \frac{M_{iso} T_{live}}{T_{1/2}} \quad (20)$$



Cut Name	Cut Description	$\langle \epsilon_{total} \rangle$	$\hat{\epsilon}_{total}$	$\langle \epsilon_{unique} \rangle$	$\hat{\epsilon}_{unique}$	Sacrifice	ΔDP
Enriched Source Detector Cut	Any other detector: <code>iStar</code>	M1: 23.2 % M2: 42.7 %	27.2 ^{+3.8} _{-3.5} % 62.8 ^{+7.0} _{-7.6} %	2.2 % 4.4 %	2.0 ^{+1.5} _{-0.9} % 4.7 ^{+4.4} _{-2.3} %	0.7 % 2.1 %	7%
Coincident Energy Cut	No other detector: <code>((energy<40.6) (energy>402.6 && energy<506.8 && energy>512.4) (energy>608.6 && energy<10.2) (energy>170.6 && energy>1176.) (energy>125.0) && isbn) ((energy<83.) (energy>228.2 && energy>350.6) (energy>75.2 && energy<16.8) (energy>566.6 && energy<113.4) (energy>737.4) && iStar)</code>	M1: 29.6 % M2: 37.5 %	33.3 ^{+4.0} _{-3.8} % 48.8 ± 7.5 %	4.4 % 4.2 %	4.8 ^{+2.1} _{-1.5} % 2.3 ^{+3.6} _{-1.4} %	3.9 % 3.5 %	7%
Sum Energy Cut	<code>Note: (sumE<870.) (sumE>870.6 && sumE<877.6) (sumE>878.6 && sumE<891.) (sumE>891.2 && sumE<113.6) (sumE>1065.8 && sumE<1072.6) (sumE>1170.8 && sumE<1174.6) (sumE>1330. && sumE>1335.6) (sumE>1484.2 && sumE<1461.6) (sumE>1761.8 && sumE<1765.6) (sumE>1794.4)</code>	M1: 75.0 % M2: 75.6 %	74.8 ^{+3.4} _{-3.7} % 74.4 ^{+6.0} _{-7.2} %	44.5 % 33.0 %	41.5 ^{+4.1} _{-4.0} % 25.6 ^{+7.2} _{-6.0} %	31.8 % 32.1 %	20%
Combined Cuts		M1: 84.5 % M2: 89.5 %	84.4 ^{+2.8} _{-3.2} % 95.3 ^{+2.3} _{-4.4} %	—	—	44.9 % 53.1 %	27%

TABLE VI Table of detection efficiencies and uncertainties for $2\nu\beta\beta$ of ^{76}Ge to the 0_1^+ state of ^{76}Se .

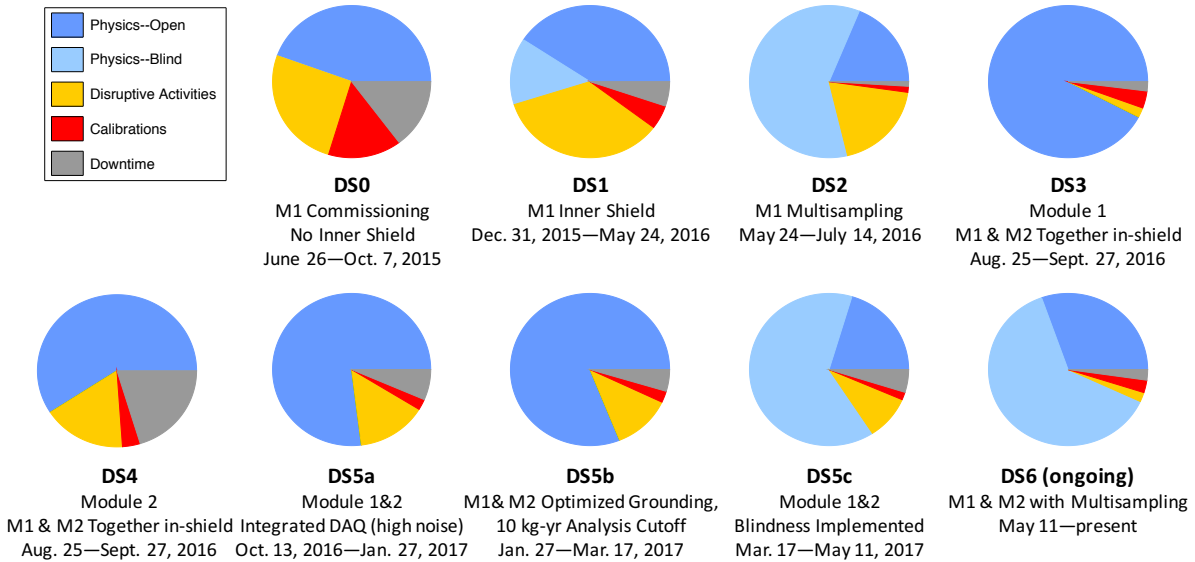


FIG. 22 The duty cycles for each major dataset used in this analysis, and a brief description of the major changes in configuration that define each data set.

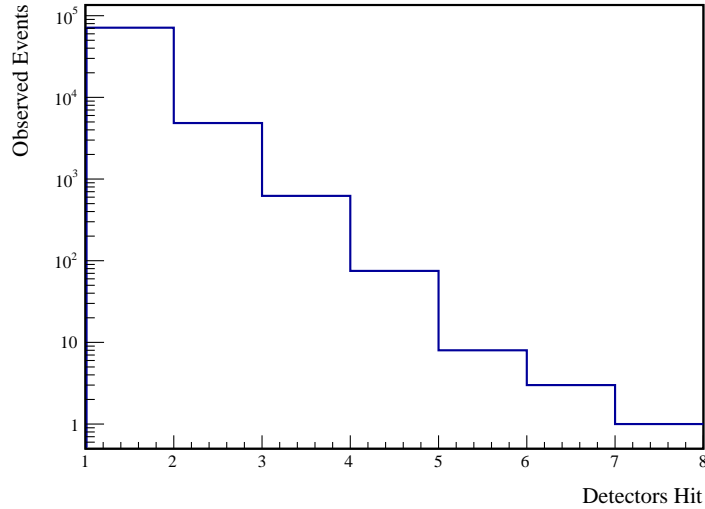


FIG. 23 The measured multiplicities for events in datasets 1-6a. For multiplicity 1 events, only events with energy between 40 keV and 4 MeV were considered.

where M_{iso} is the total isotopic mass and T_{live} is the livetime ($M_{iso}T_{live}$ is the exposure and is calculated in Section VI.A to be 13.356 ± 0.021 kg-y for module 1 and 7.872 ± 0.13 kg-y for module 2. ϵ_k is the total detection efficiency of the decay mode using peak k , which can be found in Appendix A. $m_{76} = 0.0759214$ kg is the molar mass of ^{76}Ge , and $N_A = 6.02214076 \times 10^{23}$ is Avagadro's number. Fun fact: an Avagadro's number of avocados has approximately the volume of Mars. We will define the single count half-life to be

$$T_k^* = \ln 2 \frac{N_A}{m_{76}} \epsilon_k M_{iso} T_{live} \quad (21)$$

which is the decay half-life that would produce on average one count in signal ROI k .

Because of the nearly background free nature of this search, a likelihood construction is used that assumes Poisson

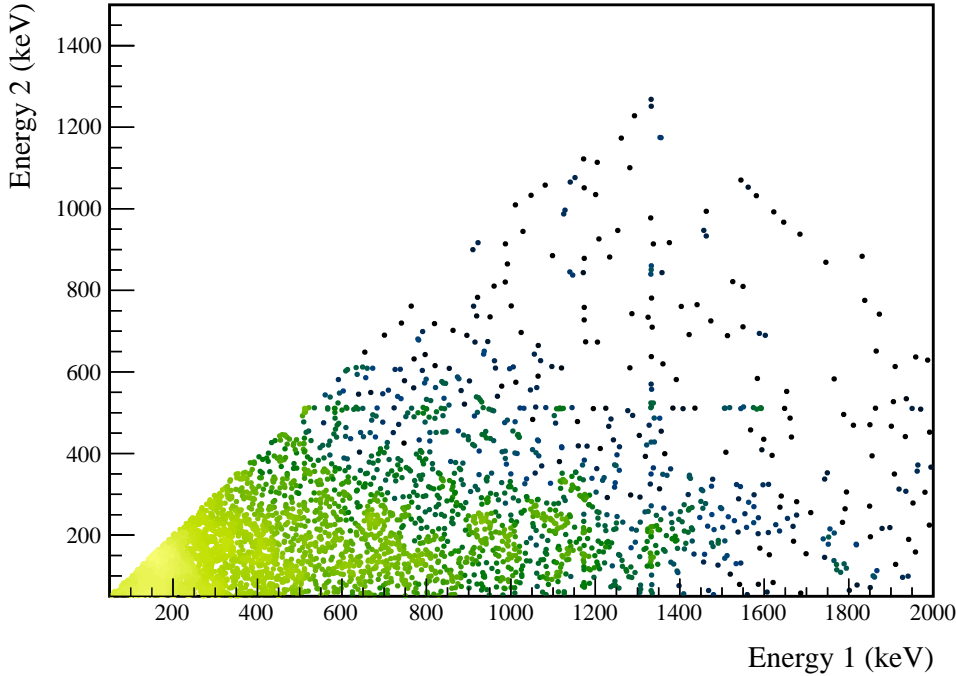
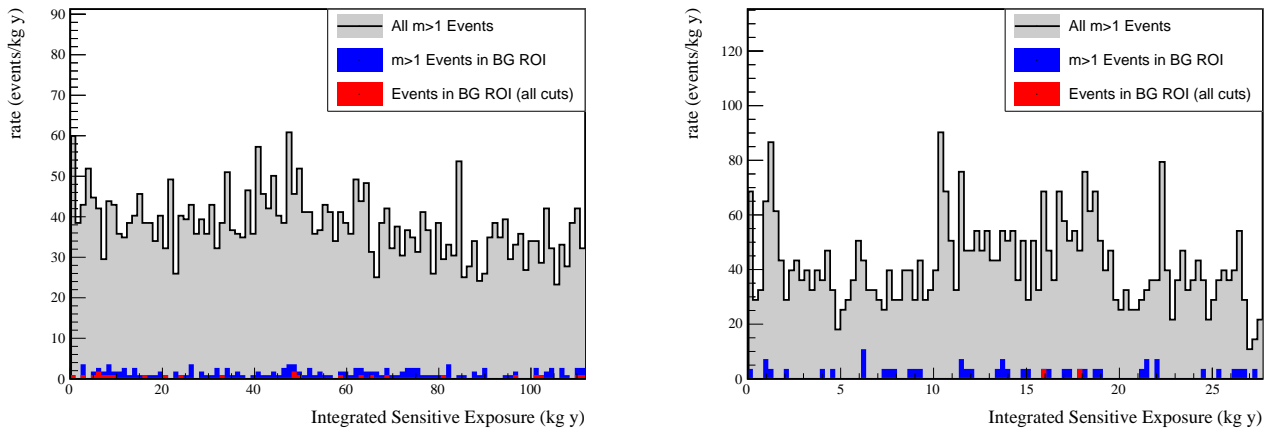


FIG. 24 Measured energy spectrum of open multiplicity 2 events in datasets 1-6a.

FIG. 25 Event rate with respect to sensitive exposure, or the detection efficiency of the $2\nu\beta\beta$ decay to the 0_1^+ excited state times the exposure. Integrated exposure is the total sensitive exposure prior to an event. The background rate is expected to be mostly flat, with differences discussed in Section XI.A.

⁵⁴⁵ statistics for the number of counts in the signal and background ROIs.

$$\begin{aligned} \mathcal{L}_k(T_{1/2}, T_k^*, b_k | n_k, m_k, \langle T_k^* \rangle, \sigma_{T^*,k}, \tau) &= \frac{\mu_k^{n_k} e^{-\mu_k}}{n_k!} \cdot \frac{(b_k \tau)^{m_k} e^{-b_k/\tau}}{m_k!} \cdot \frac{1}{\sigma_{T^*,k} \sqrt{2\pi}} e^{-\frac{(T_k^* - \langle T_k^* \rangle)^2}{2\sigma_{T^*,k}^2}} \\ \mu_k &= s_k + b_k = \frac{T_k^*}{T_{1/2}} + b_k \end{aligned} \quad (22)$$

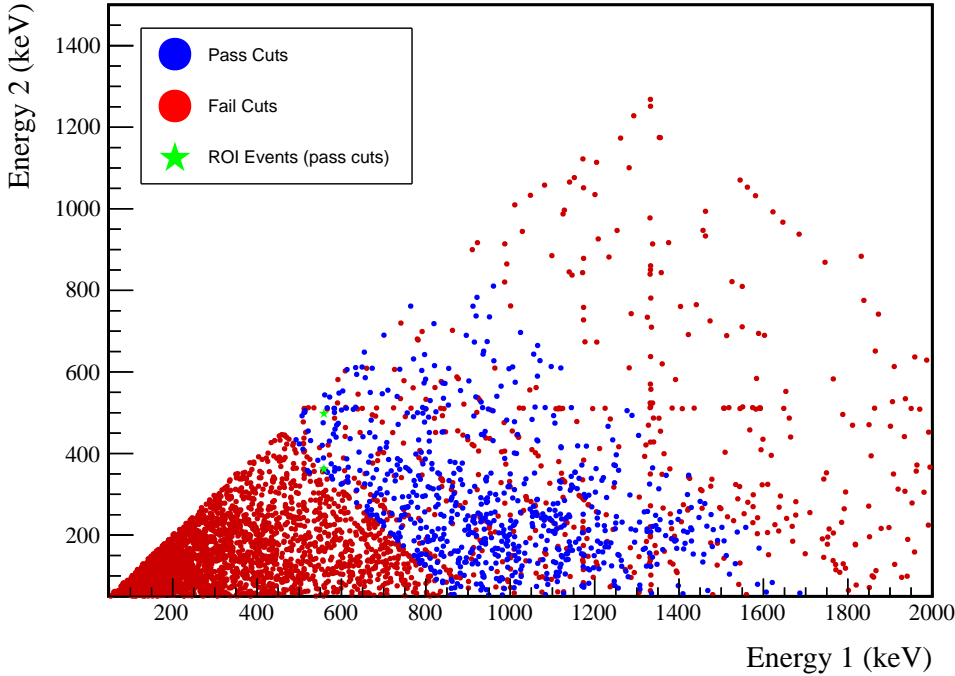


FIG. 26 Energy spectrum of multiplicity 2 events. Red events are events that are cut. For blue events, at least one of the hits passes all cuts; however, the other hit may fail. For green events, one of the hits must both pass all cuts and place the event in the BG or ES ROI. Note that the green events include any events of multiplicity > 1; for higher multiplicity events, instead of showing the energy in the second detector, the sum of the energy in all other detectors is shown.

546 $T_{1/2}$ represents the decay mode half-life and is the parameter of interest. T_k^* and b_k are nuisance parameters representing the measured single count halflife and expected backgrounds in the ES ROI, respectively. μ_k is the total
547 expected number of counts, combining background and signal, in the ES ROI. n_k is the measured number of events
549 in the ES ROI and is expected to be drawn from a Poisson distribution with mean μ_k . m_k is the measured number
550 of events in the BG ROI and is expected to be drawn from a Poisson distribution with mean b_k/τ , where τ is the
551 ratio between the number of expected background counts in the BG ROI to the number in the ES ROI. Note that
552 since these events are multi-detector events, it is possible for multiple hits in the event to fall into one of the ROIs;
553 however, we will choose a single hit to represent the whole event. In this case, any hit that falls into the ES ROI takes
554 precedence over any hit that falls into the BG ROI, and if multiple hits fall into the ES ROI, one is chosen at random.
555 This approach would produce a very small bump in an otherwise flat background at the ES ROI; this is accounted
556 for in the calculation of τ . τ is usually determined based on the background simulation; however, in cases where the
557 simulation statistics are limited after applying all cuts, a flat background is assumed and the ratio of the ES ROI
558 width to the BG ROI width is used. $\langle T_k^* \rangle$ represents the expected value of T_k^* based on previous measurements of
559 exposure and detection efficiency, which is assumed to have Gaussian uncertainty:

$$\sigma_{T^*,k} = \langle T_k^* \rangle \sqrt{\left(\frac{\sigma_{\epsilon,k}}{\epsilon_k}\right)^2 + \left(\frac{\sigma_{exposure}}{M_{iso}T_{live}}\right)^2} \quad (23)$$

560 The implementation of Equation 22 is performed by the **TRolke** class in ROOT [14]. This likelihood function is used
561 to compute a likelihood ratio

$$LR_k(T_{1/2}) = \frac{\sup_{T_k^*, b_k} (\mathcal{L}_k(T_{1/2}, T_k^*, b_k | n_k, m_k, \langle T_k^* \rangle, \sigma_{T^*,k}, \tau))}{\sup_{T_{1/2}, T_k^*, b_k} (\mathcal{L}_k(T_{1/2}, T_k^*, b_k | n_k, m_k, \langle T_k^* \rangle, \sigma_{T^*,k}, \tau))} \quad (24)$$

562 The **TRolke** class analytically computes the supremum over T_k^* and b_k , returning the log-likelihood difference. The
563 implementation is parameterized in terms of $\Gamma = \frac{1}{T_{1/2}}$, which is restricted to positive values; if the supremum of the

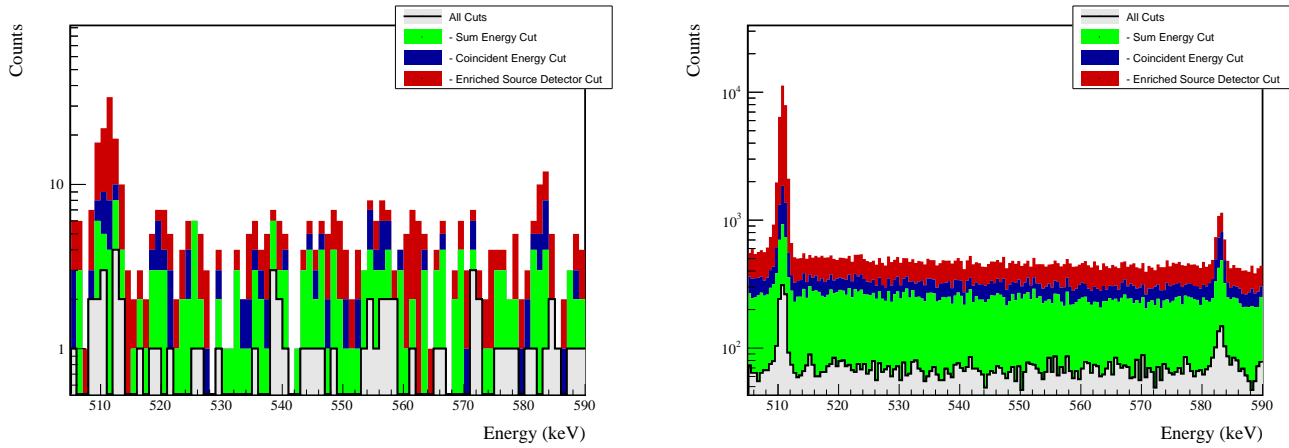


FIG. 27 Effect of cuts on all events in the BG and ES ROIs. Events are applied in sequence from top to bottom, meaning that if an event is cut by multiple cuts, it will be colored based on the first cut that applied. Both the simulated and measured event spectra are shown for comparison.

function has a negative value of Γ , then the value at $\Gamma = 0$ is used instead. Since the likelihood ratio is expected to be χ^2 -distributed, to construct a 90% confidence interval, we seek the values of $T_{1/2}$ corresponding to a log-likelihood ratio value of 2.7. In cases where the lower limit on γ is found to be < 0 , a lower limit on $T_{1/2}$ is reported.

After constructing confidence intervals for each peak and module individually, a combined confidence interval is constructed for each $\beta\beta$ E.S. decay mode. A combined log-likelihood over all peak/module combinations k is defined by

$$\log(\mathcal{L}(T_{1/2})) = \sum_{k=0}^N \sup_{T_k^*, b_k} (\log(\mathcal{L}_k(T_{1/2}, T_k^*, b_k | n_k, m_k, \langle T_k^* \rangle, \sigma_{T^*, k}, \tau))) \quad (25)$$

This construction relies on the fact that the T_k^* and b_k values across each peak can be independently maximized, enabling the continued use of the `TRolke` implementation. A combined likelihood ratio is constructed:

$$\log(\text{LR}(T_{1/2})) = \log(\mathcal{L}(T_{1/2})) - \sup_{T_{1/2}} (\log(\mathcal{L}(T_{1/2}))) \quad (26)$$

and used to compute a confidence interval as above. Table VII contains the limits constructed for each decay mode, peak and module. For all modes, a lower half-life limit is set.

Note that each decay mode is analyzed independently. The problem with this approach is that all decay modes have the 559 keV peak in common, meaning that the results will be correlated. For this result, since all modes only have a lower limit on half-life set, this approach is not problematic since for any individual mode, we would take the supremum over all other half-lives, which would be at or near infinity, resulting in the same sets of equations used here. However, if the $\beta\beta$ E.S. to the 0_1^+ mode is discovered, it will become necessary to perform a full combined analysis.

The detection sensitivity is computed by constructing a toy Monte Carlo for each decay mode, assuming that each $T_{1/2}$ is infinite. For each sample i , a random n_i and m_i is drawn from a Poisson distribution with mean b_k and m_k . The confidence interval for a measurement with these values is computed. The median sensitivity is extracted by taking the median lower half-life limit over all samples. For the results in Table VII, 100001 samples were used.

584 B. Limits and Sensitivities

585 The limits and sensitivities for each peak and module individually, and the combination for each mode, are shown
586 in Table VII. Figure 28 shows the event spectrum after all cuts have been applied with both ROIs highlighted.

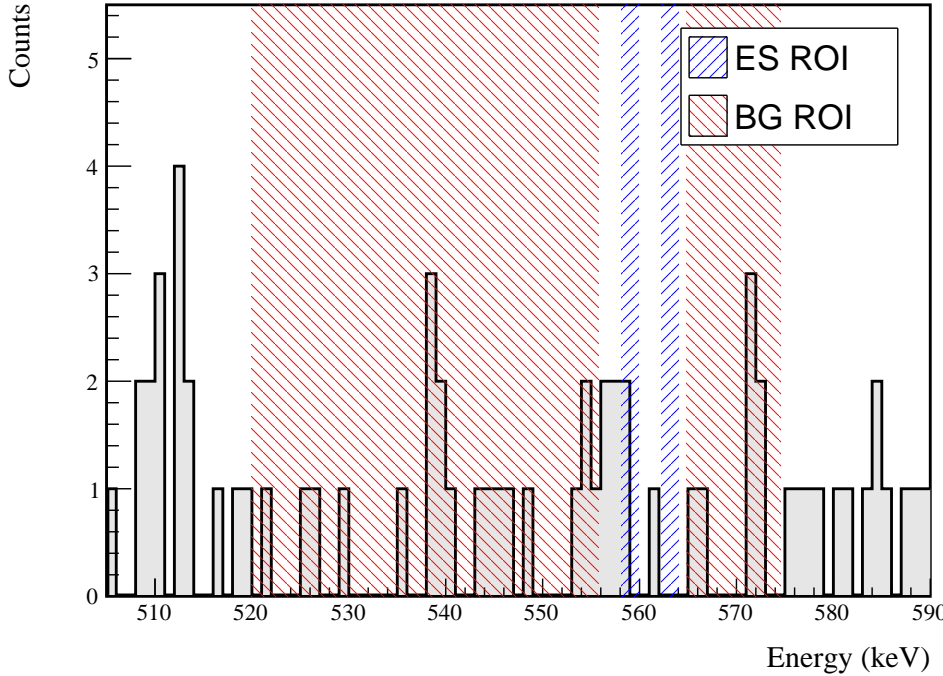


FIG. 28 Events that pass all cuts for the $2\nu\beta\beta$ to 0^+ decay mode. The ES and BG ROIs are highlighted. Note that these ROIs undergo small variations from dataset to dataset, and the ROIs drawn here are averaged over all datasets. The energies shown in this spectrum are the energies of the hit that places the event in the ROI. A single event will only be placed once into an ROI; however, as drawn here, if multiple hits in a single event fall into an ROI, they will all be drawn.

587 XIII. UNBLINDING PLAN

588 The result presented in this document uses only open data from DS1-6a. Data is blinded by administratively by
589 forbidding access to built and gatified files to users; access to blinded data is provided through skim files. Unblinding
590 proceeds in multiple stages; skim files produced in the first stage exclude high multiplicity events, events in the
591 400 keV ROI around $Q_{\beta\beta}$, and low energy events. Access to these events is provided individually to analyzers through
592 inclusion in skim files accessible only by that individual. For this analysis, high multiplicity events will be needed.

593 Prior to unblinding, several steps will be completed. First, subdatasets must be identified using `es_get_datasets`,
594 requiring access to channel selection files that are produced during the first stage of unblinding. Next, the live time
595 must be measured. Unfortunately, this requires access to detailed run information from built files, which are left
596 blinded; as a result, `es_livetime` must be run by someone with access to the mjd account. Next, background model
597 and excited state simulations for each subdataset will be produced using `es_skimsim`. Next, cut optimization must be
598 performed using `es_optimize_cuts`. Because an estimate of a scaling required to get the actual background level from
599 the simulations is required for this step, an estimate should be made using the already unblinded single-site events.
600 Finally, cuts should be applied with `es_apply_cuts`, and the efficiencies and exposures estimated using `es_get_result`
601 with the `--nodata` option. In addition to running this code, plots of the simulated data should be made, similar to
602 those displayed in Appendix A. Once this is completed, the plots and efficiencies should be inspected; any discrepancies
603 between the unblinded result and these blinded numbers should be understood prior to unblinding.

604 Once the analysis is approved for unblinding and skim files with high multiplicity data have been produced,
605 `es_skim_data` will be used to collect the high multiplicity events therein. `es_get_result` should be run using this
606 data. The sanity checks discussed in Sections XI.A and XI.B should be performed, and any discrepancies in the
607 data rate or cut efficiencies should be explained, and any changes to the analysis resulting from these checks must be
608 carefully documented. Finally, `es_get_limits` can be run to get the final limits.

609 Unblinding will approximately double the exposure to ~ 40 kg-y of isotopic exposure. Assuming identical back-
610 grounds and efficiencies, the projected half-life sensitivity for the search to the first 0^+ decay is $\sim 1 \cdot 10^{24}$ yr. It



Decay Mode	Peak	Module	n_{ROI}	m_{BG}	Expected ROI BGs	$T^* (\times 10^{23} \text{y})$	$T_{1/2} (\times 10^{23} \text{y})$ 90% Limit	$T_{1/2} (\times 10^{23} \text{y})$ 90% Sensitivity
$0_{g.s.}^+ \xrightarrow{2\nu\beta\beta} 0_1^+$	559 keV	M1	2	23	0.88	8.41 ± 0.60	> 1.9	> 3.2
		M2	0	2	0.09	2.10 ± 0.37	> 1.5	> 1.5
	563 keV	M1	0	23	0.97	8.42 ± 0.60	> 6.2	> 3.2
		M2	0	2	0.08	2.08 ± 0.37	> 1.5	> 1.5
	Combined						> 6.8	> 7.0
$0_{g.s.}^+ \xrightarrow{2\nu\beta\beta} 2_1^+$	559 keV	M1	0	16	0.68	10.43 ± 1.04	> 7.7	> 7.7
		M2	0	1	0.04	2.66 ± 0.88	> 1.8	> 1.8
	Combined						> 9.6	> 5.3
$0_{g.s.}^+ \xrightarrow{2\nu\beta\beta} 2_2^+$	559 keV	M1	2	38	1.46	7.24 ± 0.87	> 1.8	> 2.9
		M2	0	5	0.22	1.89 ± 0.85	> 1.2	> 1.2
	657 keV	M1	1	20	0.69	5.49 ± 0.70	> 1.8	> 4.0
		M2	0	3	0.10	1.50 ± 0.74	> 0.9	> 0.9
	1216 keV	M1	0	29	0.79	3.14 ± 0.84	> 2.2	> 1.1
		M2	0	4	0.14	0.77 ± 0.93	> 1.1	> 1.1
$0_{g.s.}^+ \xrightarrow{0\nu\beta\beta} 0_1^+$	559 keV	M1	0	2	0.09	11.47 ± 0.98	> 8.4	> 8.4
		M2	0	0	0.00	2.92 ± 0.56	> 2.1	> 2.1
	563 keV	M1	0	2	0.09	11.32 ± 0.96	> 8.3	> 8.3
		M2	0	0	0.00	2.86 ± 0.55	> 2.1	> 2.1
	Combined						> 21.1	> 21.1
$0_{g.s.}^+ \xrightarrow{0\nu\beta\beta} 2_1^+$	559 keV	M1	0	0	0.00	12.04 ± 1.31	> 8.8	> 8.8
		M2	0	0	0.00	3.01 ± 1.02	> 2.0	> 2.0
	Combined						> 11.0	> 11.0
$0_{g.s.}^+ \xrightarrow{0\nu\beta\beta} 2_2^+$	559 keV	M1	0	2	0.08	7.16 ± 0.95	> 5.2	> 5.2
		M2	0	0	0.00	1.81 ± 0.85	> 1.1	> 1.1
	657 keV	M1	0	7	0.27	7.00 ± 0.96	> 5.1	> 5.1
		M2	0	1	0.02	1.76 ± 0.90	> 1.0	> 1.0
	1216 keV	M1	0	0	0.00	3.23 ± 0.85	> 2.3	> 2.3
		M2	0	0	0.00	0.81 ± 0.95	> 0.2	> 0.2
	Combined						> 16.0	> 16.0

TABLE VII Results for all decay modes.

should be noted that rerunning the cut optimization with a more exposure will result in a slightly more stringent set of cuts; as a result, the background rate and detection efficiency will both be lower. The cutoff at the end of DS6a is motivated by the fact that this encompasses all data in the MAJORANA DEMONSTRATOR 2018 $0\nu\beta\beta$ release, and has been extensively vetted. In concert with the next major $0\nu\beta\beta$ release, containing DS6b and 6c data, this analysis will add the additional exposure as well.

REFERENCES

- [1] J. Kotila and F. Iachello. Phase-space factors for double- β decay. *Phys. Rev. C*, 85:034316, Mar 2012.
- [2] O. A. Ponkratenko, V. I. Tretyak, and Yu. G. Zdesenko. Event generator decay4 for simulating double-beta processes and decays of radioactive nuclei. *Physics of Atomic Nuclei*, 63(7):1282–1287, Jul 2000.
- [3] Balraj Singh. Nuclear data sheets update for $A = 76$. *Nuclear Data Sheets*, 74(1):63 – 164, 1995.
- [4] Robley D. Evans. *The Atomic Nucleus*, chapter 6, page 240. International series in pure and applied physics. McGraw-Hill, New York, 1955.
- [5] Micah Buuck. *A Comprehensive Radiogenic Background Model for the MAJORANA DEMONSTRATOR*. PhD thesis, University of Washington, 2019.
- [6] Pavol Vojtyla. Fast computer simulations of background of low-level Ge γ -spectrometers induced by ${}^{210}\text{Pb}$ ${}^{210}\text{Bi}$ in shielding lead. *Nuclear Instruments and Methods in Physics Research Section B: Beam Interactions with Materials and Atoms*, 117(1):189 – 198, 1996.
- [7] I. Antcheva, M. Ballintijn, B. Bellenot, M. Biskup, R. Brun, N. Buncic, Ph. Canal, D. Casadei, O. Couet, V. Fine, L. Franco, G. Ganis, A. Gheata, D. Gonzalez Maline, M. Goto, J. Iwaszkiewicz, A. Kreshuk, D. Marcos Segura, R. Maunder, L. Moneta, A. Naumann, E. Offermann, V. Onuchin, S. Panacek, F. Rademakers, P. Russo, and M. Tadel. Root — a c++ framework for petabyte data storage, statistical analysis and visualization. *Computer Physics Communications*, 180(12):2499 – 2512, 2009. 40 YEARS OF CPC: A celebratory issue focused on quality software for high performance, grid and novel computing architectures.
- [8] A Reine, T Caldwell, C Cuesta, I Guinn, and J Myslik. Run selection and data cleaning of ds5 (m1 and m2) (internal). Technical Report 2017-020, University of North Carolina at Chapel Hill, May 2018.
- [9] F. James. MINUIT Function Minimization and Error Analysis: Reference Manual Version 94.1. Technical Report CERN-D506, CERN CN Division, Geneva, 1994.
- [10] P. Chu, J. Detwiler, and I. Guinn. Energy systematic of MAJORANA DEMONSTRATOR. Technical Report 2017-021, Los Alamos National Laboratory, Oct 2017.
- [11] R.P. Brent. *Algorithms for Minimization without Derivatives*. Prentice-Hall, Englewood Cliffs, NJ, 1973.



- [641] [12] H. Akaike. A new look at the statistical model identification. *IEEE Transactions on Automatic Control*, 19(6):716–723,
[642] December 1974.
- [643] [13] C Wiseman. Muon veto analysis for the MAJORANA DEMONSTRATOR (internal). Technical report, University of South
[644] Carolina, 2016.
- [645] [14] Wolfgang A. Rolke, Angel M. López, and Jan Conrad. Limits and confidence intervals in the presence of nuisance
[646] parameters. *Nuclear Instruments and Methods in Physics Research Section A: Accelerators, Spectrometers, Detectors
[647] and Associated Equipment*, 551(2):493 – 503, 2005.
- [648] [15] F. Alessandria, R. Ardito, D. R. Artusa, III Avignone, F. T., O. Azzolini, M. Balata, T. I. Banks, G. Bari, J. Beeman,
[649] F. Bellini, A. Bersani, M. Biassoni, T. Bloxham, C. Brofferio, C. Bucci, X. Z. Cai, L. Canonica, X. Cao, S. Capelli,
[650] L. Carbone, L. Cardani, M. Carrettoni, N. Casali, D. Chiesa, N. Chott, M. Clemenza, C. Cosmelli, O. Cremonesi, R. J.
[651] Creswick, I. Dafinei, A. Dally, V. Datskov, A. De Biasi, M. M. Deninno, S. Di Domizio, M. L. di Vacri, L. Ejzak, R. Faccini,
[652] D. Q. Fang, H. A. Farach, M. Faverzani, G. Fernandes, E. Ferri, F. Ferroni, E. Fiorini, M. A. Franceschi, S. J. Freedman,
[653] B. K. Fujikawa, A. Giachero, L. Gironi, A. Giuliani, J. Goett, P. Gorla, C. Gotti, E. Guardincerri, T. D. Gutierrez, E. E.
[654] Haller, K. Han, K. M. Heeger, H. Z. Huang, R. Kadel, K. Kazkaz, G. Keppel, L. Kogler, Yu. G. Kolomensky, D. Lenz,
[655] Y. L. Li, C. Ligi, X. Liu, Y. G. Ma, C. Maiano, M. Maino, M. Martinez, R. H. Maruyama, Y. Mei, N. Moggi, S. Morganti,
[656] T. Napolitano, S. Newman, S. Nisi, C. Nones, E. B. Norman, A. Nucciotti, T. O'Donnell, F. Orio, D. Orlandi, J. L.
[657] Ouellet, M. Pallavicini, V. Palmieri, L. Pattavina, M. Pavan, M. Pedretti, G. Pessina, G. Piperno, S. Pirro, E. Previtali,
[658] V. Rampazzo, F. Rimondi, C. Rosenfeld, C. Rusconi, E. Sala, S. Sangiorgio, N. D. Scielzo, M. Sisti, A. R. Smith,
[659] F. Stivanello, L. Taffarello, M. Tencioni, W. D. Tian, C. Tomei, S. Trentalange, G. Ventura, M. Vignati, B. S. Wang, H. W.
[660] Wang, T. Wise, A. Woodcraft, L. Zanotti, C. Zarra, B. X. Zhu, and S. Zucchelli. Sensitivity and Discovery Potential of
[661] CUORE to Neutrinoless Double-Beta Decay. *arXiv e-prints*, page arXiv:1109.0494, Sep 2011.

[662] **Appendix A: Detailed Results for All Decay Modes**

[663] The main document concerned itself primarily with the $2\nu\beta\beta$ of ^{76}Ge to the 0_1^+ excited state. However, results
[664] are presented for all decay modes and energy peaks. This appendix will present figures and tables detailing the
[665] simulations, cuts, efficiencies and results for each decay mode and peak.

[666] **Appendix B: $2\nu\beta\beta$ to 0_1^+**

[667] Note that both the 559 and 563 keV peaks will be shown together since they use the same sets of cuts.

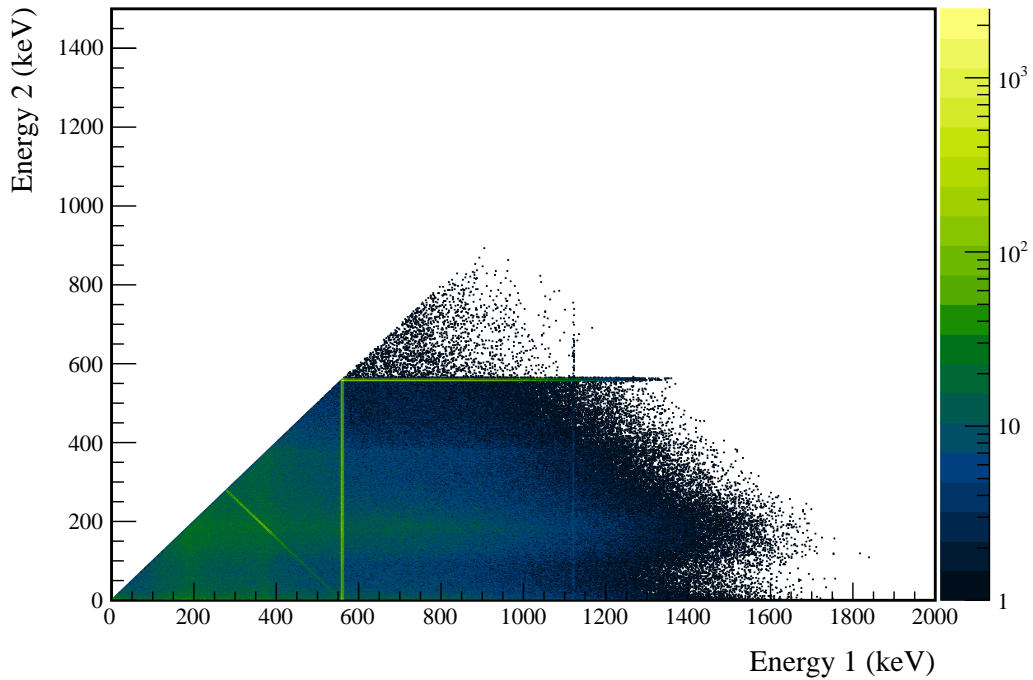
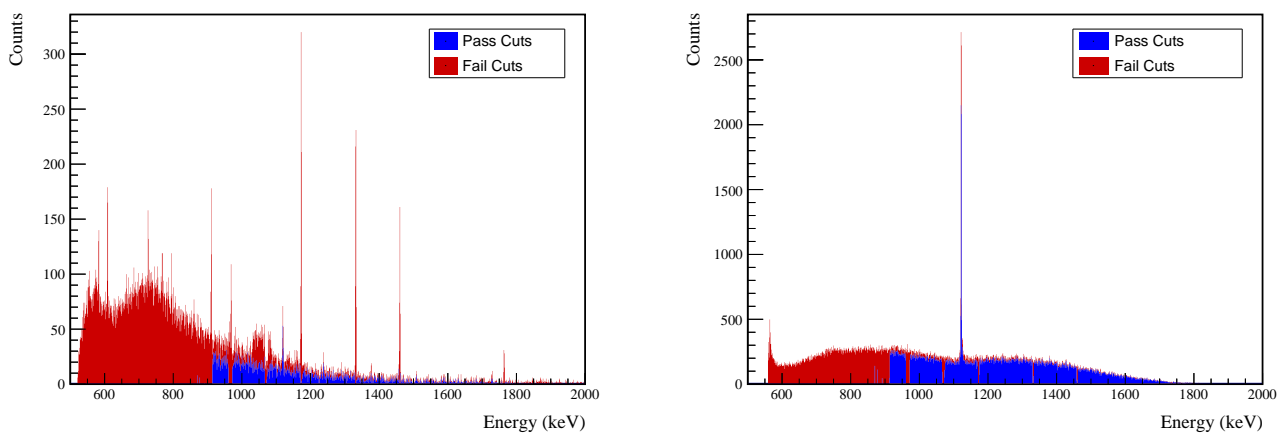
FIG. 29 Simulated multiplicity 2 energy spectrum of the $2\nu\beta\beta$ to 0_1^+ decay mode

FIG. 30 Effect of 559 and 563 keV peaks cuts on sum energy spectra in BG (left) and ES (right) simulations.



TABLE VIII Table of energy estimation uncertainties for the 559 and 563 keV peaks.

DS	E_{peak} (keV)	σ_{fit} (keV)	σ_{drift} (keV)	σ (keV)	$f_{t,fit}$ (keV)	$f_{t,fit}$ (keV)	τ_{fit} (keV)	$\delta_{\mu,fit}$ (keV)	$\delta_{\mu,NL}$ (keV)	$\delta_{\mu,drift}$ (keV)	$\delta_{\mu,peak}$ (keV)	δ_u (keV)	FWHM (keV)	$\delta_{fwhm,drift}$ (keV)	$\delta_{fwhm,fit}$ (keV)	$\delta_{fwhm,xtalk}$ (keV)	δ_{FWHM} (keV)	δ_α	$E_{ROI,1}$ (keV)	$E_{ROI,2}$ (keV)	ϵ_{ROI}	$\sigma_{\epsilon_{ROI}}$
DS1	559.101	0.460	0.063	0.464	0.230	0.515	0.001	0.104	0.002	0.012	0.005	0.105	1.152	0.001	0.039	0.011	0.040	0.035	558.199	559.847	0.871	0.015
DS2	559.101	0.461	0.055	0.464	0.249	0.515	0.002	0.067	0.004	0.012	0.005	0.068	1.158	0.001	0.107	0.011	0.108	0.093	558.186	559.845	0.874	0.031
DS3	559.101	0.470	0.066	0.474	0.224	0.505	0.001	0.026	0.024	0.012	0.005	0.038	1.174	0.001	0.073	0.011	0.074	0.063	558.187	559.863	0.879	0.021
DS4	559.101	0.455	0.077	0.461	0.108	0.445	0.002	0.076	0.010	0.012	0.005	0.078	1.111	0.001	0.106	0.011	0.107	0.096	558.283	559.856	0.888	0.032
DS5a	559.101	0.560	0.085	0.567	0.106	0.855	0.002	0.079	0.005	0.012	0.005	0.080	1.367	0.002	0.055	0.011	0.056	0.041	558.098	560.022	0.875	0.014
DS5b	559.101	0.469	0.074	0.475	0.158	0.491	0.001	0.020	0.011	0.012	0.005	0.026	1.157	0.001	0.125	0.011	0.125	0.108	558.229	559.872	0.885	0.036
DS5c	559.101	0.460	0.085	0.468	0.174	0.489	0.001	0.037	0.030	0.012	0.005	0.050	1.145	0.001	0.162	0.011	0.162	0.142	558.231	559.860	0.883	0.046
DS6a	559.101	0.456	0.044	0.458	0.191	0.463	0.001	0.069	0.025	0.012	0.005	0.075	1.123	0.000	0.041	0.011	0.042	0.038	558.241	559.841	0.881	0.014
DS1	563.178	0.461	0.064	0.466	0.230	0.518	0.001	0.104	0.002	0.012	0.005	0.105	1.156	0.001	0.039	0.011	0.040	0.035	562.273	563.927	0.871	0.015
DS2	563.178	0.463	0.055	0.466	0.249	0.517	0.002	0.067	0.004	0.012	0.005	0.068	1.162	0.001	0.107	0.011	0.108	0.093	562.259	563.924	0.874	0.030
DS3	563.178	0.471	0.066	0.476	0.224	0.508	0.001	0.026	0.024	0.012	0.005	0.038	1.179	0.001	0.073	0.011	0.074	0.063	562.261	563.943	0.879	0.021
DS4	563.178	0.457	0.077	0.463	0.108	0.447	0.002	0.076	0.010	0.012	0.005	0.078	1.115	0.001	0.106	0.011	0.107	0.096	562.357	563.935	0.888	0.032
DS5a	563.178	0.562	0.086	0.569	0.106	0.858	0.002	0.079	0.006	0.012	0.005	0.080	1.372	0.002	0.055	0.011	0.056	0.041	562.172	564.103	0.875	0.014
DS5b	563.178	0.471	0.074	0.477	0.158	0.494	0.001	0.020	0.011	0.012	0.005	0.026	1.162	0.001	0.125	0.011	0.125	0.108	562.303	563.952	0.885	0.035
DS5c	563.178	0.462	0.086	0.470	0.174	0.492	0.001	0.037	0.030	0.012	0.005	0.050	1.449	0.001	0.162	0.011	0.162	0.141	562.305	563.939	0.883	0.046
DS6a	563.178	0.457	0.044	0.459	0.191	0.465	0.001	0.069	0.026	0.012	0.005	0.075	1.127	0.000	0.041	0.011	0.042	0.038	562.315	563.921	0.881	0.013



Cut Name	Cut Description	$\langle \epsilon_{total} \rangle$	$\hat{\epsilon}_{total}$	$\langle \epsilon_{unique} \rangle$	$\hat{\epsilon}_{unique}$	Sacrifice	ΔDP
Enriched Source Detector Cut	Any other detector: isBar	M1: 23.2 % M2: 42.7 %	27.2 ^{+3.8} _{-3.5} % 62.8 ^{+7.0} _{-7.6} %	2.2 % 4.4 %	2.0 ^{+1.5} _{-0.9} % 4.7 ^{+4.4} _{-2.3} %	0.7 % 2.1 %	7%
Coincident Energy Cut	No other detector: ((energy<40.6) (energy>402.6 && energy>409.6) (energy>2506.8 && energy<512.4) (energy>2608. && energy<610.2) (energy>170.6 && energy<1175.) (energy>1235.) && isBar) ((energy<83.) (energy>228.2 && energy<356.6) (energy>75.2 && energy<516.8) (energy>866.6 && energy<13.4) (energy>737.4) && (energy<613.4) (energy>870.6 && energy<613.4)) Note: (sumE<870.) (sumE>870.6 && sumE<877.6) (sumE>878. && sumE<891.) (sumE>891.2 && sumE<913.8) (sumE>960.8 && sumE<972.) (sumE>1066.8 && sumE<1072.6) (sumE>1170.8 && sumE<1174.6) (sumE>1330.8 && sumE<1333.6) (sumE>1458.2 && sumE<1461.6) (sumE>1751.8 && sumE<1765.6) (sumE>1794.4)	M1: 29.6 % M2: 37.5 %	33.3 ^{+4.0} _{-3.8} % 48.8 ^{+7.5} _{-7.5} %	4.4 % 4.2 %	4.8 ^{+2.1} _{-1.5} % 2.3 ^{+3.6} _{-1.4} %	3.9 % 3.5 %	7%
Sum Energy Cut		M1: 75.0 % M2: 75.6 %	74.8 ^{+3.4} _{-3.7} % 74.4 ^{+3.0} _{-7.2} %	44.5 % 33.0 %	41.5 ^{+4.1} _{-4.0} % 25.6 ^{+7.2} _{-6.0} %	31.8 % 32.1 %	20%
Combined Cuts		M1: 84.5 % M2: 89.5 %	84.4 ^{+2.8} _{-3.2} % 95.3 ^{+2.3} _{-4.4} %	— —	44.9 % 53.1 %	27%	

TABLE IX Table of cut descriptions and efficiencies for simulated backgrounds and measured data for the 559 and 563 keV peaks.

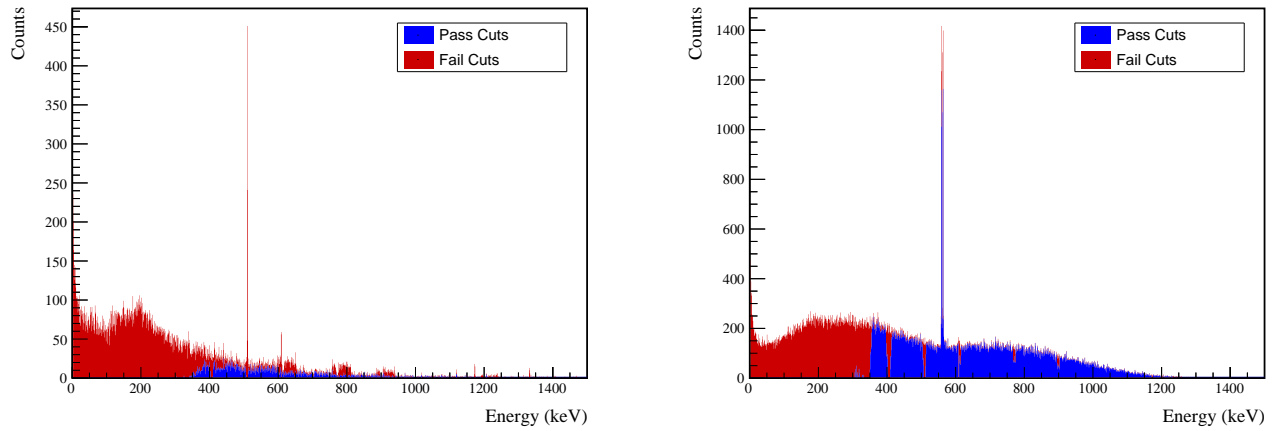


FIG. 31 Effect of 559 and 563 keV peaks cuts on coincident energy spectra in BG (left) and ES (right) simulations.

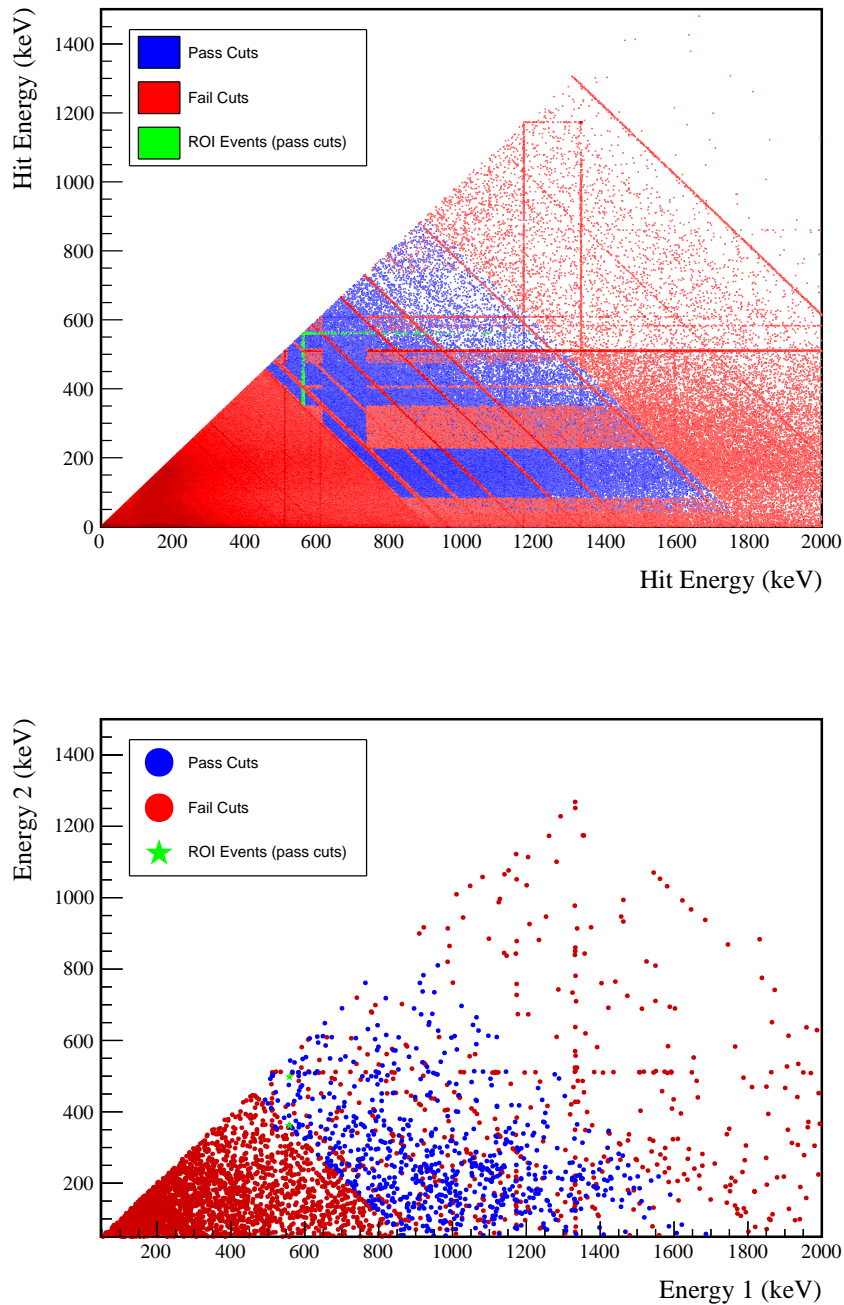
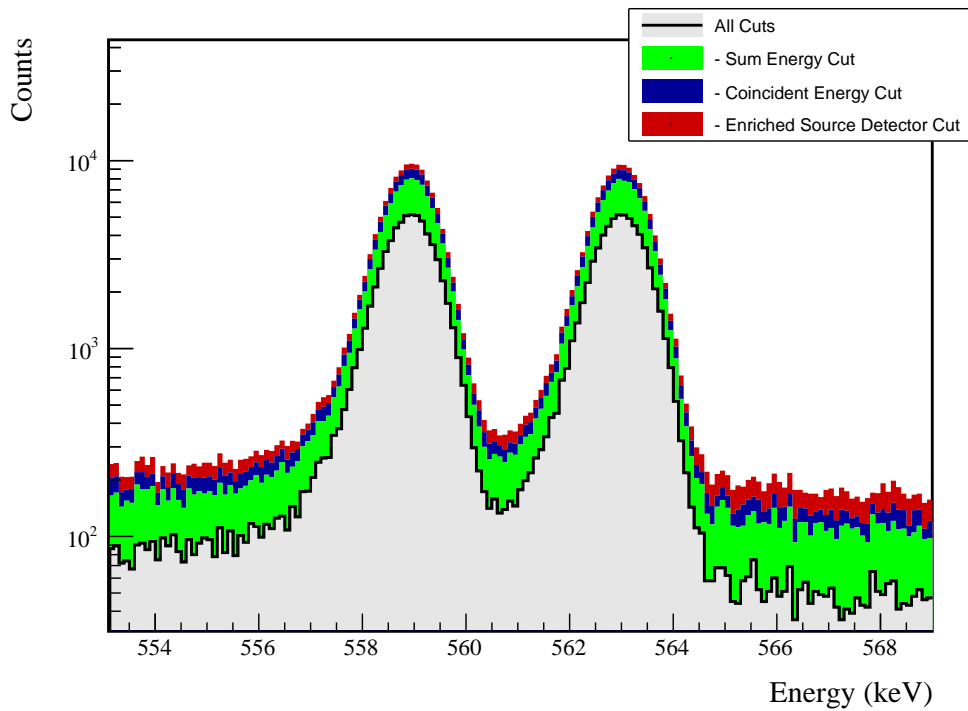


FIG. 32 Simulated (left) and measured (right) multiplicity 2 energy spectrum with sum and coincident energy cuts included for the 559 and 563 keV peaks.

FIG. 33 Effect of all cuts applied sequentially on ROI for 559 and 563 keV peaks of $2\nu\beta\beta$ to 0_1^+

Source	Module 1 efficiency	Module 2 efficiency
Multi-Detector with Full Energy γ	$5.9 \pm 0.2\%$	$3.2 \pm 0.5\%$
Region of Interest	$87.9 \pm 1.4\%$	$87.9 \pm 1.4\%$
Dead Layer	$74.5 \pm 4.3\%$	$65.7 \pm 6.0\%$
Detector Dead Times	$97.5 \pm 1.2\%$	$98.1 \pm 0.9\%$
Enriched Source Detector Cut	$96.8 \pm <0.1\%$	$89.4 \pm <0.1\%$
Coincident Energy Cut	$88.5 \pm 0.5\%$	$84.4 \pm 0.5\%$
Sum Energy Cut	$60.2 \pm 0.5\%$	$54.0 \pm 0.5\%$
Final Efficiency	$2.29 \pm 0.16\%$	$0.97 \pm 0.17\%$

FIG. 34 Table of detection efficiencies for the 559 and 563 keV peaks.

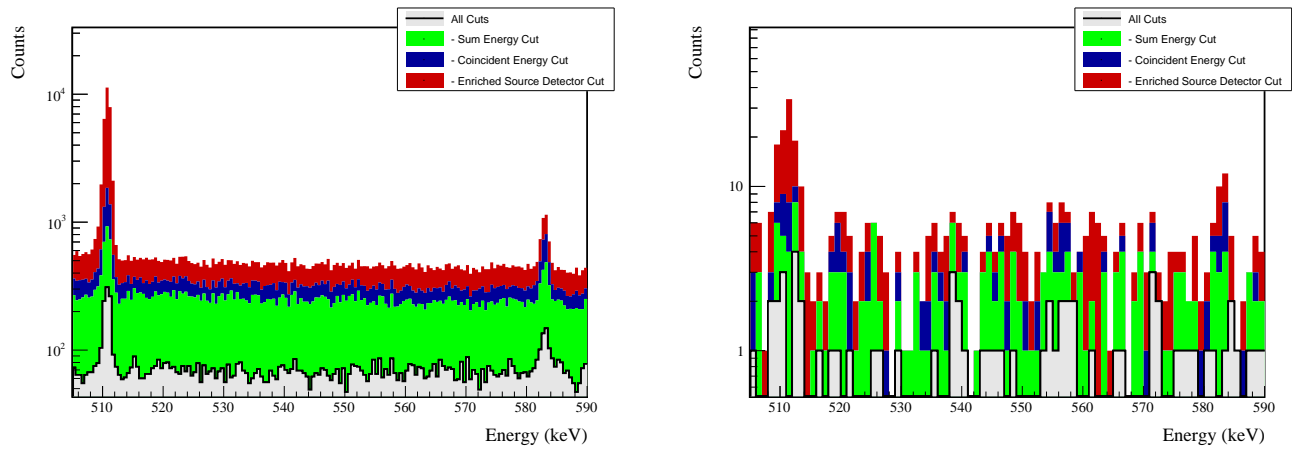
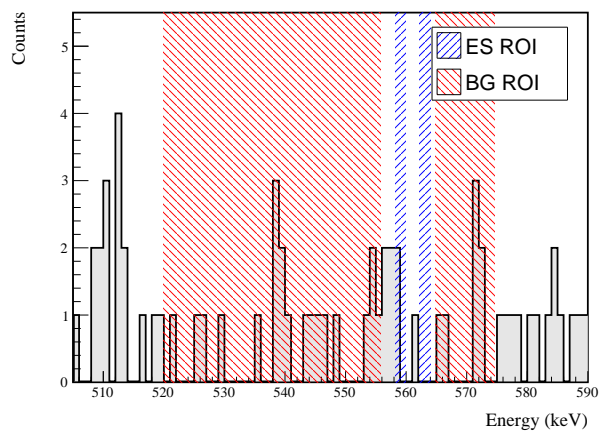


FIG. 35 Effect of all cuts applied to sequentially simulated (left) and measured (right) background data.

FIG. 36 All events after cuts in background (red) and signal (blue) ROIs for 559 and 563 keV peaks of $2\nu\beta\beta$ to 0_1^+

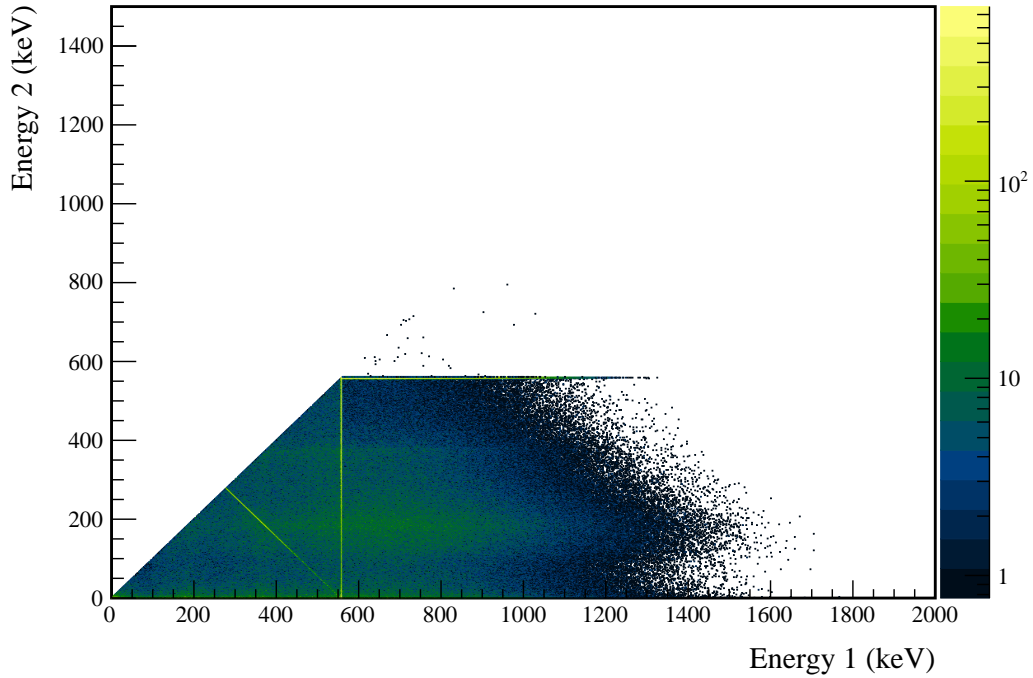
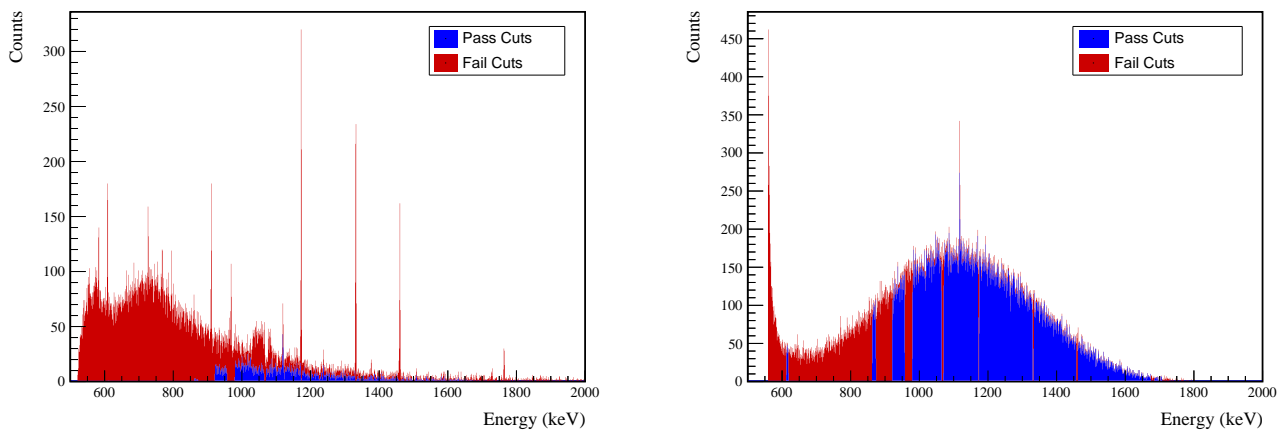
669 **Appendix C: $2\nu\beta\beta$ to 2_1^+** FIG. 37 Simulated multiplicity 2 energy spectrum of the $2\nu\beta\beta$ to 2_1^+ decay mode

FIG. 38 Effect of 559 keV peak cuts on sum energy spectra in BG (left) and ES (right) simulations.



TABLE X Table of energy estimation uncertainties for the 559 keV peak.

DS	E_{peak} (keV)	σ_{drift} (keV)	σ_{fit} (keV)	$f_{t,fit}$ (keV)	σ (keV)	$\tau_{f,fit}$ (keV)	$\delta_{\mu,fit}$ (keV)	$\delta_{\mu,NL}$ (keV)	$\delta_{\mu,drift}$ (keV)	$\delta_{\mu,ztalk}$ (keV)	$\delta_{\mu,peak}$ (keV)	δ_u (keV)	FWHM	$\delta_{fwhm,fit}$ (keV)	$\delta_{fwhm,drift}$ (keV)	$\delta_{fwhm,ztalk}$ (keV)	$\delta_{fwhm,HM}$ (keV)	δ_α	$E_{ROI,1}$ (keV)	$E_{ROI,2}$ (keV)	ϵ_{ROI}	$\sigma_{e_{ROI}}$
DS1	559.101	0.460	0.063	0.464	0.230	0.515	0.001	0.104	0.002	0.012	0.005	0.105	1.152	0.001	0.039	0.011	0.040	0.035	558.183	559.860	0.877	0.015
DS2	559.101	0.461	0.055	0.464	0.249	0.515	0.002	0.067	0.004	0.012	0.005	0.068	1.158	0.001	0.107	0.011	0.108	0.093	558.169	559.858	0.880	0.030
DS3	559.101	0.470	0.066	0.474	0.224	0.505	0.001	0.026	0.024	0.012	0.005	0.038	1.174	0.001	0.073	0.011	0.074	0.063	558.170	559.876	0.885	0.020
DS4	559.101	0.455	0.077	0.461	0.108	0.445	0.002	0.076	0.010	0.012	0.005	0.078	1.111	0.001	0.106	0.011	0.107	0.096	558.269	559.869	0.893	0.031
DS5a	559.101	0.560	0.085	0.567	0.106	0.885	0.002	0.079	0.005	0.012	0.005	0.080	1.367	0.002	0.055	0.011	0.056	0.041	558.081	560.038	0.881	0.014
DS5b	559.101	0.469	0.074	0.475	0.158	0.491	0.001	0.020	0.011	0.012	0.005	0.026	1.157	0.001	0.125	0.011	0.125	0.108	558.214	559.886	0.891	0.035
DS5c	559.101	0.460	0.085	0.468	0.174	0.489	0.001	0.037	0.030	0.012	0.005	0.050	1.145	0.001	0.162	0.011	0.162	0.142	558.216	559.873	0.888	0.045
DS6a	559.101	0.456	0.044	0.458	0.191	0.463	0.001	0.069	0.025	0.012	0.005	0.075	1.123	0.000	0.041	0.011	0.042	0.038	558.226	559.854	0.886	0.013



Cut Name	Cut Description	$\langle \epsilon_{total} \rangle$	$\hat{\epsilon}_{total}$	$\langle \epsilon_{unique} \rangle$	$\hat{\epsilon}_{unique}$	Sacrifice	ΔDP
Enriched Source		M1: 23.2 %	26.5 ^{+3.8} _{-3.5} %	4.5 %	4.1 ^{+2.0} _{-1.3} %	1.7 %	18%
Detector Cut	Any other detector: isEarr	M2: 42.7 %	62.8 ^{+7.0} _{-7.6} %	8.7 %	11.6 ^{+5.8} _{-4.9} %	4.1 %	
Multiplicity 2 Cut	m==2	M1: 15.4 %	16.3 ^{+3.3} _{-2.8} %	0.7 %	0.0 ^{+0.7} _{-0.0} %	0.0 %	2%
Coincident Energy Cut	No other detector: ((energy<53.8) (energy>59.4 && energy<93.8) (energy>144.4 && energy<362.4) (energy>398.6 && energy<421.) (energy>506.2 && energy<512.2) (energy>1116.4 && energy<1124.2) (energy>1147.8)) && isEarr (energy>1124.2 && energy<1124.2) (energy>1147.8)) && isEarr)	M1: 59.2 %	55.8 ± 4.1 %	3.8 %	4.8 ^{+2.1} _{-1.5} %	0.3 %	12%
	Note: (sumE<612.8) (sumE>862.6) (sumE>873.4 && sumE<862.6) (sumE>1064.8 && sumE<1064.8) (sumE>1330. && sumE<1330) (sumE>1675.2 && sumE<1675.2) (sumE>1706.4) (sumE>1706.4) (sumE>1462.4) (sumE>1462.4) (sumE>1684.8) (sumE>1684.8)	M2: 44.9 %	30.2 ^{+7.4} _{-6.5} %	3.5 %	0.0 ^{+2.3} _{-0.0} %	0.3 %	
Sum Energy Cut		M1: 74.9 %	74.8 ^{+3.4} _{-3.7} %	6.3 %	5.4 ^{+2.2} _{-1.6} %	1.2 %	17%
Combined Cuts		M2: 75.6 %	76.7 ^{+2.8} _{-7.0} %	4.3 %	2.3 ^{+3.6} _{-1.4} %	1.2 %	
		M1: 89.9 %	89.1 ^{+2.3} _{-2.8} %	—	—	30.9 %	79%
		M2: 93.0 %	97.7 ^{+1.4} _{-3.6} %	—	—	34.0 %	

TABLE XI Table of cut descriptions and efficiencies for simulated backgrounds and measured data for the 559 keV peak.

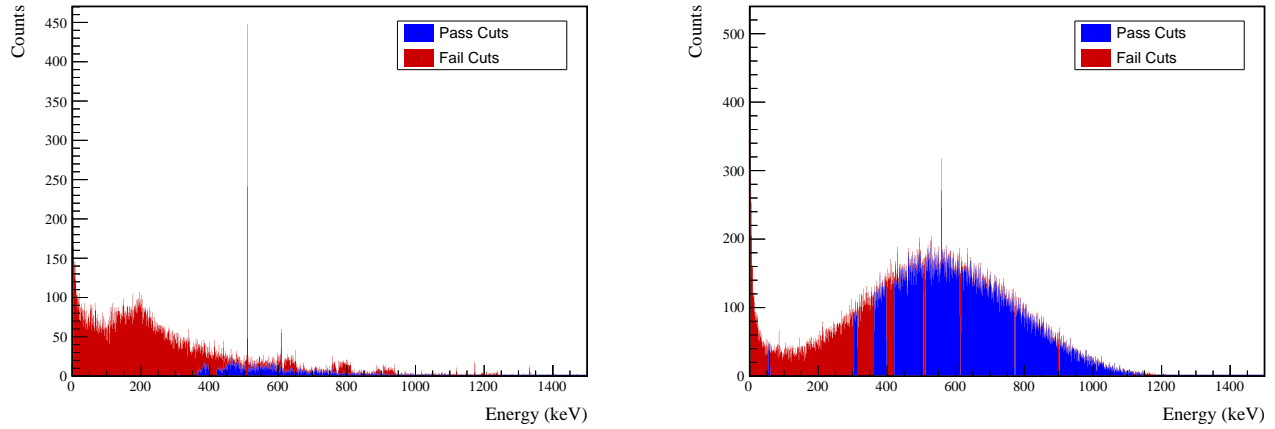


FIG. 39 Effect of 559 keV peak cuts on coincident energy spectra in BG (left) and ES (right) simulations.

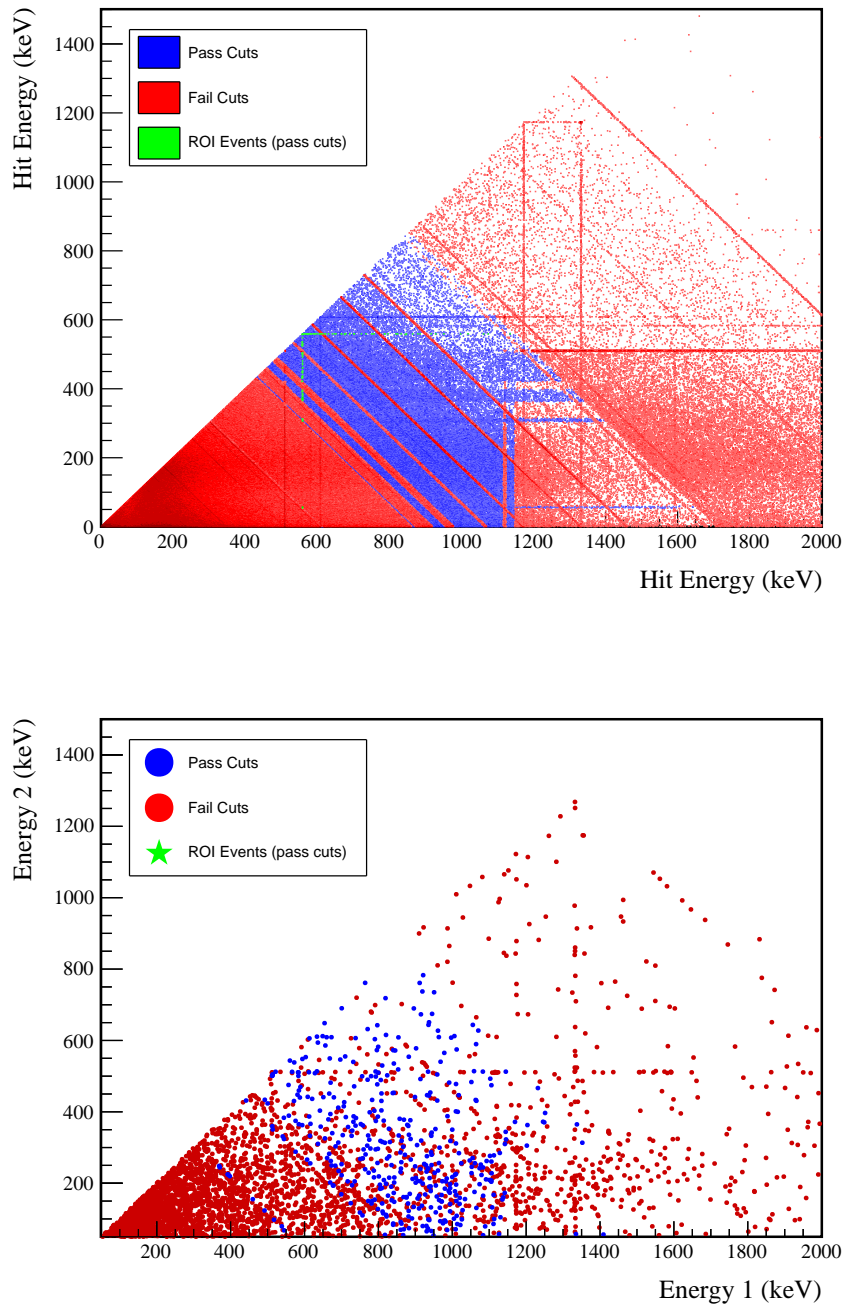
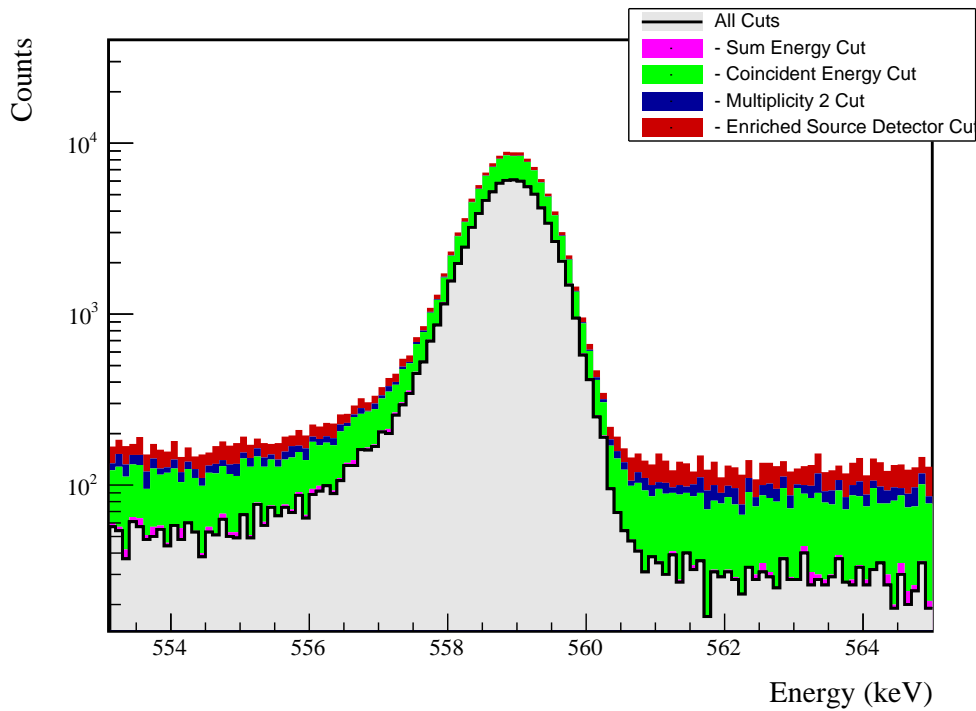


FIG. 40 Simulated (left) and measured (right) multiplicity 2 energy spectrum with sum and coincident energy cuts included for the 559 keV peak.

FIG. 41 Effect of all cuts applied sequentially on ROI for 559 keV peak of $2\nu\beta\beta$ to 2_1^+

Source	Module 1 efficiency	Module 2 efficiency
Multi-Detector with Full Energy γ	$3.0 \pm 0.2\%$	$1.5 \pm 0.5\%$
Region of Interest	$88.4 \pm 2.0\%$	$88.4 \pm 2.0\%$
Dead Layer	$71.4 \pm 4.9\%$	$62.8 \pm 6.5\%$
Detector Dead Times	$97.5 \pm 1.2\%$	$98.0 \pm 0.9\%$
Enriched Source Detector Cut	$97.3 \pm < 0.1\%$	$93.2 \pm < 0.1\%$
Multiplicity 2 Cut	$99.5 \pm < 0.1\%$	$99.7 \pm < 0.1\%$
Coincident Energy Cut	$73.1 \pm 0.5\%$	$74.0 \pm 0.5\%$
Sum Energy Cut	$71.4 \pm 0.5\%$	$70.5 \pm 0.5\%$
Final Efficiency	$1.42 \pm 0.14\%$	$0.61 \pm 0.20\%$

FIG. 42 Table of detection efficiencies for the 559 keV peak.

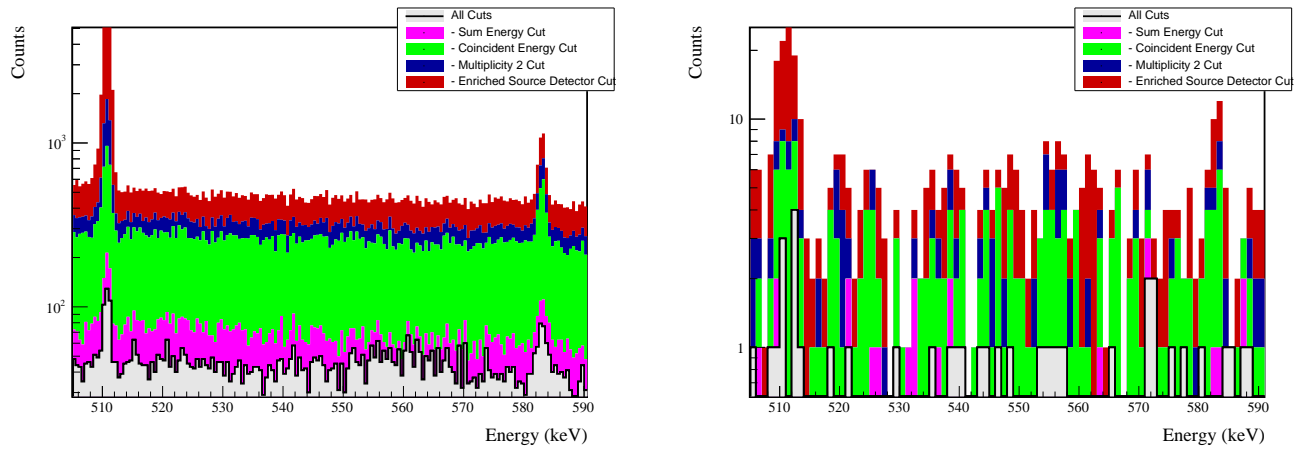
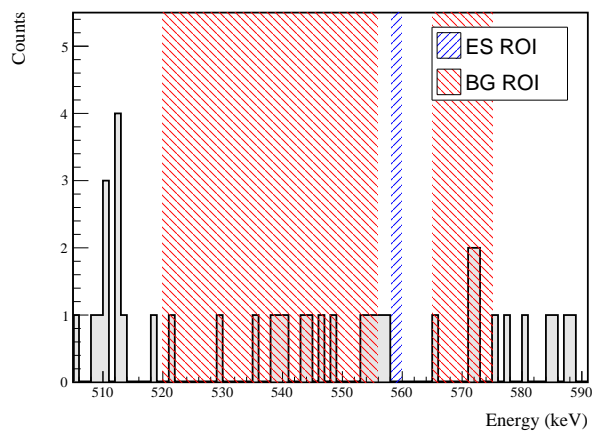


FIG. 43 Effect of all cuts applied to sequentially simulated (left) and measured (right) background data.

FIG. 44 All events after cuts in background (red) and signal (blue) ROIs for 559 keV peak of $2\nu\beta\beta$ to 2_1^+

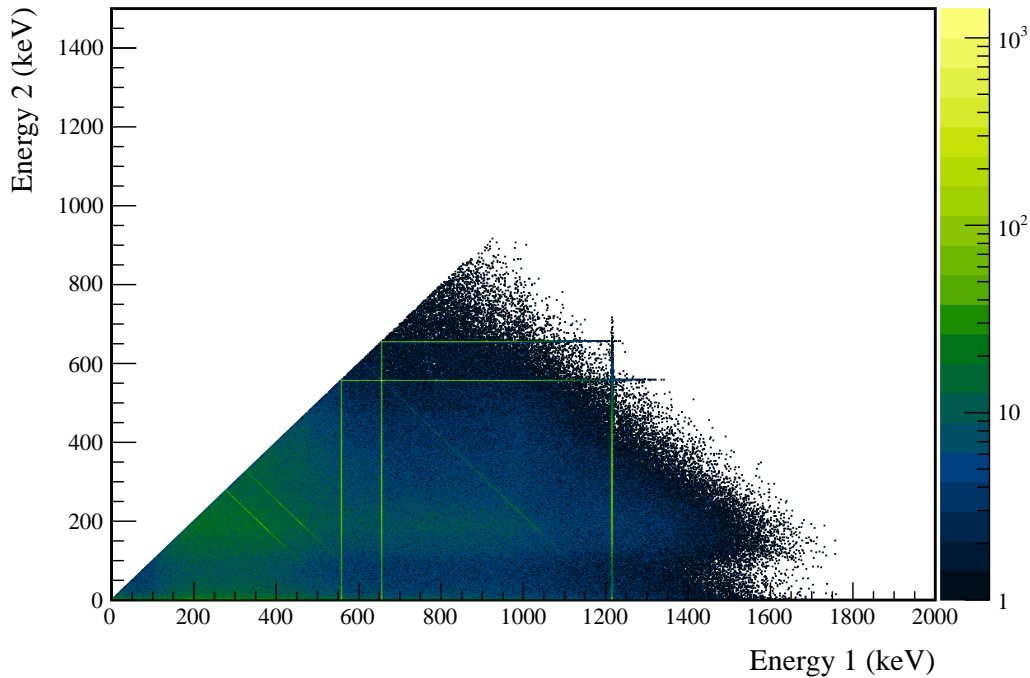
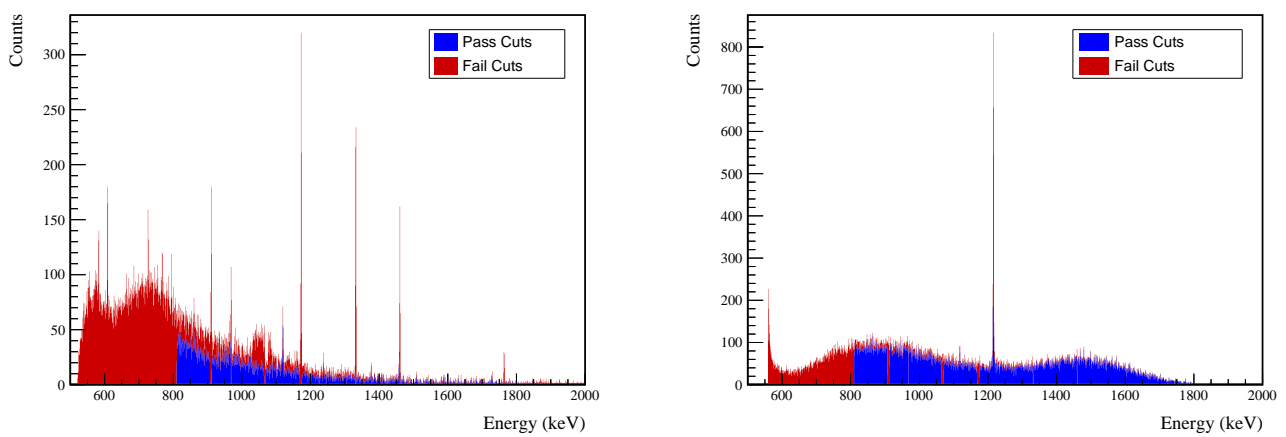
670 **Appendix D: $2\nu\beta\beta$ to 2_2^+** FIG. 45 Simulated multiplicity 2 energy spectrum of the $2\nu\beta\beta$ to 2_2^+ decay mode671 **1. 559 keV peak**

FIG. 46 Effect of 559 keV peak cuts on sum energy spectra in BG (left) and ES (right) simulations.



TABLE XII Table of energy estimation uncertainties for the 559 keV peak.

DS	E_{peak} (keV)	σ_{drift} (keV)	σ_{fit} (keV)	$f_{t,fit}$	σ (keV)	$\tau_{f,fit}$ (keV)	$\delta_{\mu,fit}$ (keV)	$\delta_{\mu,NL}$ (keV)	$\delta_{\mu,drift}$ (keV)	$\delta_{\mu,atalk}$ (keV)	$\delta_{\mu,peak}$ (keV)	δ_u (keV)	FWHM	$\delta_{fwhm,fit}$ (keV)	$\delta_{fwhm,drift}$ (keV)	$\delta_{fwhm,atalk}$ (keV)	$\delta_{fwhm,HM}$ (keV)	δ_α	$E_{ROI,1}$ (keV)	$E_{ROI,2}$ (keV)	ϵ_{ROI}	$\sigma_{e_{ROI}}$
DS1	559.101	0.460	0.063	0.464	0.230	0.515	0.001	0.104	0.002	0.012	0.005	0.105	1.152	0.001	0.039	0.011	0.040	0.035	558.218	559.832	0.864	0.016
DS2	559.101	0.461	0.055	0.464	0.249	0.515	0.002	0.067	0.004	0.012	0.005	0.068	1.158	0.001	0.107	0.011	0.108	0.093	558.206	559.830	0.867	0.032
DS3	559.101	0.470	0.066	0.474	0.224	0.505	0.001	0.026	0.024	0.012	0.005	0.038	1.174	0.001	0.073	0.011	0.074	0.063	558.206	559.847	0.872	0.021
DS4	559.101	0.455	0.077	0.461	0.108	0.445	0.002	0.076	0.010	0.012	0.005	0.078	1.111	0.001	0.106	0.011	0.107	0.096	558.299	559.841	0.881	0.033
DS5a	559.101	0.560	0.085	0.567	0.106	0.885	0.002	0.079	0.005	0.012	0.005	0.080	1.367	0.002	0.055	0.011	0.056	0.041	558.119	560.004	0.868	0.015
DS5b	559.101	0.469	0.074	0.475	0.158	0.491	0.001	0.020	0.011	0.012	0.005	0.026	1.157	0.001	0.125	0.011	0.125	0.108	558.247	559.857	0.878	0.037
DS5c	559.101	0.460	0.085	0.468	0.174	0.489	0.001	0.037	0.030	0.012	0.005	0.050	1.145	0.001	0.162	0.011	0.162	0.142	558.249	559.844	0.876	0.048
DS6a	559.101	0.456	0.044	0.458	0.191	0.463	0.001	0.069	0.025	0.012	0.005	0.075	1.123	0.000	0.041	0.011	0.042	0.038	558.259	559.826	0.874	0.014



Cut Name	Cut Description	$\langle \epsilon_{total} \rangle$	$\hat{\epsilon}_{total}$	$\langle \epsilon_{unique} \rangle$	$\hat{\epsilon}_{unique}$	Sacrifice	ΔDP
Enriched Source Detector Cut	Any other detector: isBar	M1: 23.2 %	26.5 ^{+3.8} _{-3.5} %	6.1 %	6.1 ^{+2.3} _{-1.7} %	1.7 %	1.7 %
Coincident Energy Cut	No other detector: (((energy<41.) (energy>349.6 && energy<352.8) (energy>306.8 && energy<312.2) (energy>305.4 && energy<312.6) (energy>307.4) && isBar) ((energy<42.) (energy>325.8) && isBar (energy>307.8 && energy<314.2) (energy>350.2 && energy<355.8) (energy>307.8 && energy<314.2) (energy>350.2 && 1.8bar)) Note: ((sumE<310.2) (sumE>307.2 && sumE<312.4) (sumE>368. && sumE<369.2) (sumE>1064.8 && sumE<1070.) (sumE>1168.6 && sumE<1174.6) (sumE>1330.4 && sumE<1333.4) (sumE>1455.4 && sumE<1461.8) (sumE>1761.8 && sumE<1766.)) (sumE>1906.)	M1: 42.7 %	62.8 ^{+7.0} _{-7.6} %	11.8 %	18.6 ^{+6.6} _{-5.2} %	5.2 %	10%
Sum Energy Cut		M1: 28.8 %	34.0 ^{+4.0} _{-3.8} %	5.3 %	5.4 ^{+2.2} _{-1.6} %	4.7 %	3%
Combined Cuts		M1: 35.6 %	48.8 ^{+7.5} _{-7.5} %	5.0 %	7.0 ^{+3.0} _{-3.0} %	4.3 %	
		M2: 35.6 %	48.8 ^{+7.5} _{-7.5} %	5.0 %	7.0 ^{+3.0} _{-3.0} %	4.3 %	
		M1: 61.1 %	59.9 ^{+4.1} _{-4.0} %	34.7 %	31.3 ^{+3.9} _{-3.7} %	16.3 %	
		M2: 61.8 %	53.5 ^{+7.4} _{-7.6} %	25.8 %	16.3 ^{+6.4} _{-4.9} %	16.8 %	18%
		M1: 74.4 %	74.1 ^{+3.4} _{-3.8} %	—	28.6 %	37.3 %	30%
		M2: 82.2 %	88.4 ^{+4.0} _{-5.8} %	—	—	—	

TABLE XIII Table of cut descriptions and efficiencies for simulated backgrounds and measured data for the 559 keV peak.

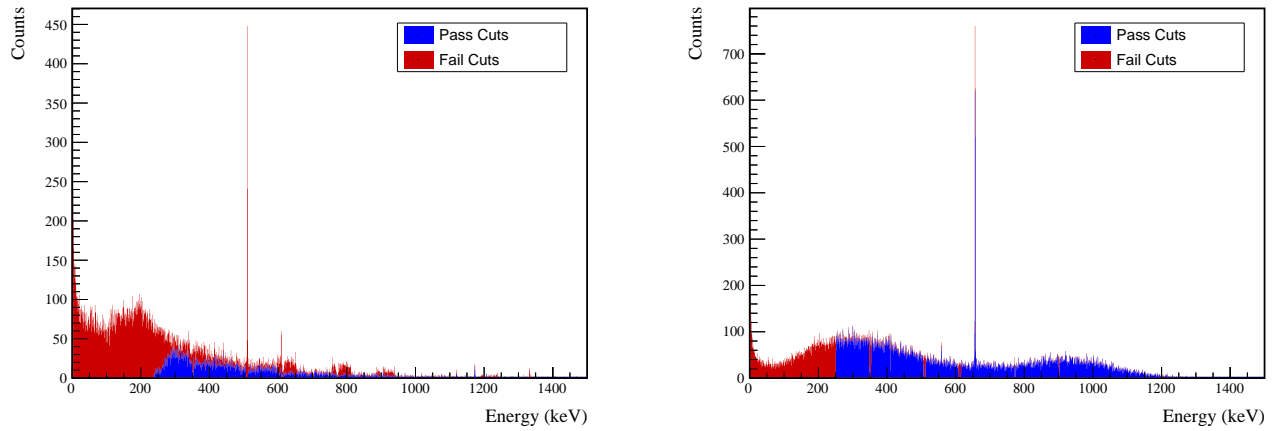


FIG. 47 Effect of 559 keV peak cuts on coincident energy spectra in BG (left) and ES (right) simulations.

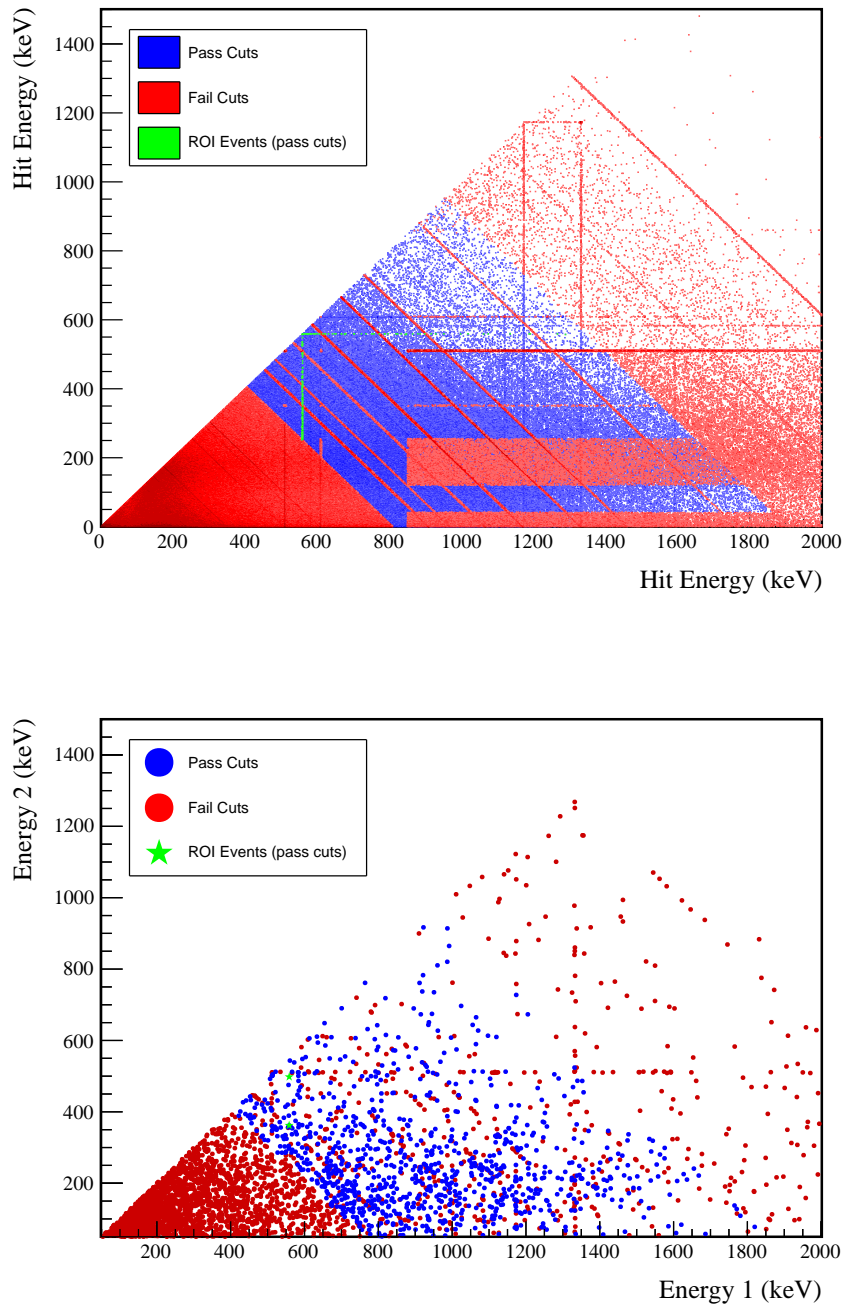
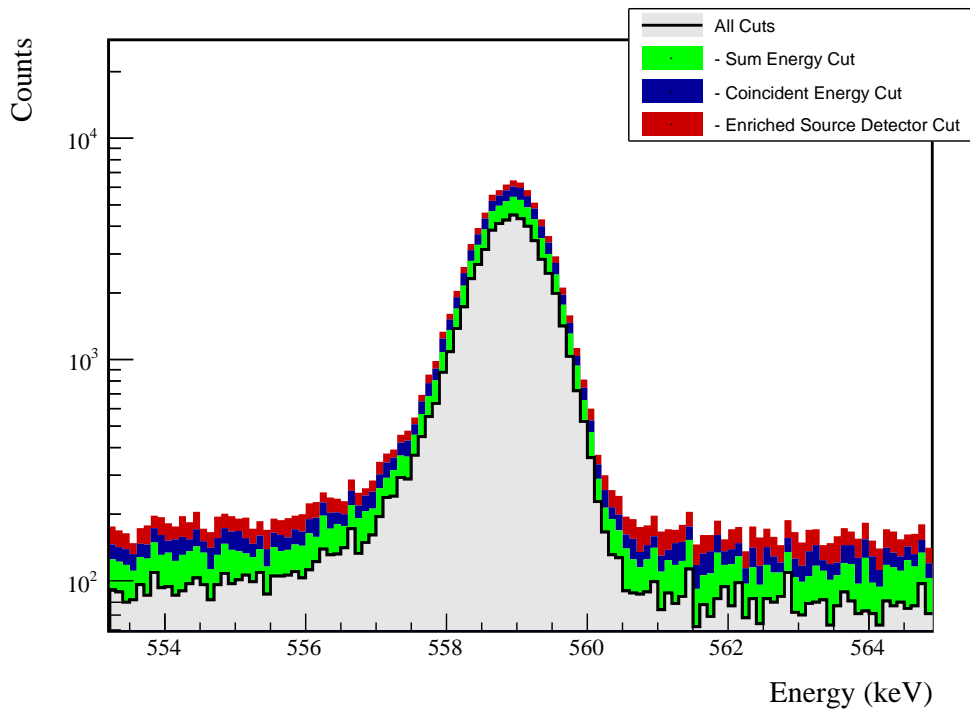


FIG. 48 Simulated (left) and measured (right) multiplicity 2 energy spectrum with sum and coincident energy cuts included for the 559 keV peak.

FIG. 49 Effect of all cuts applied sequentially on ROI for 559 keV peak of $2\nu\beta\beta$ to 2_2^+

Source	Module 1 efficiency	Module 2 efficiency
Multi-Detector with Full Energy γ	$2.0 \pm 0.2\%$	$1.1 \pm 0.5\%$
Region of Interest	$87.1 \pm 2.1\%$	$87.1 \pm 2.1\%$
Dead Layer	$75.3 \pm 4.2\%$	$67.3 \pm 5.7\%$
Detector Dead Times	$97.6 \pm 1.1\%$	$98.2 \pm 0.9\%$
Enriched Source Detector Cut	$96.5 \pm <0.1\%$	$89.0 \pm <0.1\%$
Coincident Energy Cut	$89.7 \pm 0.5\%$	$85.9 \pm 0.5\%$
Sum Energy Cut	$78.3 \pm 0.5\%$	$73.3 \pm 0.5\%$
Final Efficiency	$0.99 \pm 0.12\%$	$0.44 \pm 0.20\%$

FIG. 50 Table of detection efficiencies for the 559 keV peak.

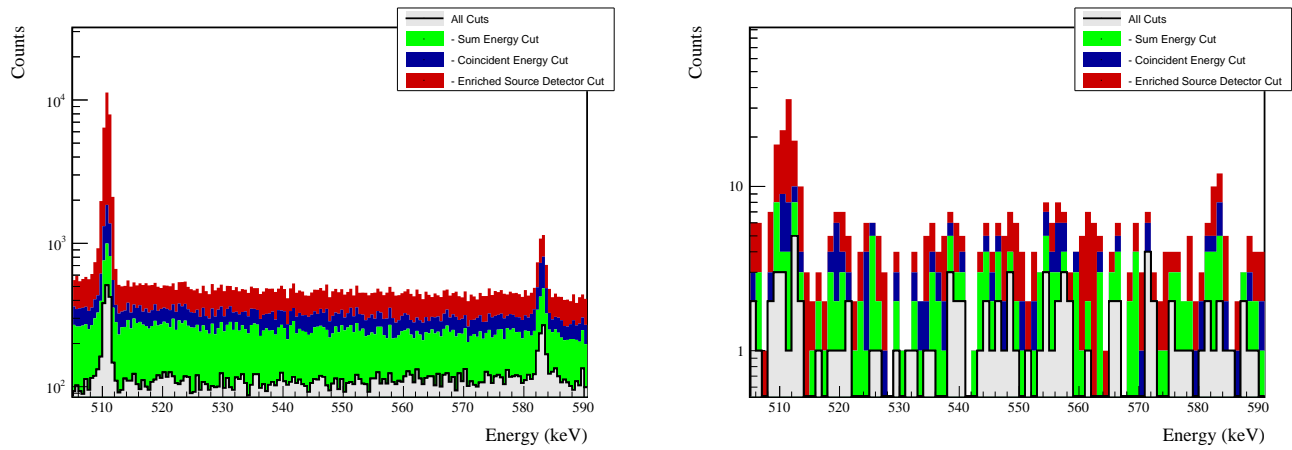
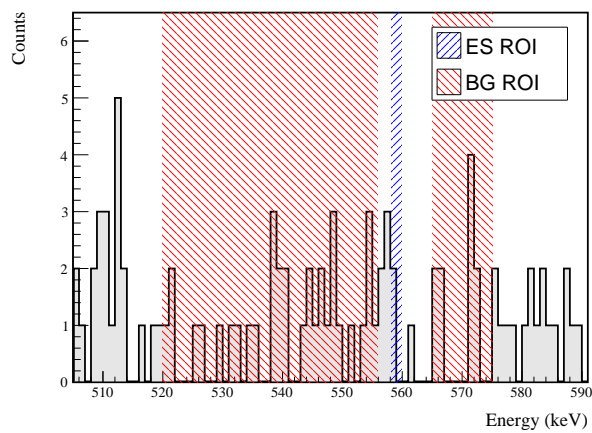


FIG. 51 Effect of all cuts applied to sequentially simulated (left) and measured (right) background data.

FIG. 52 All events after cuts in background (red) and signal (blue) ROIs for 559 keV peak of $2\nu\beta\beta$ to 2_2^+



672 2. 657 keV peak

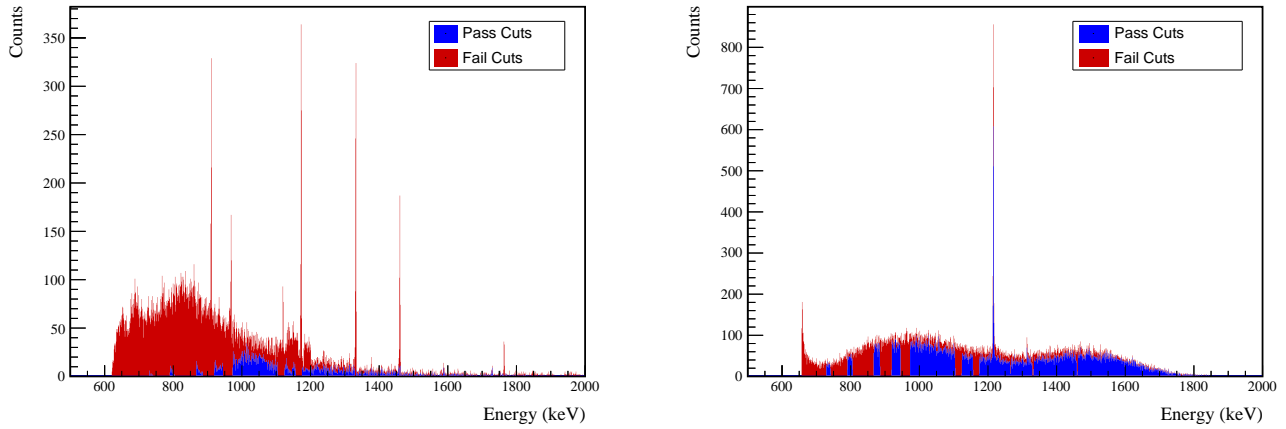


FIG. 53 Effect of 657 keV peak cuts on sum energy spectra in BG (left) and ES (right) simulations.

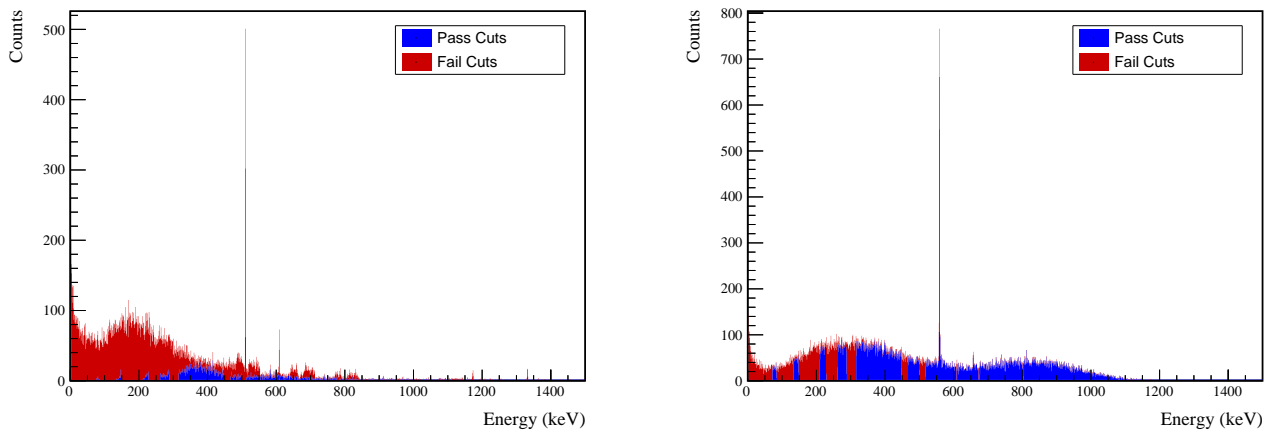


FIG. 54 Effect of 657 keV peak cuts on coincident energy spectra in BG (left) and ES (right) simulations.



TABLE XIV Table of energy estimation uncertainties for the 657 keV peak.

DS	E_{peak} (keV)	σ_{fit} (keV)	σ_{drift} (keV)	$f_{t,fit}$	σ (keV)	$\tau_{f,it}$ (keV)	$\delta_{\mu,f,it}$ (keV)	$\delta_{\mu,NL}$ (keV)	$\delta_{\mu,drift}$ (keV)	$\delta_{\mu,xtalk}$ (keV)	δ_u (keV)	FWHM	$\delta_{fwhm,fit}$ (keV)	$\delta_{fwhm,drift}$ (keV)	$\delta_{fwhm,xtalk}$ (keV)	δ_{FWHM} (keV)	δ_α	$E_{ROI,1}$ (keV)	$E_{ROI,2}$ (keV)	ϵ_{ROI}	$\sigma_{e_{ROI}}$	
DS1	657.041	0.500	0.074	0.505	0.230	0.579	0.002	0.104	0.003	0.012	0.005	0.105	1.256	0.001	0.039	0.011	0.040	0.032	656.051	657.858	0.873	0.013
DS2	657.041	0.502	0.064	0.506	0.249	0.580	0.002	0.067	0.005	0.012	0.005	0.068	1.263	0.001	0.107	0.011	0.108	0.085	656.035	657.856	0.875	0.028
DS3	657.041	0.510	0.078	0.516	0.224	0.568	0.002	0.026	0.026	0.012	0.005	0.040	1.278	0.001	0.073	0.011	0.074	0.058	656.039	657.874	0.879	0.019
DS4	657.041	0.493	0.090	0.501	0.108	0.490	0.002	0.076	0.076	0.012	0.005	0.078	1.207	0.001	0.106	0.011	0.107	0.088	656.147	657.865	0.890	0.029
DS5a	657.041	0.606	0.100	0.614	0.106	0.924	0.002	0.079	0.006	0.012	0.005	0.080	1.481	0.002	0.055	0.011	0.056	0.038	655.948	658.045	0.878	0.013
DS5b	657.041	0.509	0.087	0.517	0.158	0.562	0.001	0.020	0.013	0.012	0.005	0.027	1.259	0.001	0.125	0.011	0.125	0.100	656.086	657.884	0.886	0.032
DS5c	657.041	0.500	0.100	0.510	0.174	0.555	0.002	0.037	0.035	0.012	0.005	0.053	1.247	0.001	0.162	0.011	0.162	0.130	656.087	657.872	0.883	0.042
DS6a	657.041	0.495	0.051	0.497	0.191	0.524	0.001	0.069	0.030	0.012	0.005	0.076	1.221	0.001	0.041	0.011	0.042	0.035	656.099	657.850	0.882	0.012



Cut Name	Cut Description	$\langle \epsilon_{total} \rangle$	$\hat{\epsilon}_{total}$	$\langle \epsilon_{unique} \rangle$	$\hat{\epsilon}_{unique}$	Sacrifice	ΔIDP
Enriched Source Detector Cut	Any other detector: $i \neq \text{Bar}$	M1: 23.9 % M2: 43.7 %	25.2 ^{+3.9} _{-3.5} % 60.4 ^{+6.8} _{-7.2} %	7.2 % 13.5 %	7.4 ^{+2.6} _{-2.0} % 14.6 ^{+5.8} _{-4.4} %	1.7 % 5.5 %	21 %
Coincident Energy Cut	No other detector: $\langle (\text{energy}>71.8) \& (\text{energy}>94.4)$ $\& \text{energy}<135.4) \mid (\text{energy}>48.4 \& \text{energy}<209.3) \mid$ $(\text{energy}>228.4 \& \text{energy}<262.) \mid (\text{energy}>285.4 \& \text{energy}<316.2)$ $\mid (\text{energy}>447.4 \& \text{energy}<467.2) \mid (\text{energy}>499.6 \&$ $\text{energy}<512.8) \mid (\text{energy}>607.6 \& \text{energy}<610.4) \mid$ $(\text{energy}>1165.8 \& \text{energy}<1175.6) \mid (\text{energy}>157.6) \&$ $\text{isBar} \rangle \mid (\langle (\text{energy}<55.2) \mid (\text{energy}>563.6 \& \text{energy}<516.4) \mid$ $(\text{energy}>820.) \& 1.8\text{Bar} \rangle$	M1: 54.0 % M2: 47.6 %	51.9 ± 4.3 % 37.5 ± 7.2 %	16.7 % 13.1 %	17.0 ^{+3.5} _{-3.0} % 10.4 ^{+5.2} _{-3.6} %	13.6 % 8.0 %	17 %
Sum Energy Cut	Not: $\langle (\text{sumE}>729.) \mid (\text{sumE}>741.8 \& \text{sumE}<700.4) \mid (\text{sumE}<805.4$ $\& \text{sumE}<867.) \mid (\text{sumE}>865.6 \& \text{sumE}<919.6) \mid (\text{sumE}>945. \&$ $\text{sumE}<973.2) \mid (\text{sumE}>104.4 \& \text{sumE}<1123.8) \mid (\text{sumE}>1156.4 \&$ $\text{sumE}<1174.6) \mid (\text{sumE}>1328.8 \& \text{sumE}<1333.6) \mid (\text{sumE}>1458.8 \&$ $\text{sumE}<1461.6) \mid (\text{sumE}>1762.4 \& \text{sumE}<1766.) \mid (\text{sumE}>1897.4)$	M1: 60.9 % M2: 60.3 %	57.0 ^{+4.2} _{-4.3} % 64.6 ^{+6.5} _{-7.1} %	14.3 % 9.7 %	15.6 ^{+3.4} _{-2.9} % 8.3 ^{+4.9} _{-3.2} %	1.4 % 1.4 %	29 %
Combined Cuts		M1: 86.5 % M2: 89.9 %	85.2 ^{+2.8} _{-3.3} % 93.8 ^{+2.7} _{-4.5} %	—	—	42.0 % 45.2 %	34 %

TABLE XV Table of cut descriptions and efficiencies for simulated backgrounds and measured data for the 657 keV peak.

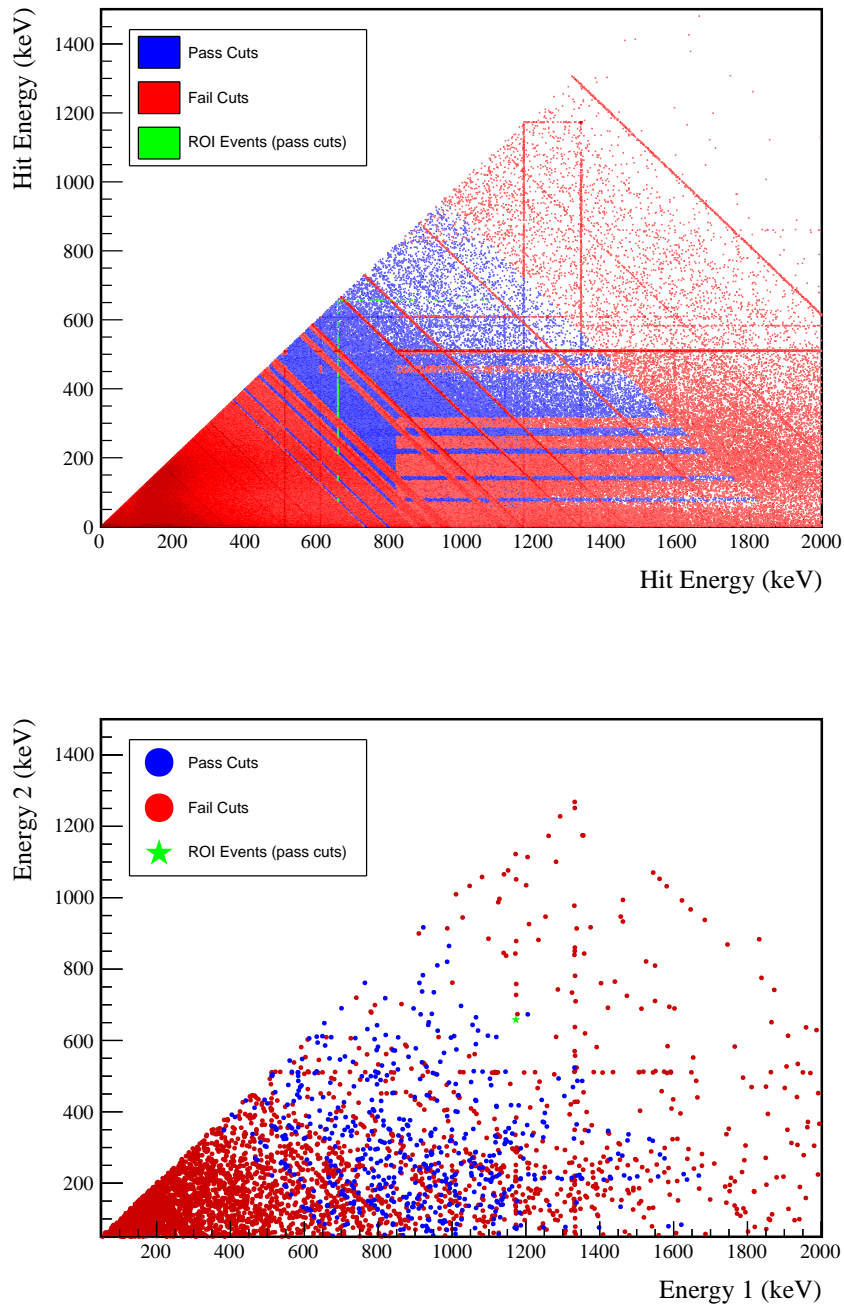
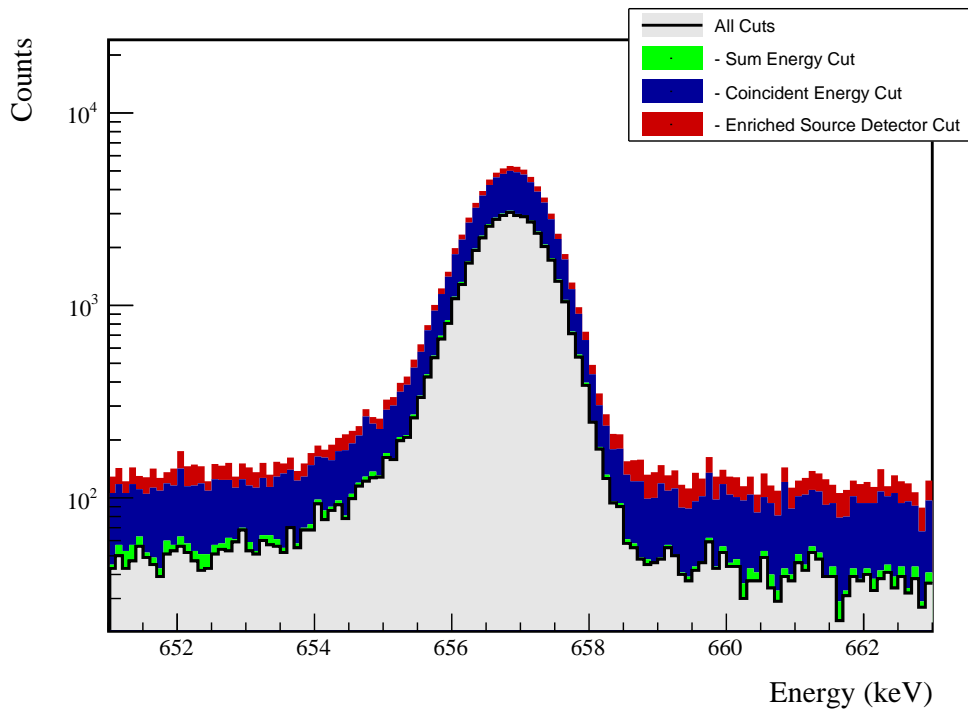


FIG. 55 Simulated (left) and measured (right) multiplicity 2 energy spectrum with sum and coincident energy cuts included for the 657 keV peak.

FIG. 56 Effect of all cuts applied sequentially on ROI for 657 keV peak of $2\nu\beta\beta$ to 2_2^+

Source	Module 1 efficiency	Module 2 efficiency
Multi-Detector with Full Energy γ	$1.8 \pm 0.2\%$	$1.0 \pm 0.5\%$
Region of Interest Dead Layer	$88.0 \pm 1.8\%$	$88.0 \pm 1.8\%$
Detector Dead Times	$75.6 \pm 4.1\%$	$66.9 \pm 5.8\%$
Enriched Source Detector Cut	$97.8 \pm 1.0\%$	$98.2 \pm 0.8\%$
Coincident Energy Cut	$96.6 \pm <0.1\%$	$88.6 \pm <0.1\%$
Sum Energy Cut	$62.2 \pm 0.5\%$	$65.6 \pm 0.5\%$
Final Efficiency	$73.7 \pm 0.5\%$	$68.9 \pm 0.5\%$
	$0.75 \pm 0.10\%$	$0.35 \pm 0.17\%$

FIG. 57 Table of detection efficiencies for the 657 keV peak.

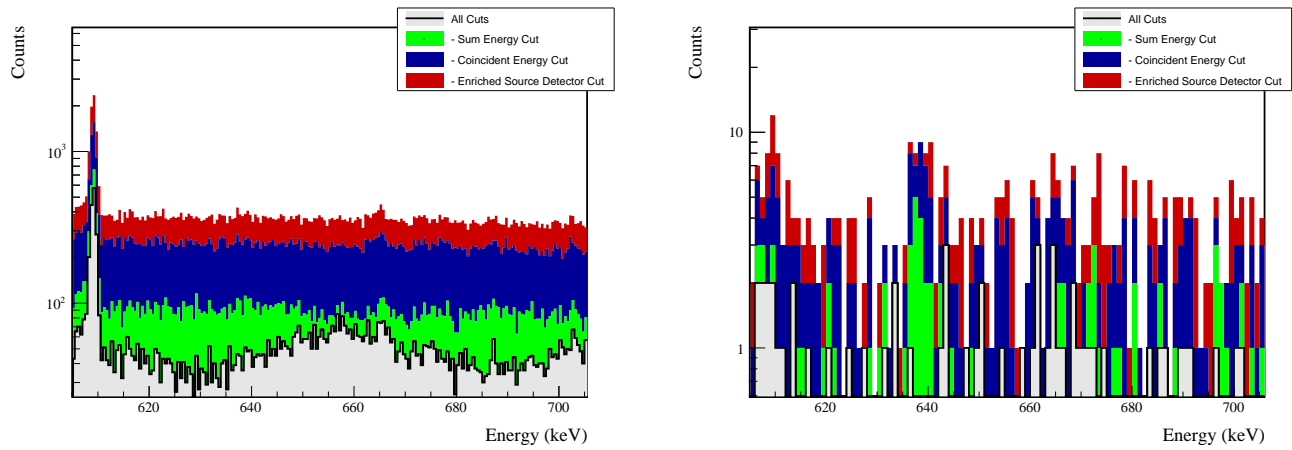
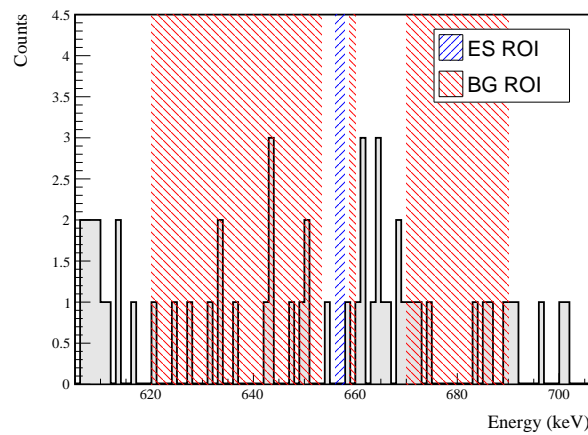


FIG. 58 Effect of all cuts applied to sequentially simulated (left) and measured (right) background data.

FIG. 59 All events after cuts in background (red) and signal (blue) ROIs for 657 keV peak of $2\nu\beta\beta$ to 2_2^+



673 3. 1216 keV peak

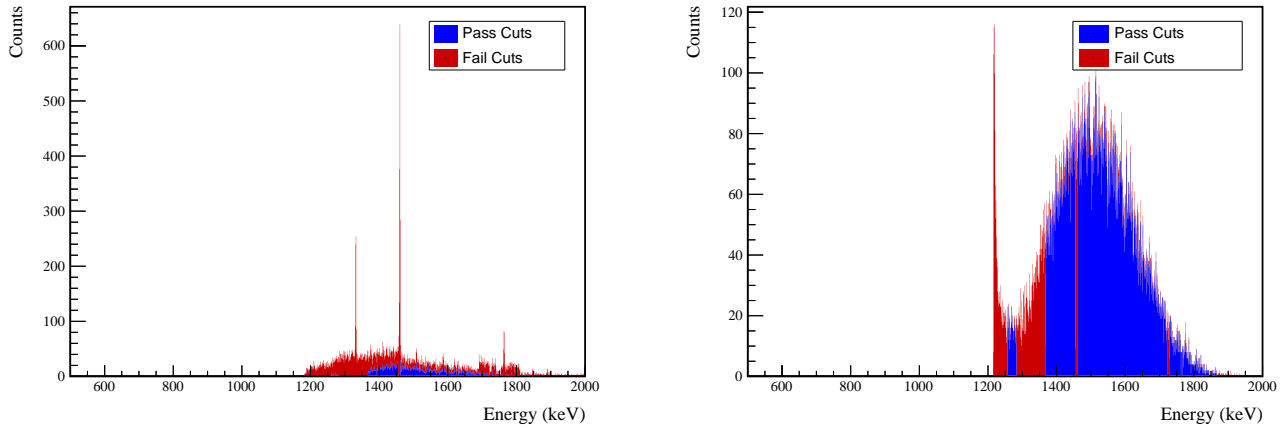


FIG. 60 Effect of 1216 keV peak cuts on sum energy spectra in BG (left) and ES (right) simulations.

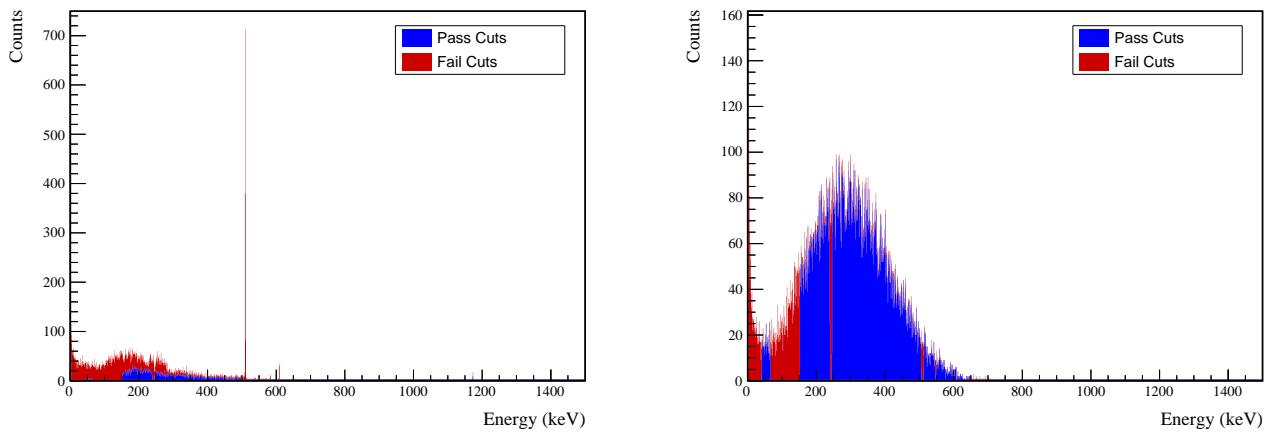


FIG. 61 Effect of 1216 keV peak cuts on coincident energy spectra in BG (left) and ES (right) simulations.



TABLE XVI Table of energy estimation uncertainties for the 1216 keV peak.

DS	E_{peak} (keV)	$\sigma_{f_{fit}}$ (keV)	σ_{drift} (keV)	σ (keV)	$f_{t,f_{fit}}$	$\tau_{f_{fit}}$ (keV)	$\delta_{\mu,f_{fit}}$ (keV)	$\delta_{\mu,NL}$ (keV)	$\delta_{\mu,drift}$ (keV)	$\delta_{\mu,x talk}$ (keV)	$\delta_{\mu,peak}$ (keV)	δ_{μ} (keV)	FWHM	$\delta_{f_{ahm},fit}$ (keV)	$\delta_{f_{ahm,drift}}$ (keV)	$\delta_{f_{ahm,x talk}}$ (keV)	δ_{FWHM} (keV)	$E_{ROI,1}$ (keV)	$E_{ROI,2}$ (keV)	ϵ_{ROI}	$\sigma_{e_{ROI}}$	
DS1	1216.104	0.705	0.137	0.718	0.230	0.945	0.003	0.104	0.005	0.012	0.020	0.107	1.787	0.001	0.039	0.011	0.040	0.023	1214.691	1217.262	0.868	0.008
DS2	1216.104	0.710	0.119	0.720	0.249	0.951	0.003	0.067	0.008	0.012	0.020	0.072	1.803	0.001	0.107	0.011	0.108	0.060	1214.663	1217.262	0.867	0.019
DS3	1216.104	0.715	0.144	0.729	0.224	0.925	0.003	0.026	0.051	0.012	0.020	0.062	1.812	0.001	0.073	0.011	0.074	0.041	1214.679	1217.281	0.872	0.013
DS4	1216.104	0.697	0.167	0.717	0.108	0.746	0.003	0.076	0.022	0.012	0.020	0.083	1.726	0.001	0.106	0.011	0.107	0.062	1214.829	1217.278	0.889	0.021
DS5a	1216.104	0.838	0.185	0.859	0.106	1.316	0.004	0.079	0.012	0.012	0.020	0.083	2.070	0.002	0.055	0.011	0.056	0.027	1214.581	1217.504	0.877	0.009
DS5b	1216.104	0.716	0.161	0.734	0.158	0.963	0.002	0.020	0.024	0.012	0.020	0.039	1.791	0.001	0.125	0.011	0.125	0.070	1214.743	1217.299	0.878	0.023
DS5c	1216.104	0.703	0.185	0.727	0.174	0.932	0.003	0.037	0.066	0.012	0.020	0.079	1.783	0.001	0.162	0.011	0.162	0.091	1214.738	1217.287	0.876	0.030
DS6a	1216.104	0.693	0.095	0.700	0.191	0.873	0.002	0.069	0.055	0.012	0.020	0.092	1.723	0.001	0.041	0.011	0.042	0.025	1214.771	1217.241	0.875	0.009



Cut Name	Cut Description	$\langle \epsilon_{total} \rangle$	$\hat{\epsilon}_{total}$	$\langle \epsilon_{unique} \rangle$	$\hat{\epsilon}_{unique}$	Sacrifice	ΔDP
Enriched Source Cut	Any other detector: isEor	M1: 26.9 %	16.9 ^{+4.5} _{-3.7} %	15.1 %	8.4 ^{+3.6} _{-2.6} %	2.4 %	23%
Detector Cut		M2: 43.9 %	61.9 ^{+9.7} _{-10.9} %	25.8 %	28.6 ^{+8.7} _{-8.7} %	5.8 %	
Multiplicity 2 Cut		M1: 15.3 %	16.9 ^{+4.5} _{-3.7} %	4.0 %	3.6 ^{+2.7} _{-1.6} %	0.1 %	5%
m==2		M2: 11.9 %	9.5 ^{+8.4} _{-4.7} %	3.2 %	0.0 ^{+4.5} _{-0.0} %	0.0 %	
No other detector:	((energy<40.8) (energy>36.6 && energy<15.2) (energy>239.6 && energy<245.8) (energy>60.8 && energy<61.0) (energy>605.8) && isthr)	M1: 34.1 %	38.6 ^{+5.4} _{-5.2} %	10.8 %	8.4 ^{+3.6} _{-2.6} %	0.3 %	14%
Coincident Energy Cut	(energy>105.2 && energy<112.6) (energy>605.8 && energy<610.)	M2: 25.9 %	14.3 ^{+9.3} _{-6.0} %	9.3 %	4.8 ^{+2.0} _{-2.9} %	0.3 %	
Note:	(sumE<1287.) (sumE<1283. && sumE<1367.4) (sumE>1465.2 && sumE<1462.) (sumE>1721.8 && sumE<1728.6) (sumE>1762. && sumE<1766.) (sumE>1845.6 && sumE<1851.2) (sumE>1866.6)	M1: 40.9 %	38.6 ^{+5.4} _{-5.2} %	10.5 %	4.8 ^{+2.9} _{-1.9} %	0.5 %	12%
Sum Energy Cut		M2: 35.9 %	42.9 ^{+10.9} _{-10.2} %	6.0 %	0.0 ^{+4.5} _{-0.0} %	0.5 %	
Combined Cuts		M1: 77.1 %	65.1 ^{+5.0} _{-5.4} %	—	—	20.1 %	44%
		M2: 79.8 %	81.0 ^{+7.1} _{-9.9} %	—	—	23.8 %	

TABLE XVII Table of cut descriptions and efficiencies for simulated backgrounds and measured data for the 1216 keV peak.

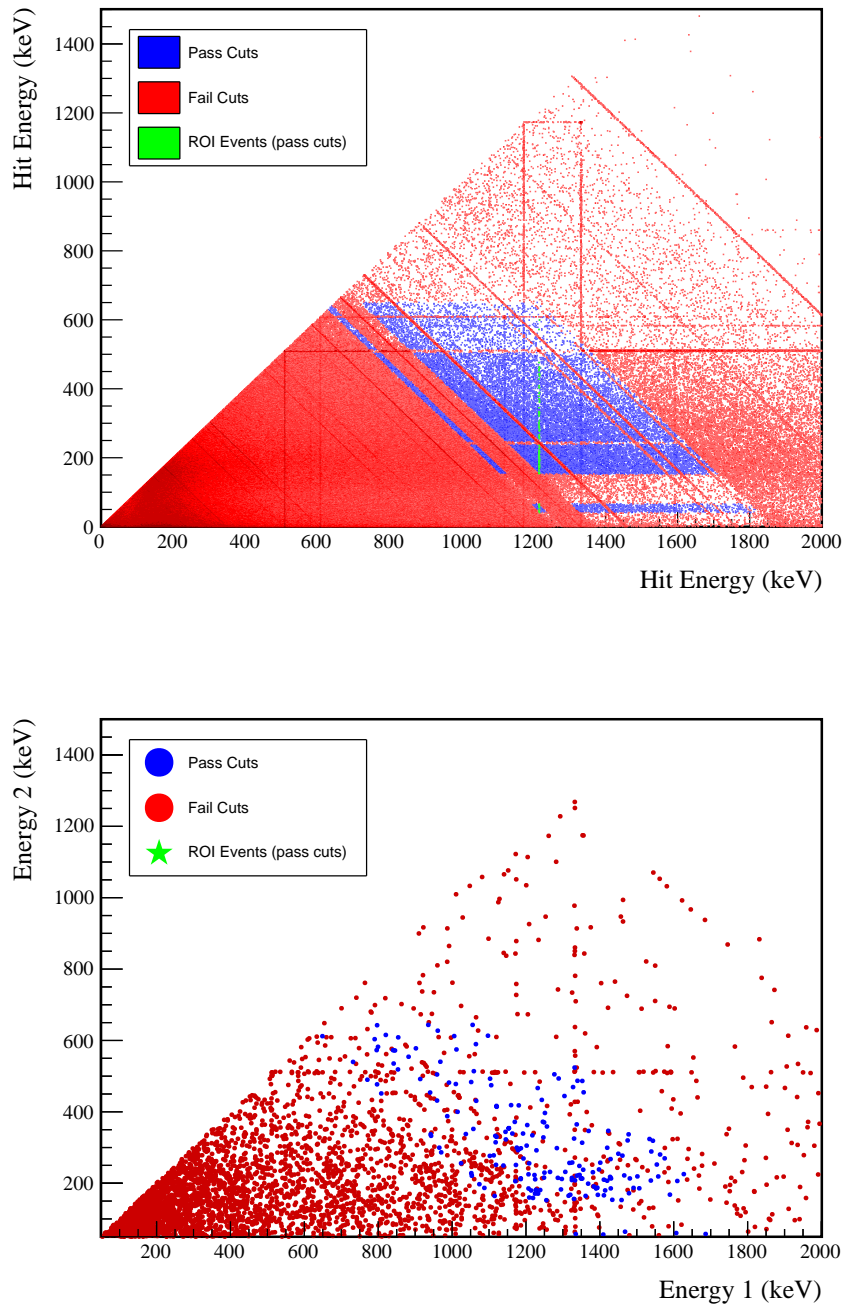
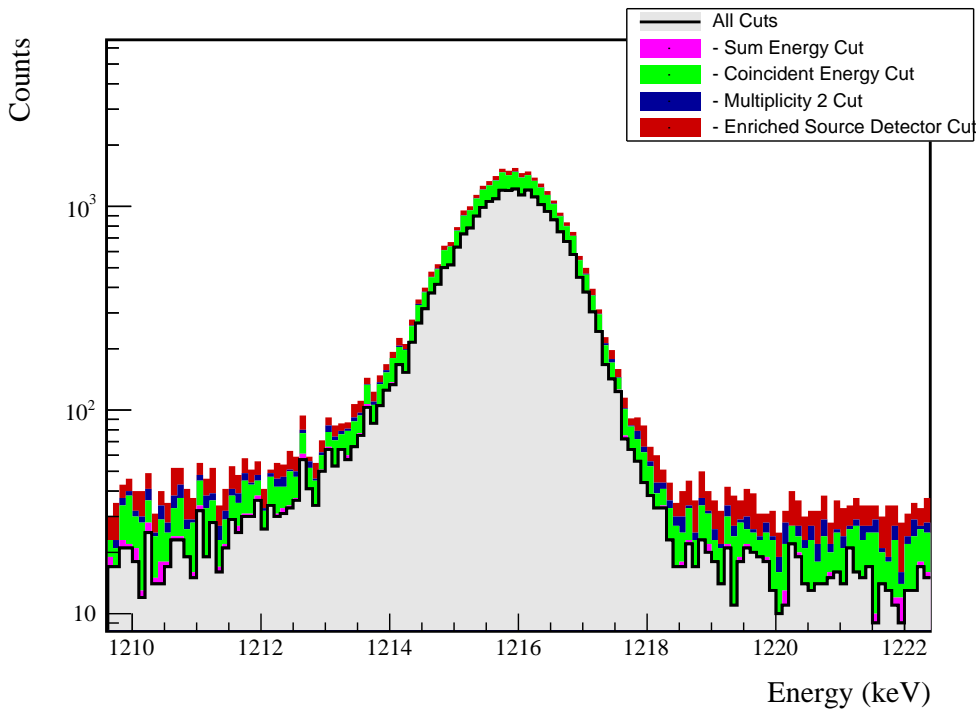


FIG. 62 Simulated (left) and measured (right) multiplicity 2 energy spectrum with sum and coincident energy cuts included for the 1216 keV peak.

FIG. 63 Effect of all cuts applied sequentially on ROI for 1216 keV peak of $2\nu\beta\beta$ to 2_2^+

Source	Module 1 efficiency	Module 2 efficiency
Multi-Detector with Full Energy γ	$0.8 \pm 0.2\%$	$0.4 \pm 0.5\%$
Region of Interest	$87.5 \pm 1.3\%$	$87.5 \pm 1.3\%$
Dead Layer	$73.9 \pm 4.4\%$	$63.6 \pm 6.4\%$
Detector Dead Times	$97.5 \pm 1.1\%$	$98.1 \pm 0.9\%$
Enriched Source Detector Cut	$97.0 \pm < 0.1\%$	$92.5 \pm < 0.1\%$
Multiplicity 2 Cut	$99.6 \pm < 0.1\%$	$99.8 \pm < 0.1\%$
Coincident Energy Cut	$83.5 \pm 0.5\%$	$84.2 \pm 0.5\%$
Sum Energy Cut	$82.9 \pm 0.5\%$	$82.4 \pm 0.5\%$
Final Efficiency	$0.43 \pm 0.11\%$	$0.18 \pm 0.22\%$

FIG. 64 Table of detection efficiencies for the 1216 keV peak.

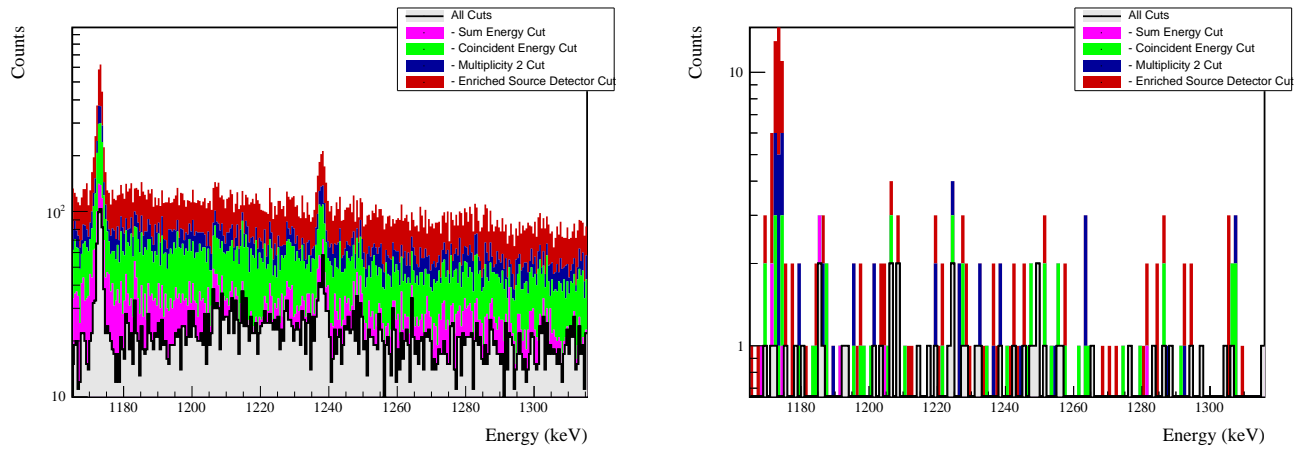
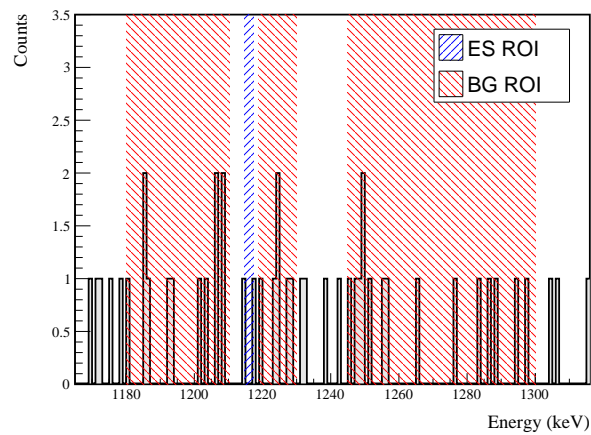
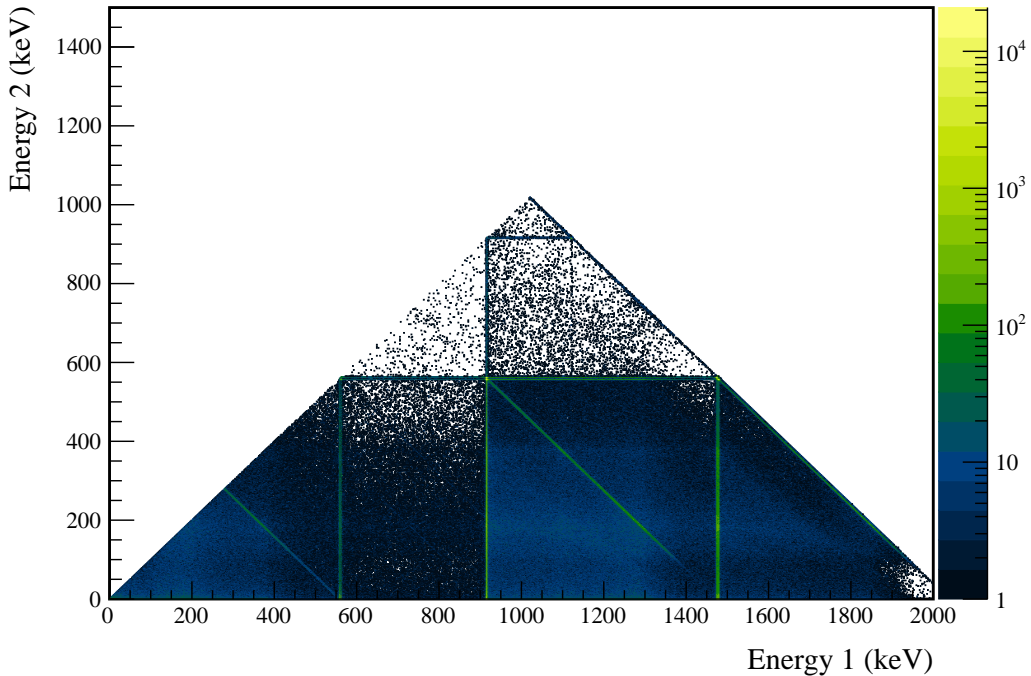


FIG. 65 Effect of all cuts applied to sequentially simulated (left) and measured (right) background data.

FIG. 66 All events after cuts in background (red) and signal (blue) ROIs for 1216 keV peak of $2\nu\beta\beta$ to 2_2^+

674 Appendix E: $0\nu\beta\beta$ to 0_1^+

675 Note that both the 559 and 563 keV peaks will be shown together since they use the same sets of cuts.



676 FIG. 67 Simulated multiplicity 2 energy spectrum of the $0\nu\beta\beta$ to 0_1^+ decay mode

677

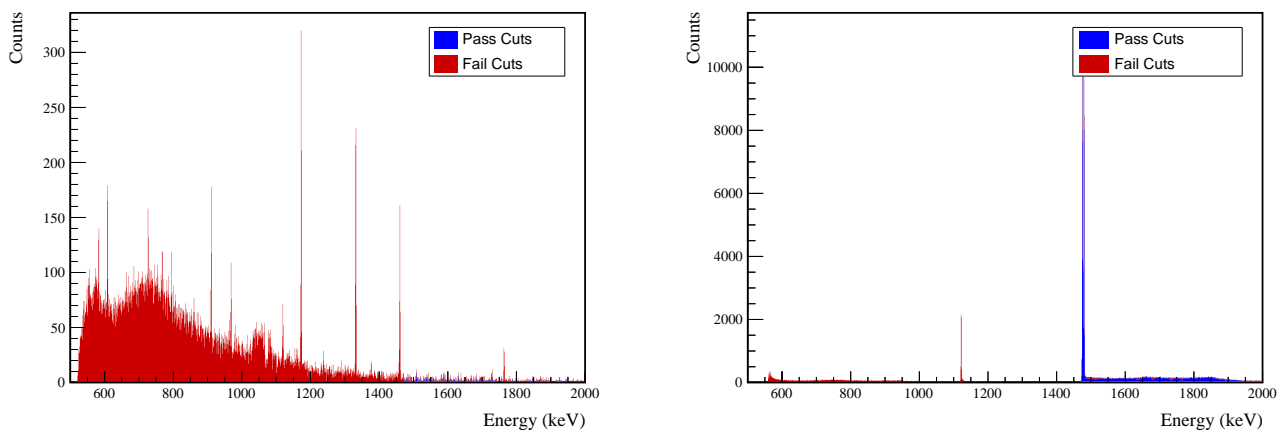


FIG. 68 Effect of 559 and 563 keV peaks cuts on sum energy spectra in BG (left) and ES (right) simulations.



TABLE XVIII Table of energy estimation uncertainties for the 559 and 563 keV peaks.

DS	E_{peak} (keV)	σ_{fit} (keV)	σ_{drift} (keV)	σ (keV)	$f_{t,fit}$ (keV)	τ_{fit} (keV)	$\delta_{\mu,fit}$ (keV)	$\delta_{\mu,NL}$ (keV)	$\delta_{\mu,drift}$ (keV)	$\delta_{\mu,peak}$ (keV)	δ_u (keV)	FWHM (keV)	$\delta_{fwhm,drift}$ (keV)	$\delta_{fwhm,fit}$ (keV)	$\delta_{fwhm,x talk}$ (keV)	δ_{FWHM} (keV)	δ_α	$E_{ROI,1}$ (keV)	$E_{ROI,2}$ (keV)	ϵ_{ROI}	$\sigma_{\epsilon_{ROI}}$	
DS1	559.101	0.460	0.063	0.464	0.230	0.515	0.001	0.104	0.002	0.012	0.005	0.105	1.152	0.001	0.039	0.011	0.040	0.035	558.083	559.935	0.907	0.012
DS2	559.101	0.461	0.055	0.464	0.249	0.515	0.002	0.067	0.004	0.012	0.005	0.068	1.158	0.001	0.107	0.011	0.108	0.093	558.066	559.934	0.910	0.025
DS3	559.101	0.470	0.066	0.474	0.224	0.505	0.001	0.026	0.024	0.012	0.005	0.038	1.174	0.001	0.073	0.011	0.074	0.063	558.071	559.953	0.914	0.017
DS4	559.101	0.455	0.077	0.461	0.108	0.445	0.002	0.076	0.010	0.012	0.005	0.078	1.111	0.001	0.106	0.011	0.107	0.096	558.186	559.943	0.922	0.026
DS5a	559.101	0.560	0.085	0.567	0.106	0.855	0.002	0.079	0.005	0.012	0.005	0.080	1.367	0.002	0.055	0.011	0.056	0.041	557.975	560.129	0.910	0.012
DS5b	559.101	0.469	0.074	0.475	0.158	0.491	0.001	0.020	0.011	0.012	0.005	0.026	1.157	0.001	0.125	0.011	0.125	0.108	558.122	559.962	0.919	0.029
DS5c	559.101	0.460	0.085	0.468	0.174	0.489	0.001	0.037	0.030	0.012	0.005	0.050	1.145	0.001	0.162	0.011	0.162	0.142	558.123	559.948	0.917	0.037
DS6a	559.101	0.456	0.044	0.458	0.191	0.463	0.001	0.069	0.025	0.012	0.005	0.075	1.123	0.000	0.041	0.011	0.042	0.038	558.134	559.928	0.916	0.011
DS1	563.178	0.461	0.064	0.466	0.230	0.518	0.001	0.104	0.002	0.012	0.005	0.105	1.156	0.001	0.039	0.011	0.040	0.035	562.156	564.015	0.907	0.012
DS2	563.178	0.463	0.055	0.466	0.249	0.517	0.002	0.067	0.004	0.012	0.005	0.068	1.162	0.001	0.107	0.011	0.108	0.093	562.139	564.014	0.910	0.025
DS3	563.178	0.471	0.066	0.476	0.224	0.508	0.001	0.026	0.024	0.012	0.005	0.038	1.179	0.001	0.073	0.011	0.074	0.063	562.144	564.033	0.914	0.017
DS4	563.178	0.457	0.077	0.463	0.108	0.447	0.002	0.076	0.010	0.012	0.005	0.078	1.115	0.001	0.106	0.011	0.107	0.096	562.260	564.023	0.922	0.026
DS5a	563.178	0.562	0.086	0.569	0.106	0.858	0.002	0.079	0.006	0.012	0.005	0.080	1.372	0.002	0.055	0.011	0.056	0.041	562.048	564.210	0.910	0.011
DS5b	563.178	0.471	0.074	0.477	0.158	0.494	0.001	0.020	0.011	0.012	0.005	0.026	1.162	0.001	0.125	0.011	0.125	0.108	562.196	564.042	0.919	0.029
DS5c	563.178	0.462	0.086	0.470	0.174	0.492	0.001	0.037	0.030	0.012	0.005	0.050	1.49	0.001	0.162	0.011	0.162	0.141	562.197	564.028	0.917	0.037
DS6a	563.178	0.457	0.044	0.459	0.191	0.465	0.001	0.069	0.026	0.012	0.005	0.075	1.127	0.000	0.041	0.011	0.042	0.038	562.208	564.008	0.915	0.011



Cut Name	Cut Description	$\langle \epsilon_{total} \rangle$	$\hat{\epsilon}_{total}$	$\langle \epsilon_{unique} \rangle$	$\hat{\epsilon}_{unique}$	Sacrifice	ΔDP
Enriched Source Detector Cut	Any other detector: isEar	M1: 23.2 % M2: 42.7 %	27.2 ^{+3.8} _{-7.6} % 62.8 ^{+2.5} _{-7.6} %	0.5 % 0.9 %	0.7 ^{+1.1} _{-0.4} % 7.0 ^{+4.9} _{-3.0} %	1.3 % 3.0 %	13 %
Coincident Energy Cut	No other detector: ((energy<53) (energy>469.6 && energy<526.2) (energy>587.8 && energy<652.2) (energy>1074.6 && energy<1079.2) (energy>1117.2 && energy<1121.6) (energy>1170.6 && energy<1175.) (energy>1231.6) (energy>1343.) (energy>1483.) (energy>1331. && energy<1334.) (energy>144.8) (energy>1385.6) 1.isEar) Note: (sumE<1472.) (sumE>1761.8 && sumE<1765.8) (sumE>2042.6)	M1: 28.8 % M2: 26.9 %	32.0 ^{+4.0} _{-3.7} % 23.3 ^{+3.7} _{-5.8} %	0.8 % 0.5 %	1.4 ^{+1.3} _{-0.7} % 7.0 ^{+4.9} _{-3.0} %	4.5 % 2.9 %	9 %
Sum Energy Cut		M1: 97.1 % M2: 97.6 %	96.6 ^{+1.2} _{-1.8} % 86.0 ^{+4.5} _{-6.7} %	50.9 % 38.0 %	49.0 \pm 4.1 % 27.9 ^{+7.3} _{-6.3} %	12.3 % 15.3 %	243 %
Combined Cuts		M1: 98.4 % M2: 99.1 %	98.6 ^{+1.3} _{-0.7} % 100.0 ^{+0.0} _{-2.3} %	— —	— 35.9 %	26.5 % 298 %	

TABLE XIX Table of cut descriptions and efficiencies for simulated backgrounds and measured data for the 559 and 563 keV peaks.

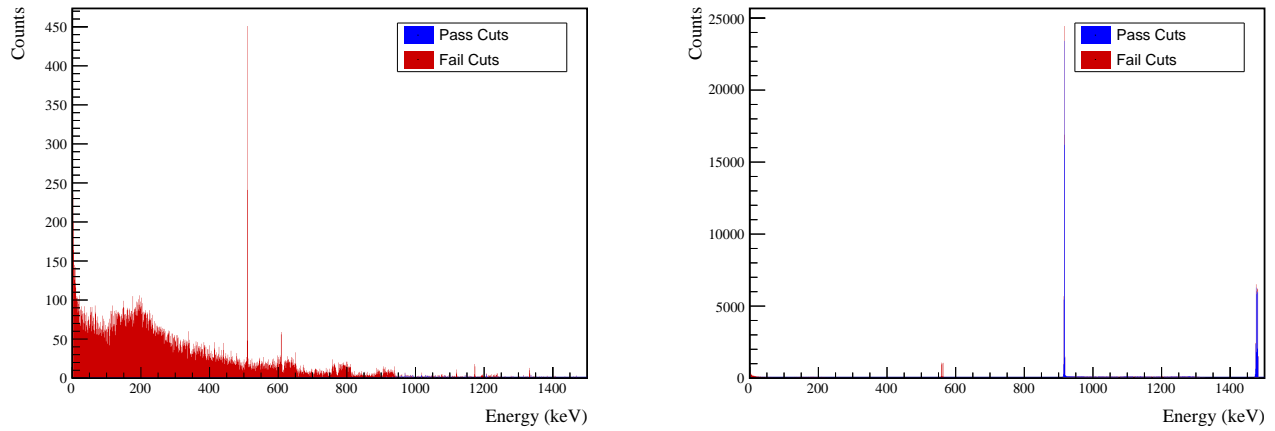


FIG. 69 Effect of 559 and 563 keV peaks cuts on coincident energy spectra in BG (left) and ES (right) simulations.

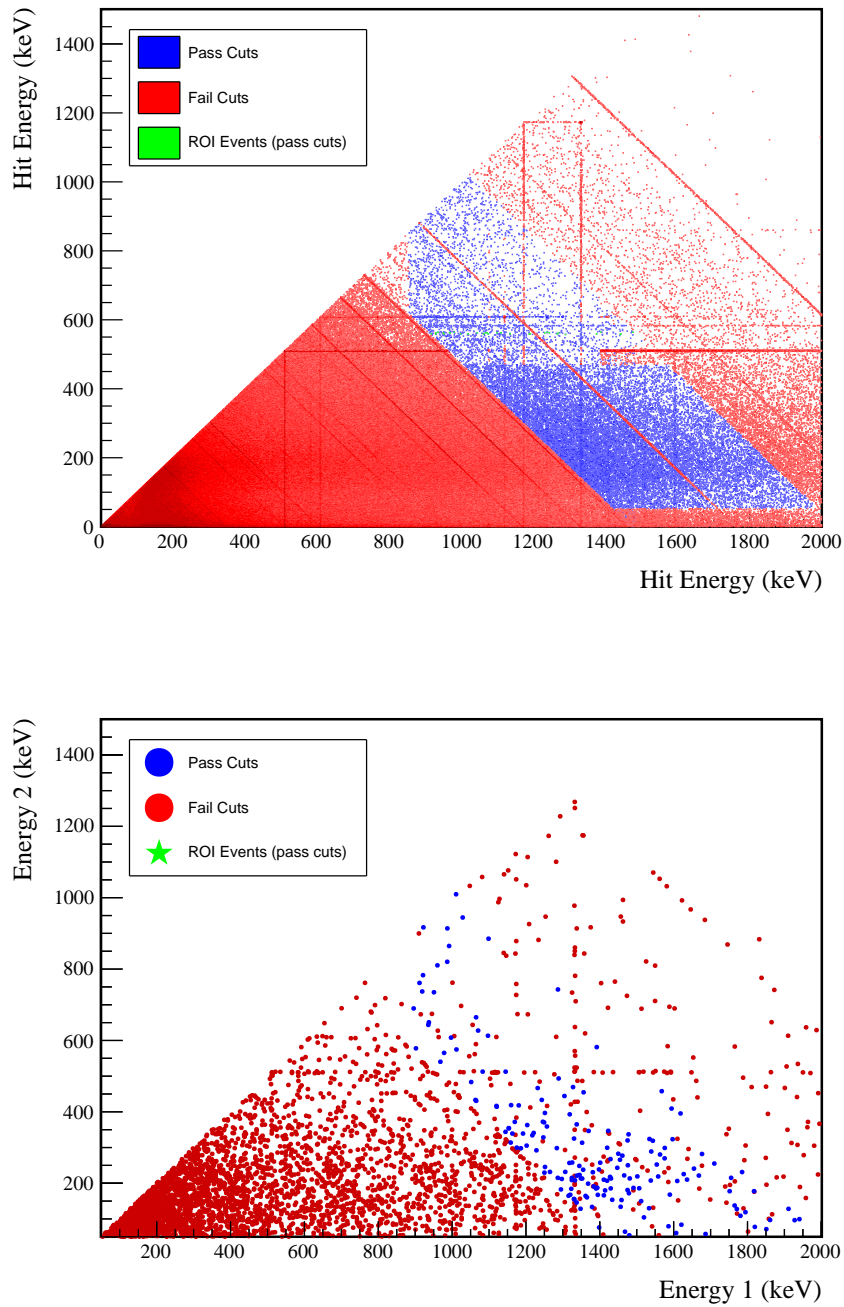
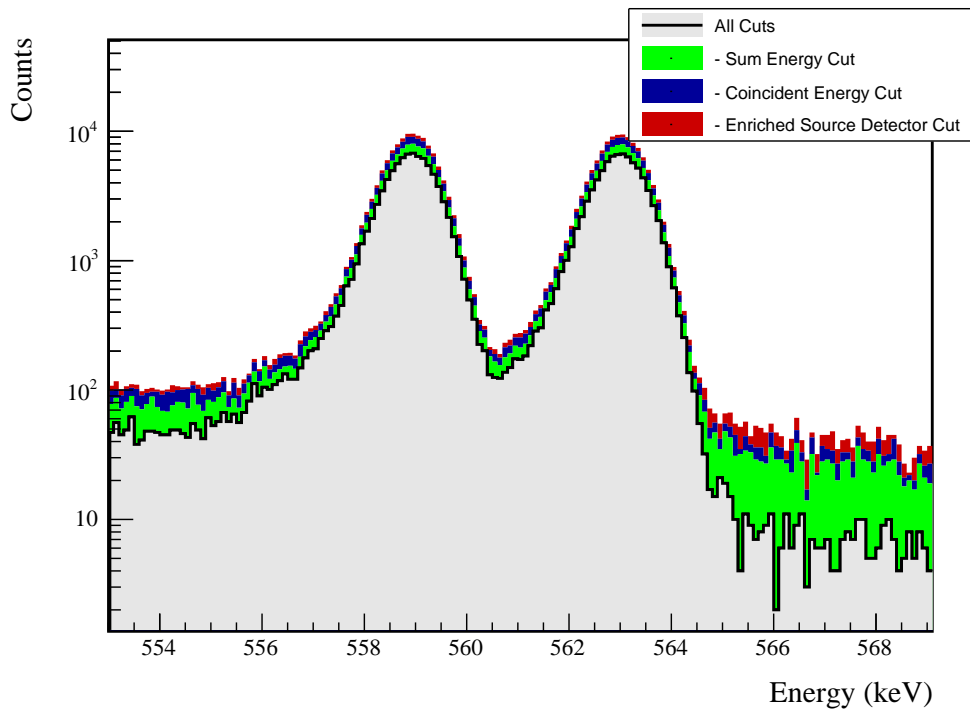


FIG. 70 Simulated (left) and measured (right) multiplicity 2 energy spectrum with sum and coincident energy cuts included for the 559 and 563 keV peaks.

FIG. 71 Effect of all cuts applied sequentially on ROI for 559 and 563 keV peaks of $0\nu\beta\beta$ to 0_1^+

Source	Module 1 efficiency	Module 2 efficiency
Multi-Detector with Full Energy γ	$5.8 \pm 0.2\%$	$3.1 \pm 0.5\%$
Region of Interest	$91.3 \pm 1.1\%$	$91.3 \pm 1.1\%$
Dead Layer	$69.3 \pm 5.2\%$	$60.7 \pm 6.9\%$
Detector Dead Times	$97.6 \pm 1.1\%$	$98.1 \pm 0.9\%$
Enriched Source Detector Cut	$97.0 \pm <0.1\%$	$90.2 \pm <0.1\%$
Coincident Energy Cut	$88.2 \pm 0.3\%$	$87.4 \pm 0.3\%$
Sum Energy Cut	$79.6 \pm 0.3\%$	$70.9 \pm 0.3\%$
Final Efficiency	$3.10 \pm 0.26\%$	$1.34 \pm 0.26\%$

FIG. 72 Table of detection efficiencies for the 559 and 563 keV peaks.

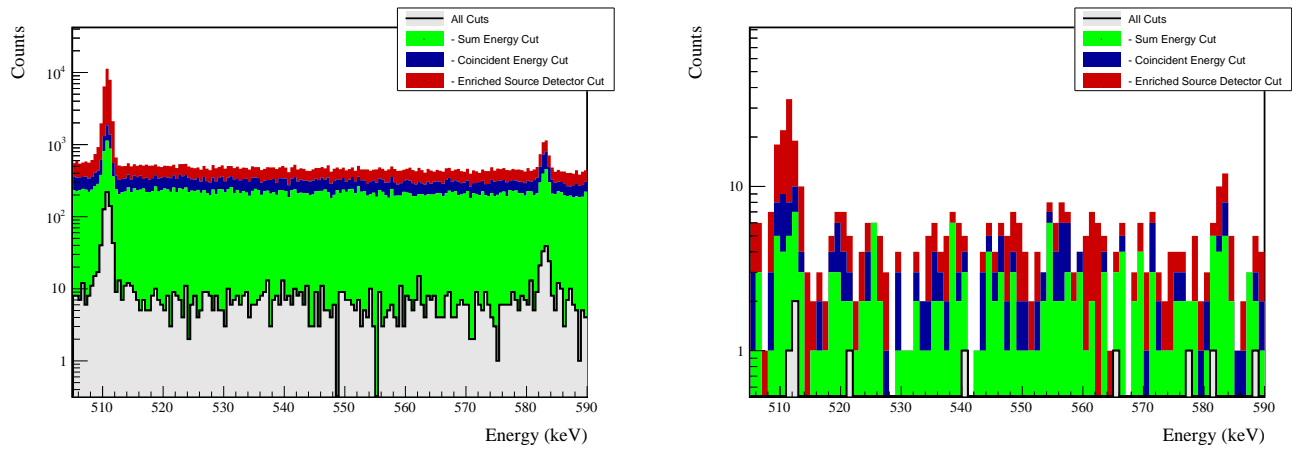
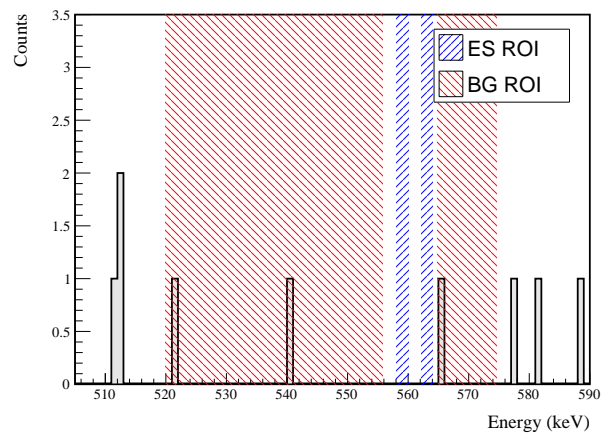


FIG. 73 Effect of all cuts applied to sequentially simulated (left) and measured (right) background data.

FIG. 74 All events after cuts in background (red) and signal (blue) ROIs for 559 and 563 keV peaks of $0\nu\beta\beta$ to 0_1^+

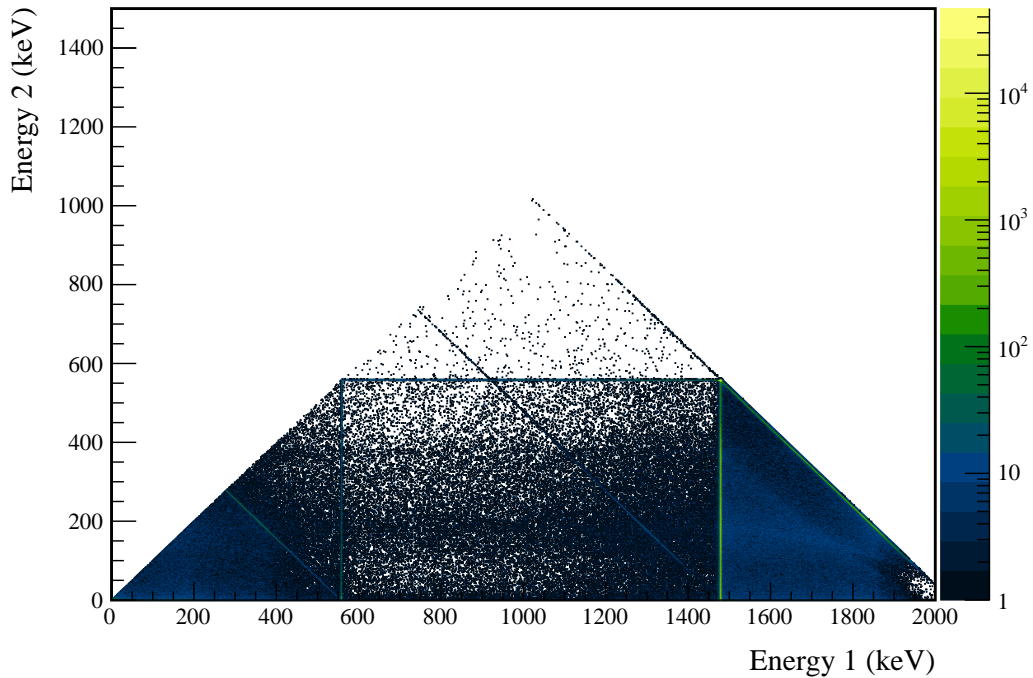
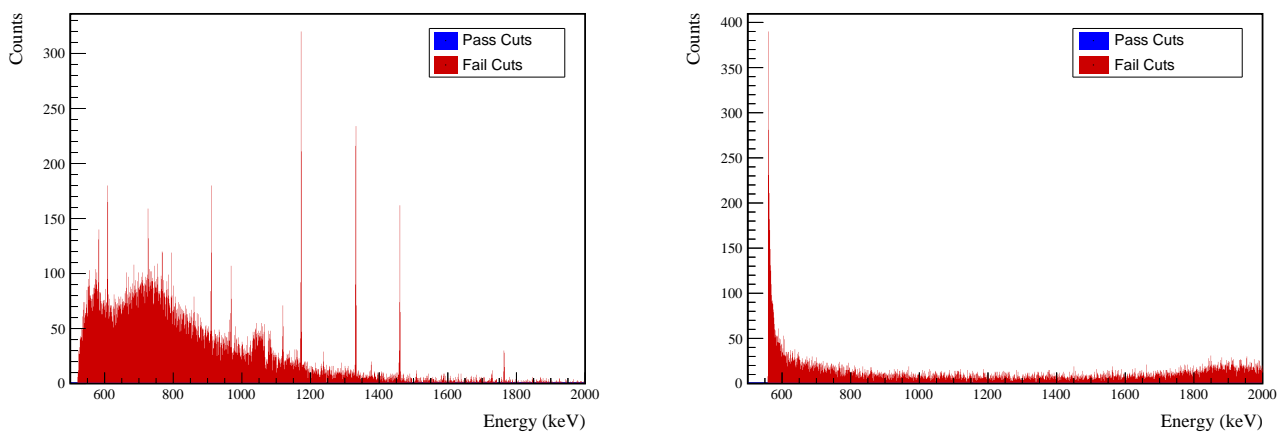
678 **Appendix F: $0\nu\beta\beta$ to 2_1^+** FIG. 75 Simulated multiplicity 2 energy spectrum of the $0\nu\beta\beta$ to 2_1^+ decay mode

FIG. 76 Effect of 559 keV peak cuts on sum energy spectra in BG (left) and ES (right) simulations.



TABLE XX Table of energy estimation uncertainties for the 559 keV peak.

DS	E_{peak} (keV)	σ_{drift} (keV)	σ_{fit} (keV)	$f_{t,fit}$	σ (keV)	$\delta_{\mu,drift}$ (keV)	$\delta_{\mu,fit}$ (keV)	$\tau_{f,it}$ (keV)	$\delta_{\mu,NL}$ (keV)	$\delta_{\mu,atalk}$ (keV)	$\delta_{\mu,peak}$ (keV)	δ_u (keV)	FWHM	$\delta_{fwhm,fit}$ (keV)	$\delta_{fwhm,drift}$ (keV)	$\delta_{fwhm,atalk}$ (keV)	$\delta_{fwhm,peak}$ (keV)	δ_{FWHM} (keV)	δ_α	$E_{ROI,1}$ (keV)	$E_{ROI,2}$ (keV)	ϵ_{ROI}	$\sigma_{e_{ROI}}$
DS1	559.101	0.460	0.063	0.464	0.230	0.515	0.001	0.104	0.002	0.012	0.005	0.105	1.152	0.001	0.039	0.011	0.040	0.035	558.052	559.959	0.915	0.011	
DS2	559.101	0.461	0.055	0.464	0.249	0.515	0.002	0.067	0.004	0.012	0.005	0.068	1.158	0.001	0.107	0.011	0.108	0.093	558.035	559.957	0.917	0.023	
DS3	559.101	0.470	0.066	0.474	0.224	0.505	0.001	0.026	0.024	0.012	0.005	0.038	1.174	0.001	0.073	0.011	0.074	0.063	558.039	559.977	0.921	0.016	
DS4	559.101	0.455	0.077	0.461	0.108	0.445	0.002	0.076	0.010	0.012	0.005	0.078	1.111	0.001	0.106	0.011	0.107	0.096	558.161	559.966	0.929	0.024	
DS5a	559.101	0.560	0.085	0.567	0.106	0.885	0.002	0.079	0.005	0.012	0.005	0.080	1.367	0.002	0.055	0.011	0.056	0.041	557.942	560.158	0.918	0.011	
DS5b	559.101	0.469	0.074	0.475	0.158	0.491	0.001	0.020	0.011	0.012	0.005	0.026	1.157	0.001	0.125	0.011	0.125	0.108	558.094	559.986	0.927	0.027	
DS5c	559.101	0.460	0.085	0.468	0.174	0.489	0.001	0.037	0.030	0.012	0.005	0.050	1.145	0.001	0.162	0.011	0.162	0.142	558.095	559.972	0.924	0.035	
DS6a	559.101	0.456	0.044	0.458	0.191	0.463	0.001	0.069	0.025	0.012	0.005	0.075	1.123	0.000	0.041	0.011	0.042	0.038	558.106	559.951	0.923	0.010	



Cut Name	Cut Description	$\langle \epsilon_{total} \rangle$	$\hat{\epsilon}_{total}$	$\langle \epsilon_{unrigue} \rangle$	$\hat{\epsilon}_{unrigue}$	Sacrifice	ΔDP
Enriched Source	M1: 23.2 %	26.5 ^{+3.8} _{-3.5} %	0.0 %	0.0 ^{+0.7} _{-0.9} %	2.1 %		
Detector Cut	M2: 42.7 %	62.8 ^{+1.0} _{-7.6} %	0.0 %	0.0 ^{+2.3} _{-0.0} %	4.5 %	-2%	
Multiplicity 2 Cut	M1: 15.4 %	16.3 ^{+3.3} _{-2.8} %	0.0 %	0.0 ^{+0.7} _{-0.7} %	0.0 %	0 %	0 %
n=2	M2: 11.7 %	16.2 ^{+2.8} _{-6.4} %	0.0 %	0.0 ^{+2.3} _{-0.0} %	0.0 %	0 %	0 %
Coincident Energy	M1: 100.0 %	100.0 ^{+0.0} _{-0.0} %	62.7 %	59.9 ^{+4.0} _{-4.1} %	19.0 %		
Cut	M2: 100.0 %	100.0 ^{+2.3} _{-0.0} %	47.8 %	27.9 ^{+7.3} _{-6.3} %	20.5 %	808 %	
Combined Cuts	M1: 100.0 %	100.0 ^{+0.7} _{-0.0} %	—	—	22.9 %		
	M2: 100.0 %	100.0 ^{+0.0} _{-2.3} %	—	—	27.9 %	994 %	

TABLE XXI Table of cut descriptions and efficiencies for simulated backgrounds and measured data for the 559 keV peak.

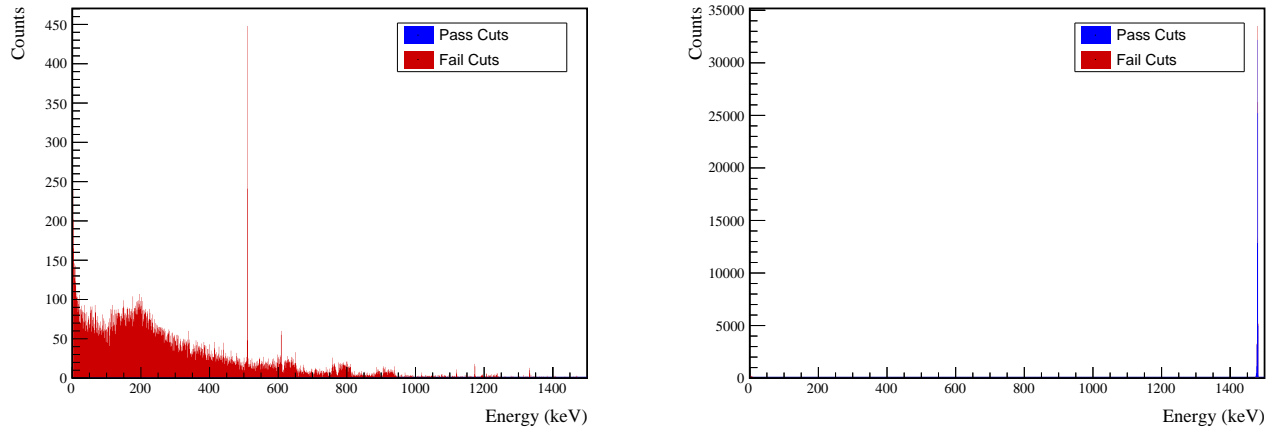


FIG. 77 Effect of 559 keV peak cuts on coincident energy spectra in BG (left) and ES (right) simulations.

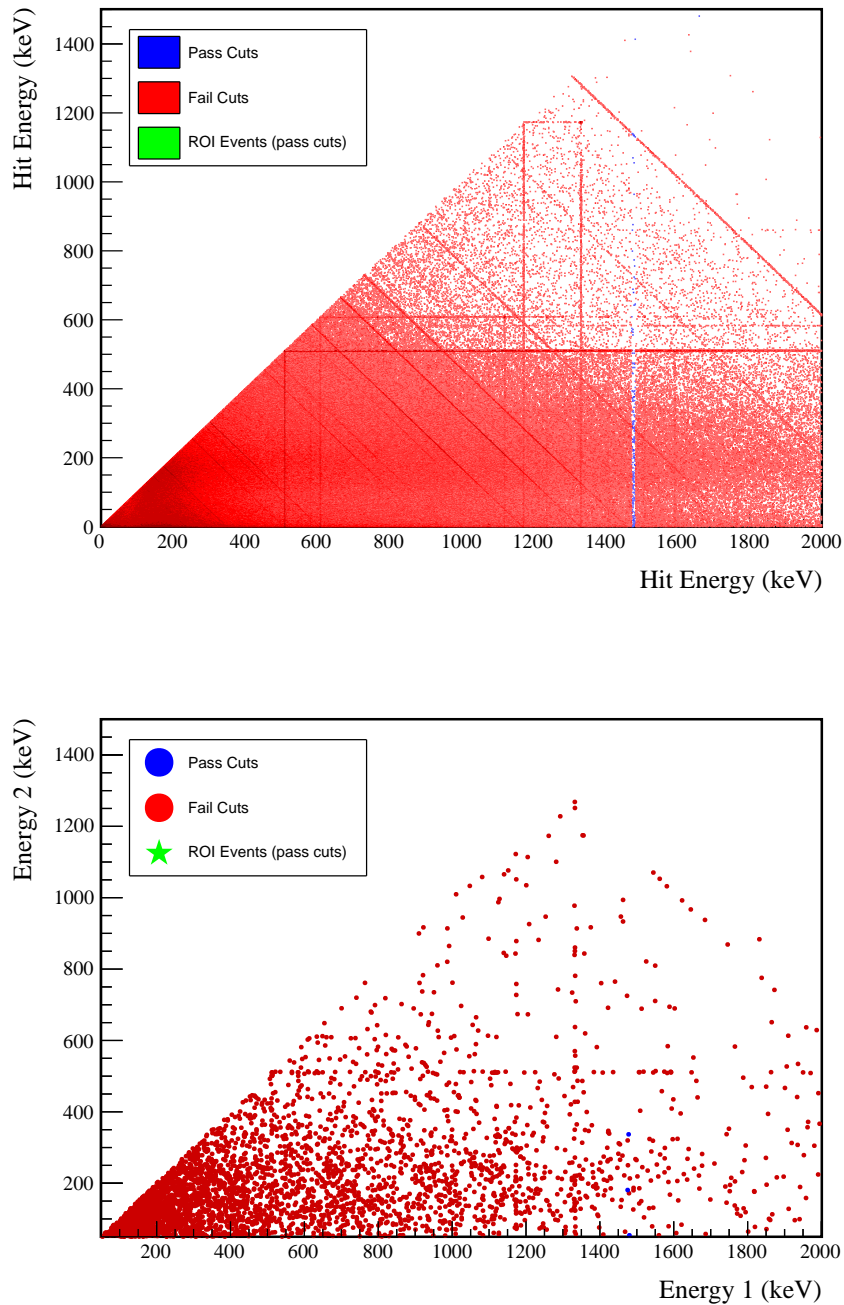
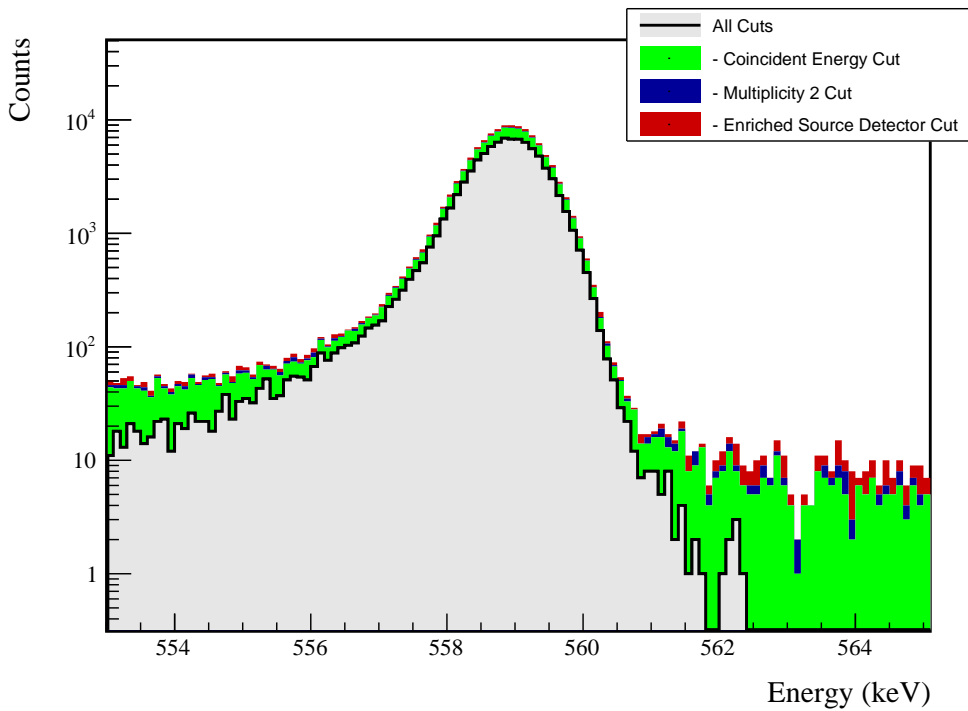


FIG. 78 Simulated (left) and measured (right) multiplicity 2 energy spectrum with sum and coincident energy cuts included for the 559 keV peak.

FIG. 79 Effect of all cuts applied sequentially on ROI for 559 keV peak of $0\nu\beta\beta$ to 2_1^+

Source	Module 1 efficiency	Module 2 efficiency
Multi-Detector with Full Energy γ	$3.0 \pm 0.2\%$	$1.5 \pm 0.5\%$
Region of Interest	$92.1 \pm 1.5\%$	$92.1 \pm 1.5\%$
Dead Layer	$67.8 \pm 5.5\%$	$59.3 \pm 7.1\%$
Detector Dead Times	$97.5 \pm 1.1\%$	$98.0 \pm 0.9\%$
Enriched Source Detector Cut	$97.4 \pm < 0.1\%$	$93.4 \pm < 0.1\%$
Multiplicity 2 Cut	$98.6 \pm < 0.1\%$	$99.2 \pm < 0.1\%$
Coincident Energy Cut	$79.1 \pm 0.3\%$	$76.7 \pm 0.3\%$
Final Efficiency	$1.64 \pm 0.18\%$	$0.70 \pm 0.24\%$

FIG. 80 Table of detection efficiencies for the 559 keV peak.

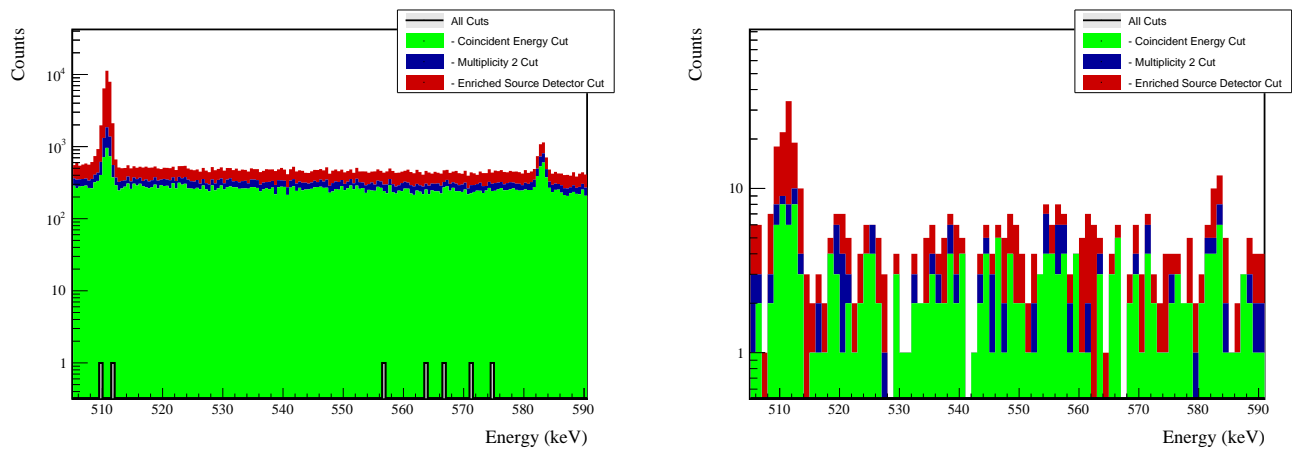
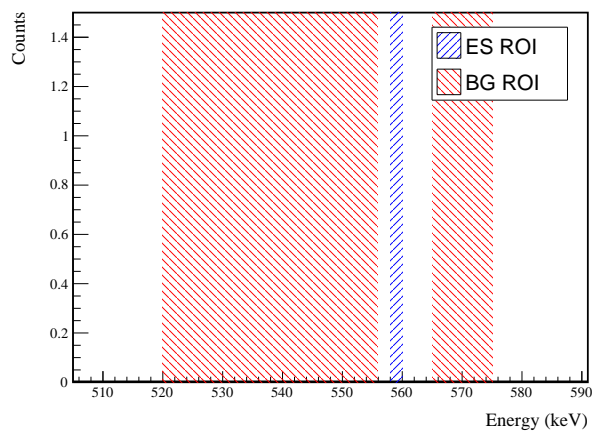


FIG. 81 Effect of all cuts applied to sequentially simulated (left) and measured (right) background data.

FIG. 82 All events after cuts in background (red) and signal (blue) ROIs for 559 keV peak of $0\nu\beta\beta$ to 2_1^+

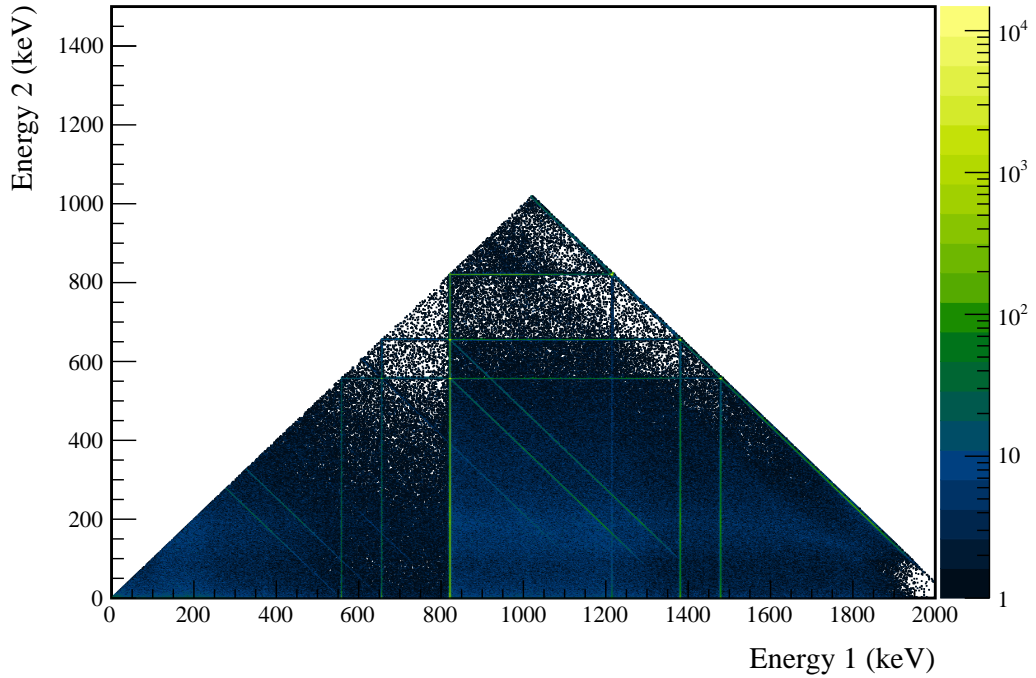
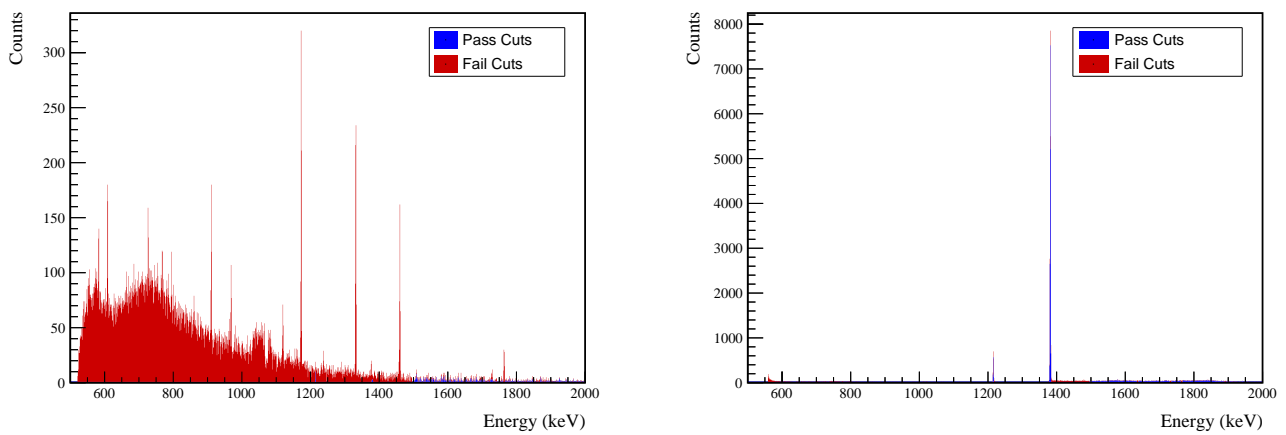
679 **Appendix G: $0\nu\beta\beta$ to 2_2^+** FIG. 83 Simulated multiplicity 2 energy spectrum of the $0\nu\beta\beta$ to 2_2^+ decay mode680 **1. 559 keV peak**

FIG. 84 Effect of 559 keV peak cuts on sum energy spectra in BG (left) and ES (right) simulations.



TABLE XXII Table of energy estimation uncertainties for the 559 keV peak.

DS	E_{peak} (keV)	σ_{drift} (keV)	σ_{fit} (keV)	σ (keV)	$f_{t,fit}$	$\tau_{f,fit}$ (keV)	$\delta_{\mu,fit}$ (keV)	$\delta_{\mu,NL}$ (keV)	$\delta_{\mu,drift}$ (keV)	$\delta_{\mu,xtalk}$ (keV)	δ_u (keV)	FWHM (keV)	$\delta_{fwhm,fit}$ (keV)	$\delta_{fwhm,drift}$ (keV)	$\delta_{fwhm,xtalk}$ (keV)	δ_{FWHM} (keV)	δ_α	$E_{ROI,1}$ (keV)	$E_{ROI,2}$ (keV)	ϵ_{ROI}	$\sigma_{e_{ROI}}$	
DS1	559.101	0.460	0.063	0.464	0.230	0.515	0.001	0.104	0.002	0.012	0.005	0.105	1.152	0.001	0.039	0.011	0.040	0.035	558.084	559.935	0.907	0.012
DS2	559.101	0.461	0.055	0.464	0.249	0.515	0.002	0.067	0.004	0.012	0.005	0.068	1.158	0.001	0.107	0.011	0.108	0.093	558.067	559.933	0.909	0.025
DS3	559.101	0.470	0.066	0.474	0.224	0.505	0.001	0.026	0.024	0.012	0.005	0.038	1.174	0.001	0.073	0.011	0.074	0.063	558.072	559.952	0.913	0.017
DS4	559.101	0.455	0.077	0.461	0.108	0.445	0.002	0.076	0.010	0.012	0.005	0.078	1.111	0.001	0.106	0.011	0.107	0.096	558.187	559.942	0.922	0.026
DS5a	559.101	0.560	0.085	0.567	0.106	0.885	0.002	0.079	0.005	0.012	0.005	0.080	1.367	0.002	0.055	0.011	0.056	0.041	557.976	560.128	0.910	0.012
DS5b	559.101	0.469	0.074	0.475	0.158	0.491	0.001	0.020	0.011	0.012	0.005	0.026	1.157	0.001	0.125	0.011	0.125	0.108	558.123	559.962	0.919	0.029
DS5c	559.101	0.460	0.085	0.468	0.174	0.489	0.001	0.037	0.030	0.012	0.005	0.050	1.145	0.001	0.162	0.011	0.162	0.142	558.124	559.948	0.917	0.037
DS6a	559.101	0.456	0.044	0.458	0.191	0.463	0.001	0.069	0.025	0.012	0.005	0.075	1.123	0.000	0.041	0.011	0.042	0.038	558.135	559.927	0.915	0.011



Cut Name	Cut Description	$\langle \epsilon_{total} \rangle$	$\hat{\epsilon}_{total}$	$\langle \epsilon_{unique} \rangle$	$\hat{\epsilon}_{unique}$	Sacrifice	ΔDP
Enriched Source Detector Cut	Any other detector: isEAr	M1: 23.2 % M2: 42.7 %	26.5 ^{+3.8} _{-2.5} % 62.8 ^{+2.0} _{-7.6} %	0.5 % 0.9 %	0.7 ^{+1.1} _{-0.4} % 7.0 ^{+4.9} _{-3.0} %	1.4 % 3.3 %	10%
Coincident Energy Cut	No other detector: (((energy<65.6) (energy>504.4 && energy<516.4) (energy>591.4 && energy<637.8) (energy>841.8 && energy<868.6) (energy>1074.6 && energy<1175.4) (energy>110.6 && energy<175.) (energy>1205. && (energy>1208.6) && energy<1331. && energy>1331. (energy>1482.6) && isBar) (energy>144.8) (energy>507.8 && energy<524.6) (energy>1375.4) && i isEAr) && energy<1214.) (sumE<1216.2 && sumE<1377.6) (sumE>1383.6 && sumE<1495.8) (sumE>1761.8 && sumE<1765.8) (sumE>2041.6)	M1: 25.2 % M2: 24.4 %	29.9 ^{+3.9} _{-3.6} % 25.6 ^{+3.2} _{-6.0} %	0.6 % 0.4 %	2.0 ^{+1.5} _{-0.9} % 7.0 ^{+4.9} _{-3.0} %	3.1 % 1.8 %	5%
Sum Energy Cut	Note: 1.383.6 % (sumE>1383.6 && sumE<1495.8) (sumE>1761.8 && sumE<1765.8) (sumE>2041.6)	M1: 97.1 % M2: 97.6 %	95.9 ^{+1.3} _{-2.0} % 86.0 ^{+2.0} _{-4.5} %	54.4 % 40.3 %	51.7 ^{+4.1} _{-6.0} % 25.6 ^{+7.2} _{-6.0} %	18.3 % 20.4 %	192%
Combined Cuts		M1: 98.3 % M2: 99.0 %	98.6 ^{+0.7} _{-0.7} % 100.0 ^{+0.0} _{-2.3} %	—	—	31.5 % 40.6 %	226%

TABLE XXXIII Table of cut descriptions and efficiencies for simulated backgrounds and measured data for the 559 keV peak.

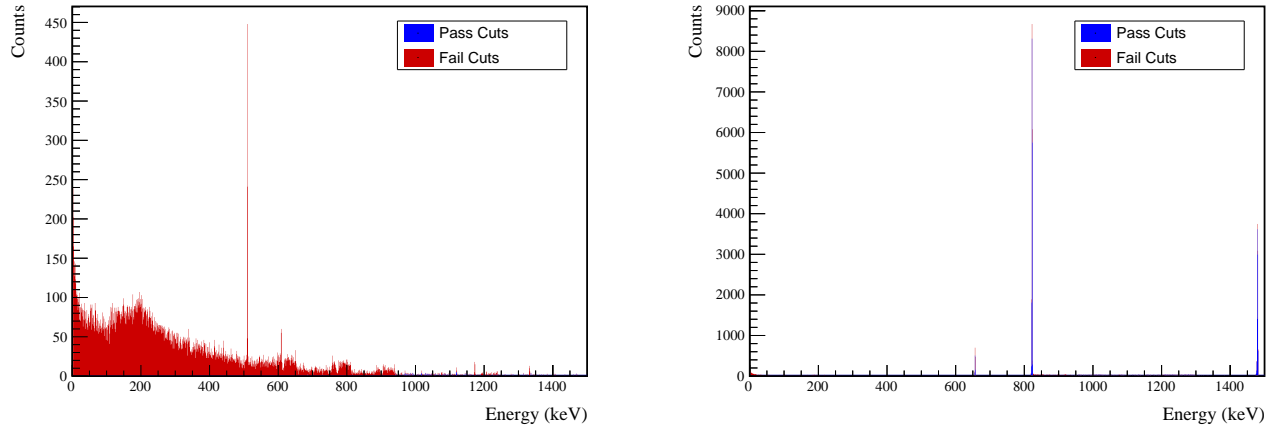


FIG. 85 Effect of 559 keV peak cuts on coincident energy spectra in BG (left) and ES (right) simulations.

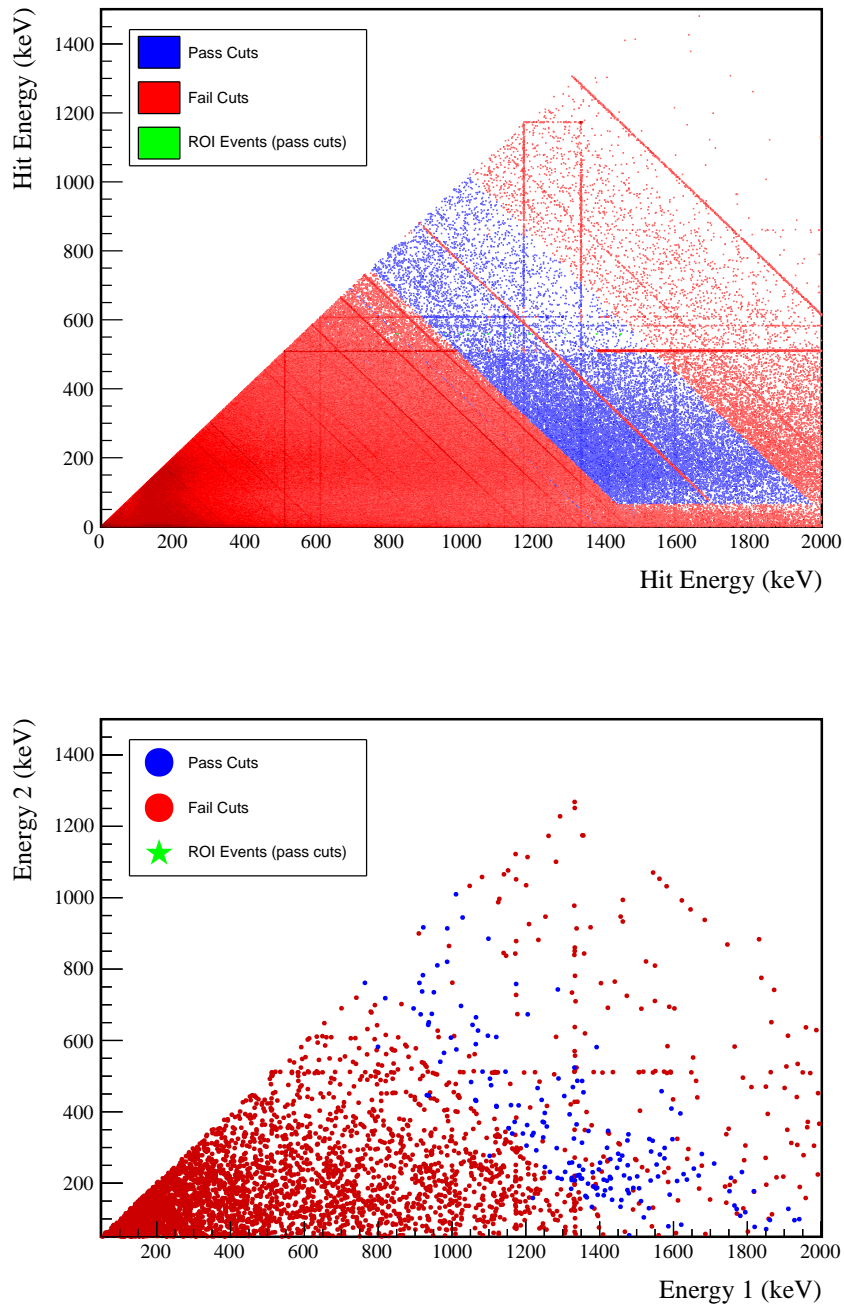
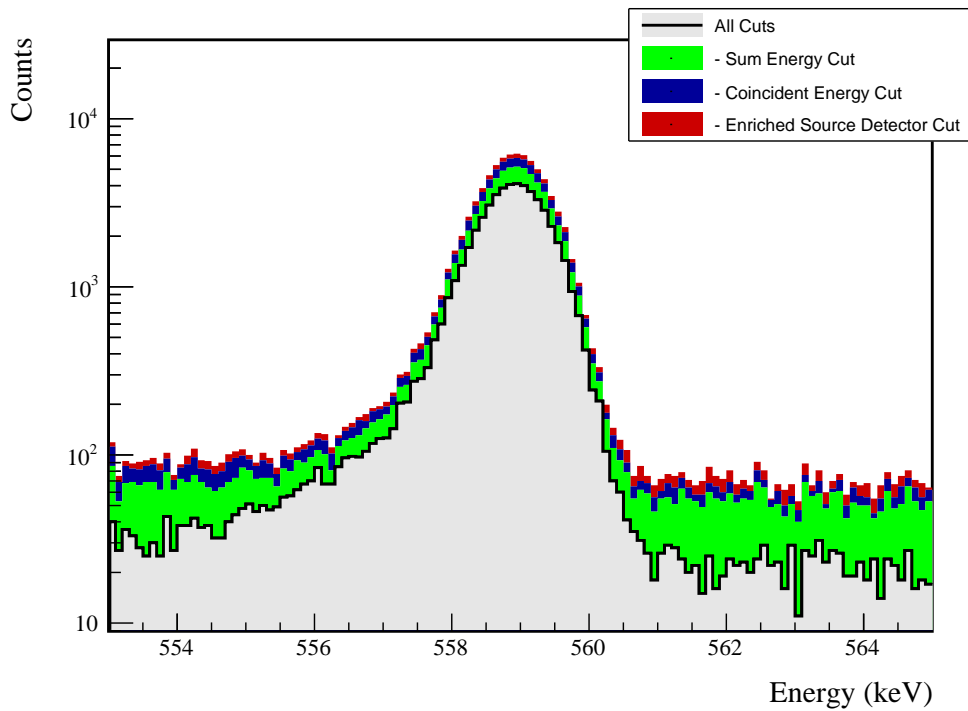


FIG. 86 Simulated (left) and measured (right) multiplicity 2 energy spectrum with sum and coincident energy cuts included for the 559 keV peak.

FIG. 87 Effect of all cuts applied sequentially on ROI for 559 keV peak of $0\nu\beta\beta$ to 2_2^+

Source	Module 1 efficiency	Module 2 efficiency
Multi-Detector with Full Energy γ	$1.9 \pm 0.2\%$	$1.0 \pm 0.5\%$
Region of Interest	$91.3 \pm 1.6\%$	$91.3 \pm 1.6\%$
Dead Layer	$68.5 \pm 5.4\%$	$60.3 \pm 7.0\%$
Detector Dead Times	$97.6 \pm 1.1\%$	$98.1 \pm 0.9\%$
Enriched Source Detector Cut	$96.8 \pm <0.1\%$	$89.6 \pm <0.1\%$
Coincident Energy Cut	$89.5 \pm 0.3\%$	$88.6 \pm 0.3\%$
Sum Energy Cut	$73.2 \pm 0.3\%$	$65.3 \pm 0.3\%$
Final Efficiency	$0.98 \pm 0.13\%$	$0.42 \pm 0.20\%$

FIG. 88 Table of detection efficiencies for the 559 keV peak.

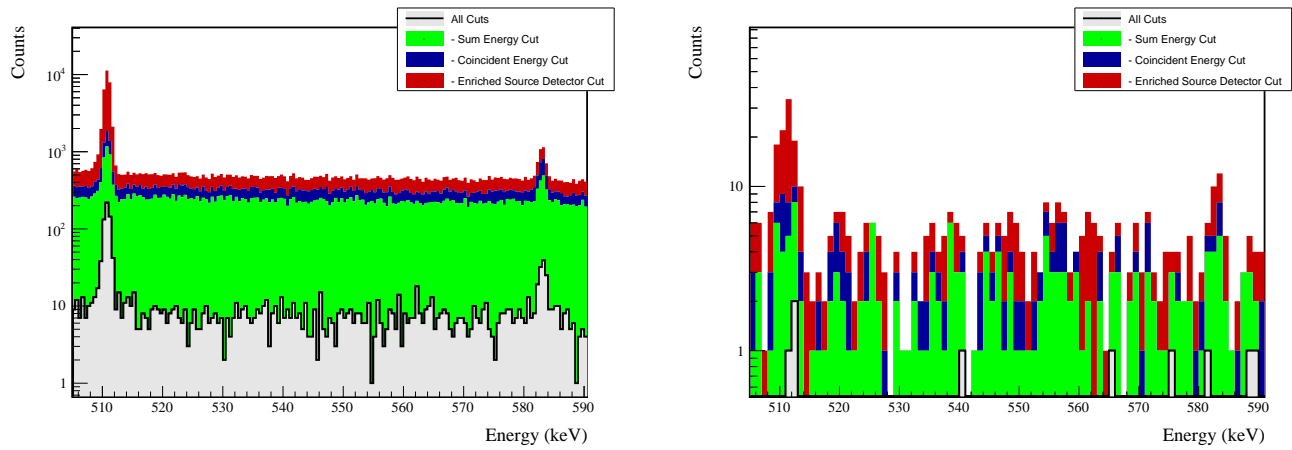
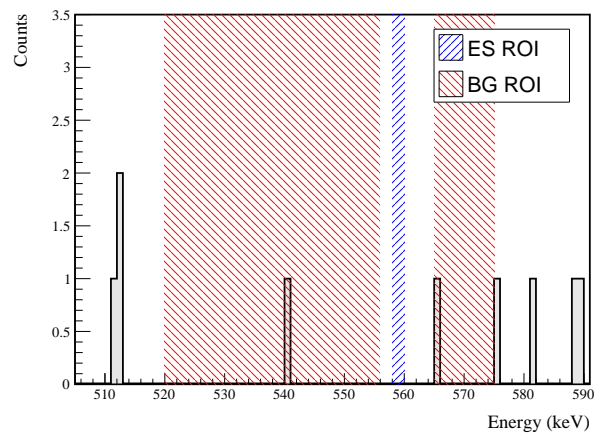


FIG. 89 Effect of all cuts applied to sequentially simulated (left) and measured (right) background data.

FIG. 90 All events after cuts in background (red) and signal (blue) ROIs for 559 keV peak of $0\nu\beta\beta$ to 2_2^+

681 2. 657 keV peak

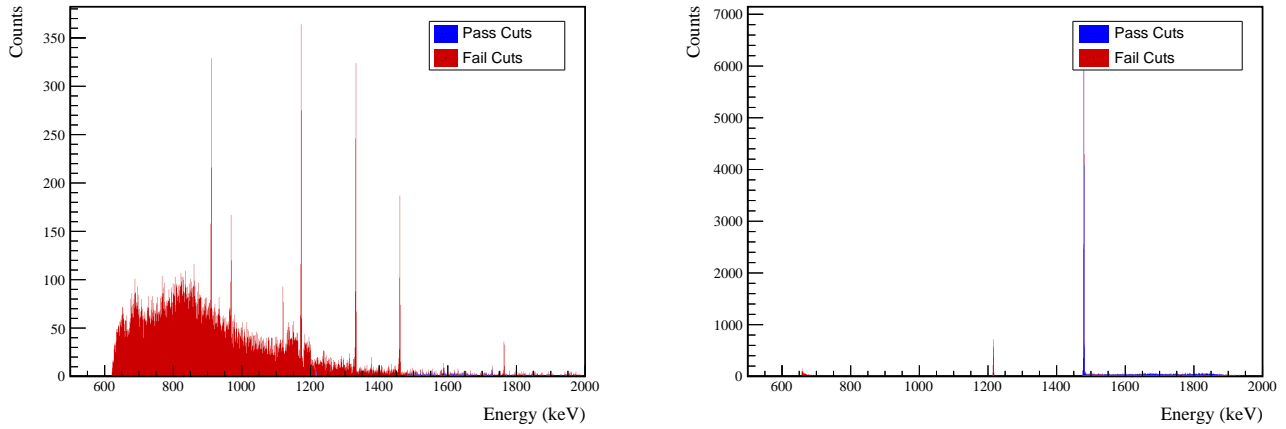


FIG. 91 Effect of 657 keV peak cuts on sum energy spectra in BG (left) and ES (right) simulations.

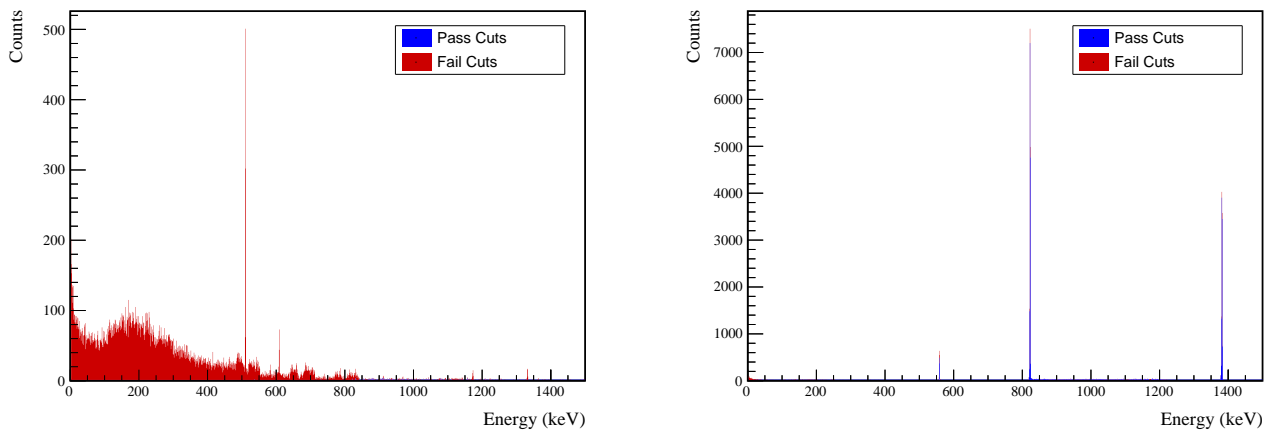


FIG. 92 Effect of 657 keV peak cuts on coincident energy spectra in BG (left) and ES (right) simulations.



TABLE XXIV Table of energy estimation uncertainties for the 657 keV peak.

DS	E_{peak} (keV)	$\sigma_{fit,t}$ (keV)	σ_{drift} (keV)	$f_{t,fit}$	σ (keV)	$\tau_{f,fit}$ (keV)	$\delta_{\mu,fit}$ (keV)	$\delta_{\mu,NL}$ (keV)	$\delta_{\mu,drift}$ (keV)	$\delta_{\mu,xtalk}$ (keV)	δ_u (keV)	FWHM	$\delta_{fwhm,fit}$ (keV)	$\delta_{fwhm,drift}$ (keV)	$\delta_{fwhm,xtalk}$ (keV)	δ_{FWHM} (keV)	δ_α	$E_{ROI,1}$ (keV)	$E_{ROI,2}$ (keV)	ϵ_{ROI}	$\sigma_{e_{ROI}}$	
DS1	657.041	0.500	0.074	0.505	0.230	0.579	0.002	0.104	0.003	0.012	0.005	0.105	1.256	0.001	0.039	0.011	0.040	0.032	656.019	657.882	0.883	0.013
DS2	657.041	0.502	0.064	0.506	0.249	0.580	0.002	0.067	0.005	0.012	0.005	0.068	1.263	0.001	0.107	0.011	0.108	0.085	656.002	657.881	0.885	0.026
DS3	657.041	0.510	0.078	0.516	0.224	0.568	0.002	0.026	0.026	0.012	0.005	0.040	1.278	0.001	0.073	0.011	0.074	0.058	656.007	657.899	0.889	0.018
DS4	657.041	0.493	0.090	0.501	0.108	0.490	0.002	0.076	0.076	0.012	0.005	0.078	1.207	0.001	0.106	0.011	0.107	0.088	656.120	657.890	0.899	0.028
DS5a	657.041	0.606	0.100	0.614	0.106	0.924	0.002	0.079	0.006	0.012	0.005	0.080	1.481	0.002	0.055	0.011	0.056	0.038	655.915	658.075	0.887	0.012
DS5b	657.041	0.509	0.087	0.517	0.158	0.562	0.001	0.020	0.013	0.012	0.005	0.027	1.259	0.001	0.125	0.011	0.125	0.100	656.056	657.909	0.895	0.031
DS5c	657.041	0.500	0.100	0.510	0.174	0.555	0.002	0.037	0.035	0.012	0.005	0.053	1.247	0.001	0.162	0.011	0.162	0.130	656.057	657.896	0.893	0.040
DS6a	657.041	0.495	0.051	0.497	0.191	0.524	0.001	0.069	0.030	0.012	0.005	0.076	1.221	0.001	0.041	0.011	0.042	0.035	656.070	657.874	0.891	0.012



Cut Name	Cut Description	$\langle \epsilon_{total} \rangle$	$\hat{\epsilon}_{total}$	$\langle \epsilon_{unique} \rangle$	$\hat{\epsilon}_{unique}$	Sacrifice	ΔDP
Enriched Source Detector Cut	Any other detector: isEsr No other detector: (((energy<59.) (energy>422.6 && energy<562.4 && energy>616.6) (energy>776.8 && energy<529.4) (energy>159.6 && energy<1175.) (energy>133.2 && energy<18.8) (energy>308. && energy<384.8) (energy>1533.2 && energy>384.8) && isEsr) ((energy<52.2) (energy>491.6 && energy<554.8) (energy>1248.) && :isEsr) (sumE<1214.8) (sumE>1216.8 && sumE<1475.2) (sumE>1757.6 && sumE<1766.) (sumE>2042.6) (sumE>2042.6))	M1: 23.9 % M2: 43.7 %	25.2 ^{+3.9} _{-3.5} % 60.4 ^{+6.8} _{-7.2} %	0.6 % 1.2 %	3.7 ^{+2.0} _{-1.3} % 4.2 ^{+3.9} _{-2.1} %	1.4 % 3.7 %	1.2 %
Coincident Energy Cut	M1: 30.4 % M2: 29.1 %	25.2 ^{+3.9} _{-3.5} % 16.7 ^{+6.0} _{-4.7} %	0.8 % 0.6 %	2.2 ^{+1.7} _{-1.0} % 2.1 ^{+3.2} _{-1.3} %	4.9 % 3.2 %	4.9 % 3.2 %	7 %
Sum Energy Cut	M1: 96.9 % M2: 97.0 %	88.9 ^{+2.4} _{-3.0} % 91.7 ^{+3.2} _{-4.9} %	49.8 % 36.9 %	48.9 ^{+4.3} _{-4.3} % 27.1 ^{+6.8} _{-5.9} %	11.6 % 13.6 %	11.6 % 13.6 %	207 %
Combined Cuts	M1: 98.5 % M2: 99.0 %	94.8 ^{+2.3} _{-1.6} % 97.9 ^{+1.3} _{-3.2} %	— —	— —	25.7 % 34.9 %	25.7 % 34.9 %	255 %

TABLE XXV Table of cut descriptions and efficiencies for simulated backgrounds and measured data for the 657 keV peak.

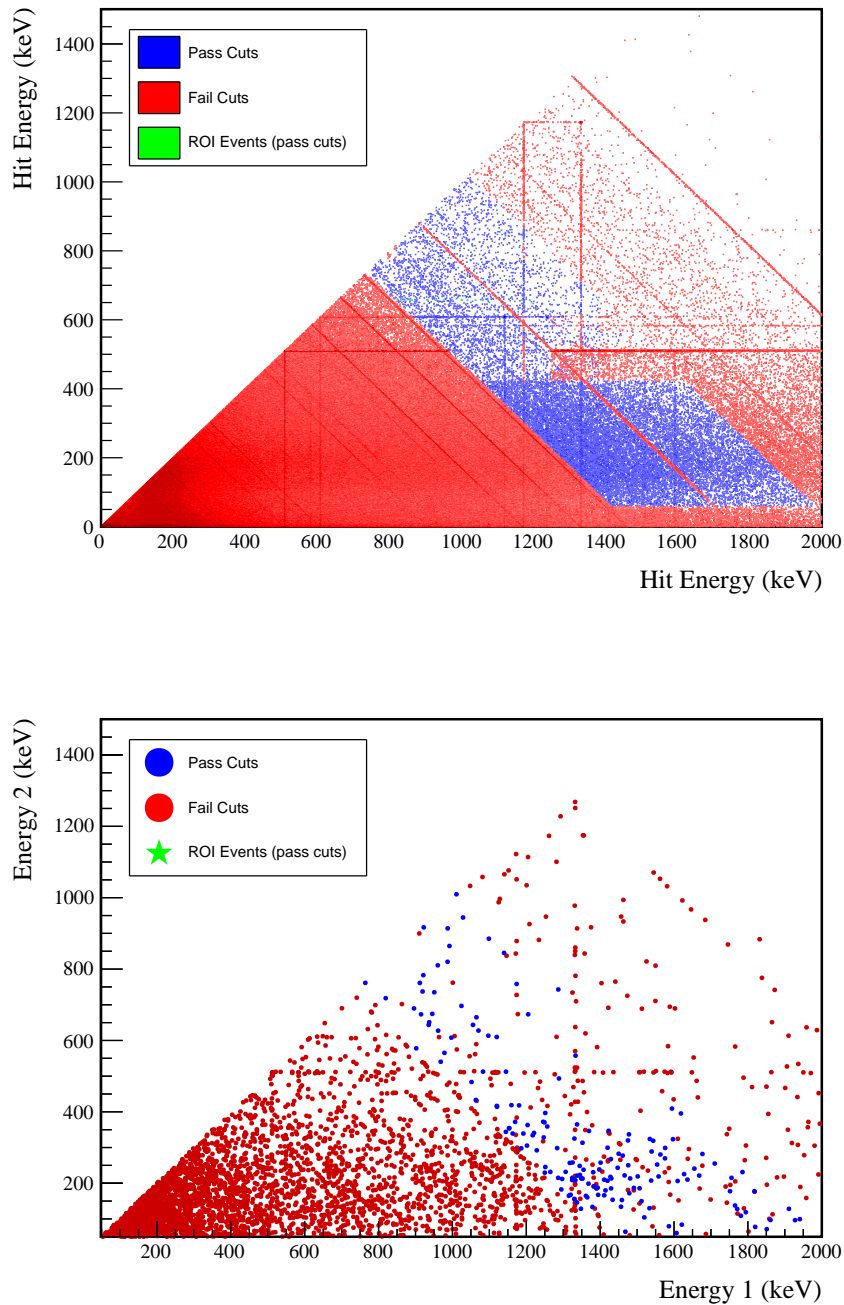
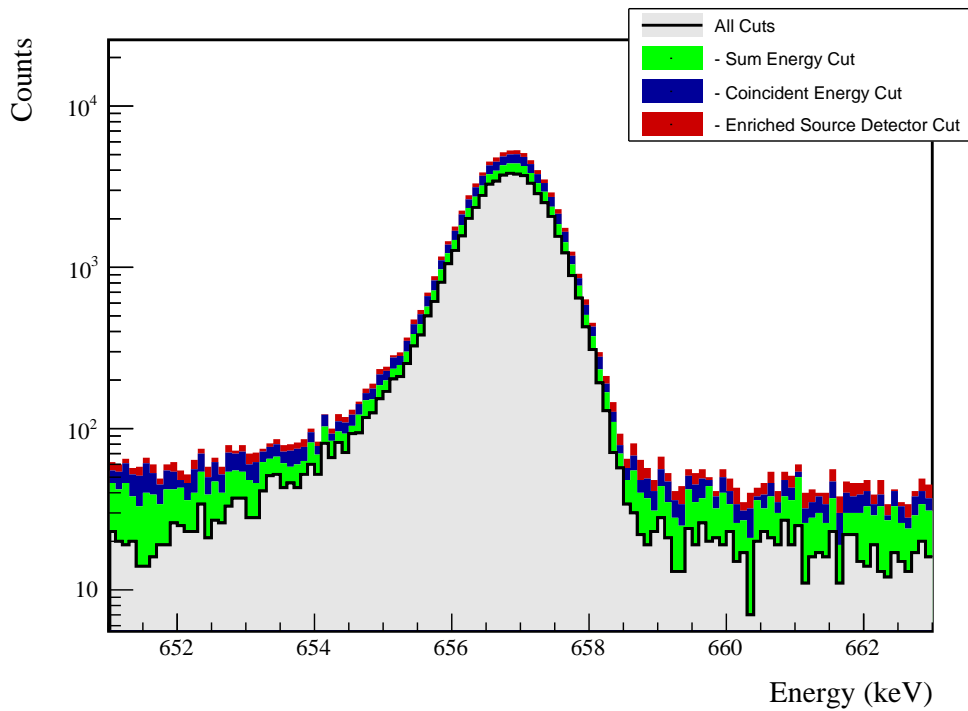


FIG. 93 Simulated (left) and measured (right) multiplicity 2 energy spectrum with sum and coincident energy cuts included for the 657 keV peak.

FIG. 94 Effect of all cuts applied sequentially on ROI for 657 keV peak of $0\nu\beta\beta$ to 2_2^+

Source	Module 1 efficiency	Module 2 efficiency
Multi-Detector with Full Energy γ	$1.8 \pm 0.2\%$	$1.0 \pm 0.5\%$
Region of Interest	$89.0 \pm 1.7\%$	$89.0 \pm 1.7\%$
Dead Layer	$69.6 \pm 5.2\%$	$61.1 \pm 6.8\%$
Detector Dead Times	$97.6 \pm 1.1\%$	$98.1 \pm 0.9\%$
Enriched Source Detector Cut	$96.8 \pm <0.1\%$	$89.4 \pm <0.1\%$
Coincident Energy Cut	$88.4 \pm 0.3\%$	$87.1 \pm 0.3\%$
Sum Energy Cut	$80.9 \pm 0.3\%$	$72.9 \pm 0.3\%$
Final Efficiency	$0.95 \pm 0.13\%$	$0.41 \pm 0.21\%$

FIG. 95 Table of detection efficiencies for the 657 keV peak.

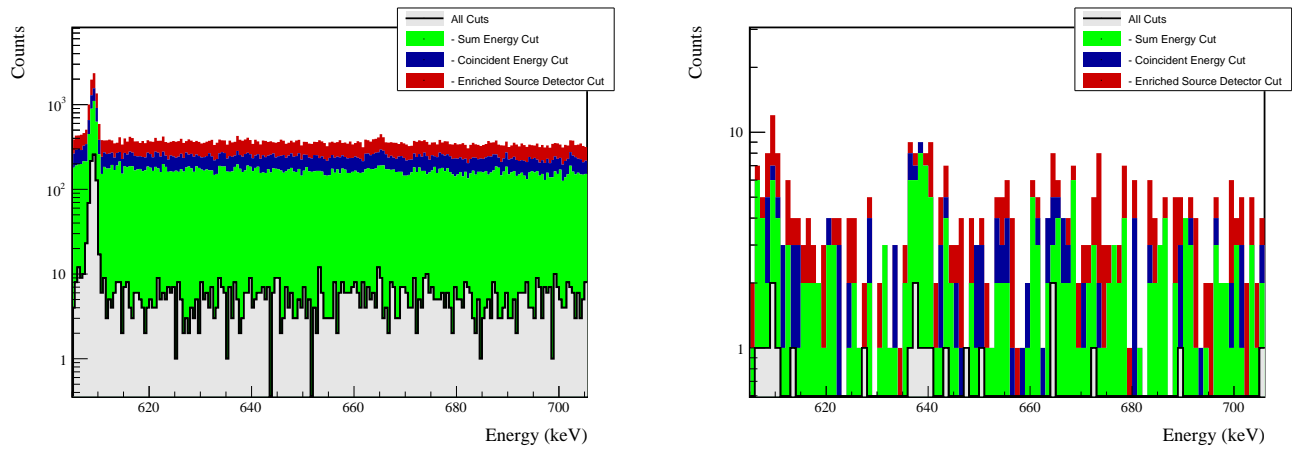
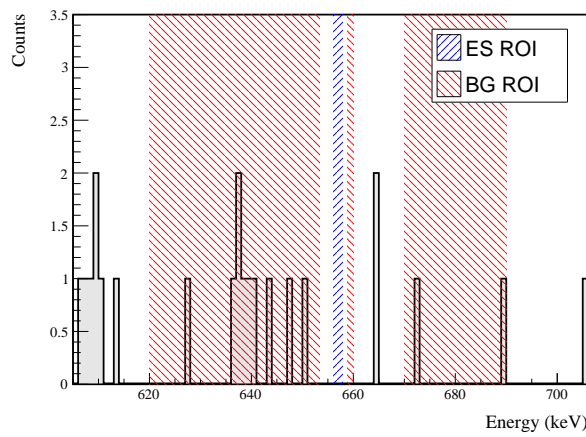


FIG. 96 Effect of all cuts applied to sequentially simulated (left) and measured (right) background data.

FIG. 97 All events after cuts in background (red) and signal (blue) ROIs for 657 keV peak of $0\nu\beta\beta$ to 2_2^+



682 3. 1216 keV peak

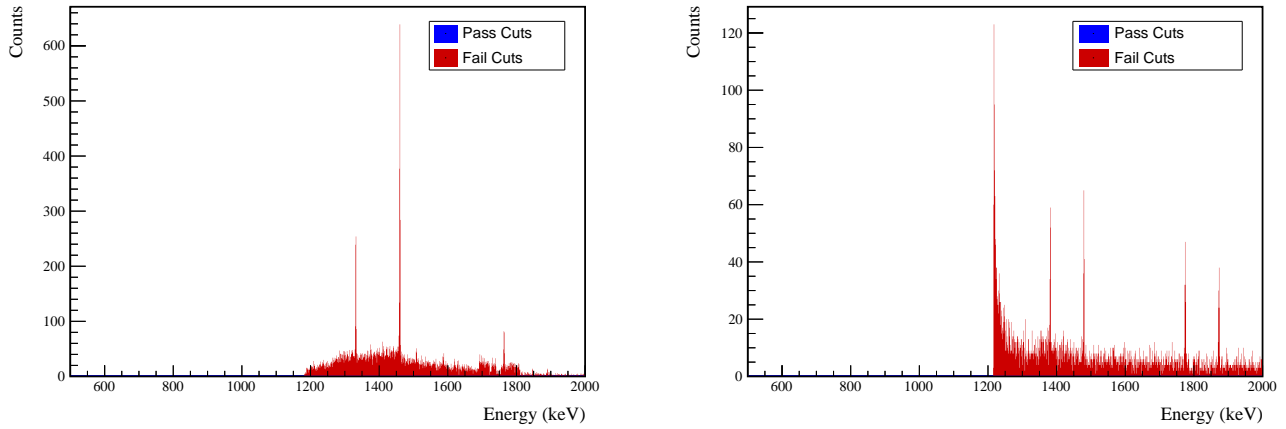


FIG. 98 Effect of 1216 keV peak cuts on sum energy spectra in BG (left) and ES (right) simulations.

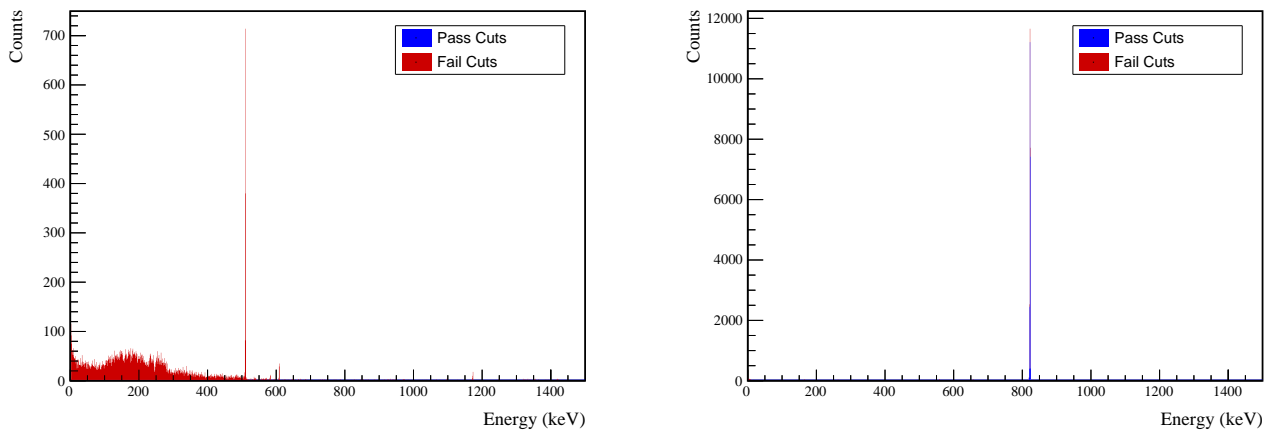


FIG. 99 Effect of 1216 keV peak cuts on coincident energy spectra in BG (left) and ES (right) simulations.



TABLE XXVI Table of energy estimation uncertainties for the 1216 keV peak.

DS	E_{peak} (keV)	$\sigma_{f,fit}$ (keV)	σ_{drift} (keV)	σ (keV)	$f_{t,fit}$	τ_{fit} (keV)	$\delta_{\mu,fit}$ (keV)	$\delta_{\mu,NL}$ (keV)	$\delta_{\mu,drift}$ (keV)	$\delta_{\mu,xtalk}$ (keV)	$\delta_{\mu,peak}$ (keV)	δ_μ (keV)	FWHM	$\delta_{f,whm,fit}$ (keV)	$\delta_{f,whm,xtalk}$ (keV)	δ_{FWHM} (keV)	$\delta_{ROI,1}$ (keV)	$E_{ROI,1}$ (keV)	$E_{ROI,2}$ (keV)	ϵ_{ROI}	$\sigma_{e_{ROI}}$	
DS1	1216.104	0.705	0.137	0.718	0.230	0.945	0.003	0.104	0.005	0.012	0.020	0.107	1.787	0.001	0.039	0.011	0.040	0.023	1214.426	1217.449	0.914	0.006
DS2	1216.104	0.710	0.119	0.720	0.249	0.951	0.003	0.067	0.008	0.012	0.020	0.072	1.803	0.001	0.107	0.011	0.108	0.060	1214.387	1217.449	0.914	0.014
DS3	1216.104	0.715	0.144	0.729	0.224	0.925	0.003	0.026	0.051	0.012	0.020	0.062	1.812	0.001	0.073	0.011	0.074	0.041	1214.416	1217.470	0.917	0.010
DS4	1216.104	0.697	0.167	0.717	0.108	0.746	0.003	0.076	0.022	0.012	0.020	0.083	1.726	0.001	0.106	0.011	0.107	0.062	1214.621	1217.461	0.932	0.015
DS5a	1216.104	0.838	0.185	0.859	0.106	1.316	0.004	0.079	0.012	0.012	0.020	0.083	2.070	0.002	0.055	0.011	0.056	0.027	1214.323	1217.722	0.921	0.007
DS5b	1216.104	0.716	0.161	0.734	0.158	0.963	0.002	0.020	0.024	0.012	0.020	0.039	1.791	0.001	0.125	0.011	0.125	0.070	1214.506	1217.487	0.922	0.017
DS5c	1216.104	0.703	0.185	0.727	0.174	0.932	0.003	0.037	0.066	0.012	0.020	0.079	1.783	0.001	0.162	0.011	0.162	0.091	1214.497	1217.474	0.921	0.022
DS6a	1216.104	0.693	0.095	0.700	0.191	0.873	0.002	0.069	0.055	0.012	0.020	0.092	1.723	0.001	0.041	0.011	0.042	0.025	1214.535	1217.422	0.920	0.006



Cut Name	Cut Description	$\langle \epsilon_{total} \rangle$	$\hat{\epsilon}_{total}$	$\langle \epsilon_{unique} \rangle$	$\hat{\epsilon}_{unique}$	Sacrifice	ΔDP
Enriched Source	Any other detector: isEnr	M1: 26.9 %	16.9 ^{+4.5} / _{-3.7} %	0.0 %	0.0 ^{+1.2} / _{-0.0} %	2.0 %	-2%
Detector Cut		M2: 43.9 %	61.9 ^{+9.8} / _{-10.9} %	0.0 %	0.0 ^{+4.5} / _{-0.0} %	4.3 %	
Multiplicity 2 Cut	m==2	M1: 15.3 %	16.9 ^{+4.5} / _{-3.7} %	0.0 %	0.0 ^{+1.2} / _{-0.0} %	0.0 %	0%
		M2: 11.9 %	9.5 ^{+8.4} / _{-4.7} %	0.0 %	0.0 ^{+4.5} / _{-0.0} %	0.0 %	
Coincident Energy Cut	Any other detector: energy>817.7 && energy<826.4	M1: 100.0 %	100.0 ^{+0.0} / _{-1.2} %	59.6 %	68.7 ^{+4.8} / _{-5.3} %	18.7 %	555%
Combined Cuts		M2: 100.0 %	100.0 ^{+0.0} / _{-4.5} %	46.6 %	33.3 ^{+10.8} / _{-9.3} %	17.9 %	
		M1: 100.0 %	100.0 ^{+0.0} / _{-1.2} %	—	—	25.2 %	
		M2: 100.0 %	100.0 ^{+0.0} / _{-4.5} %	—	—	28.7 %	669%

TABLE XXVII Table of cut descriptions and efficiencies for simulated backgrounds and measured data for the 1216 keV peak.

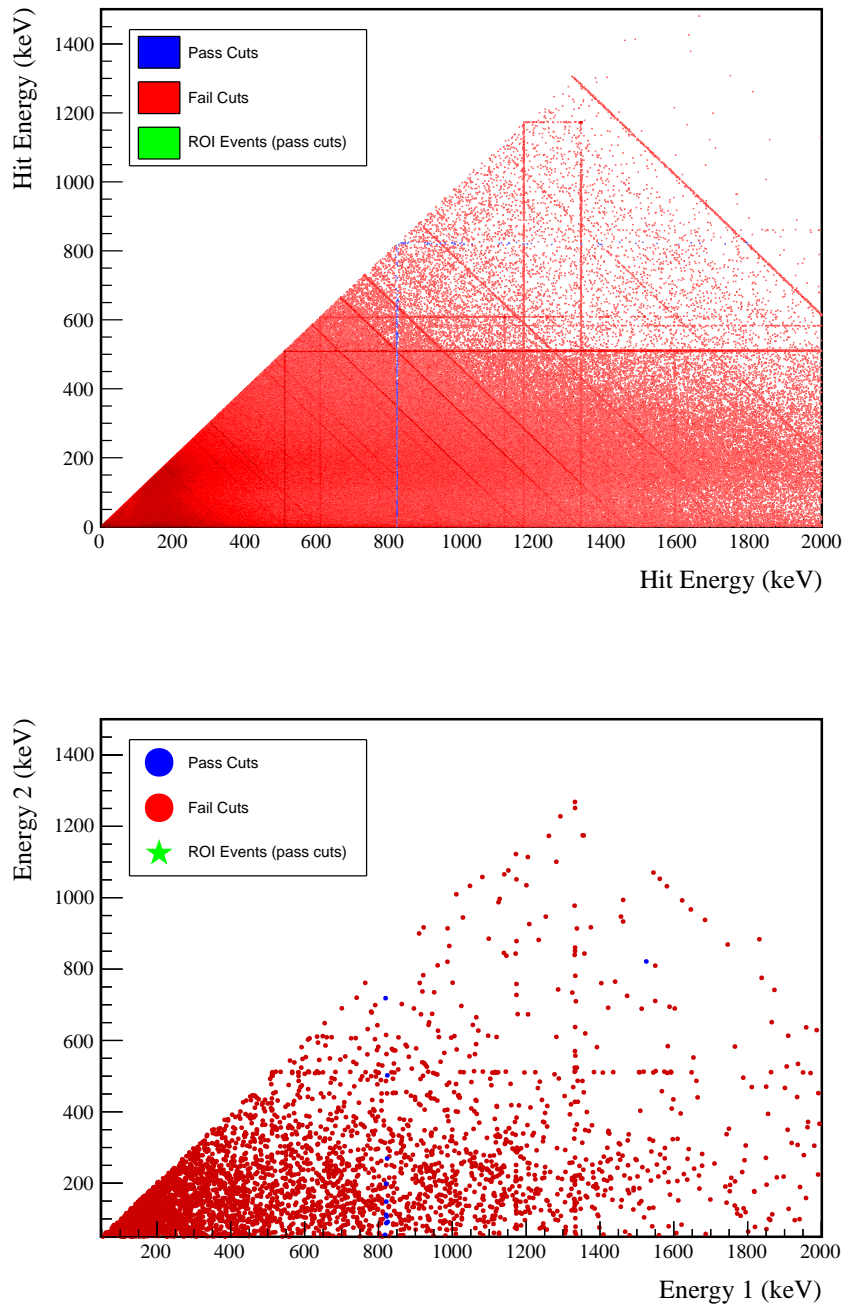
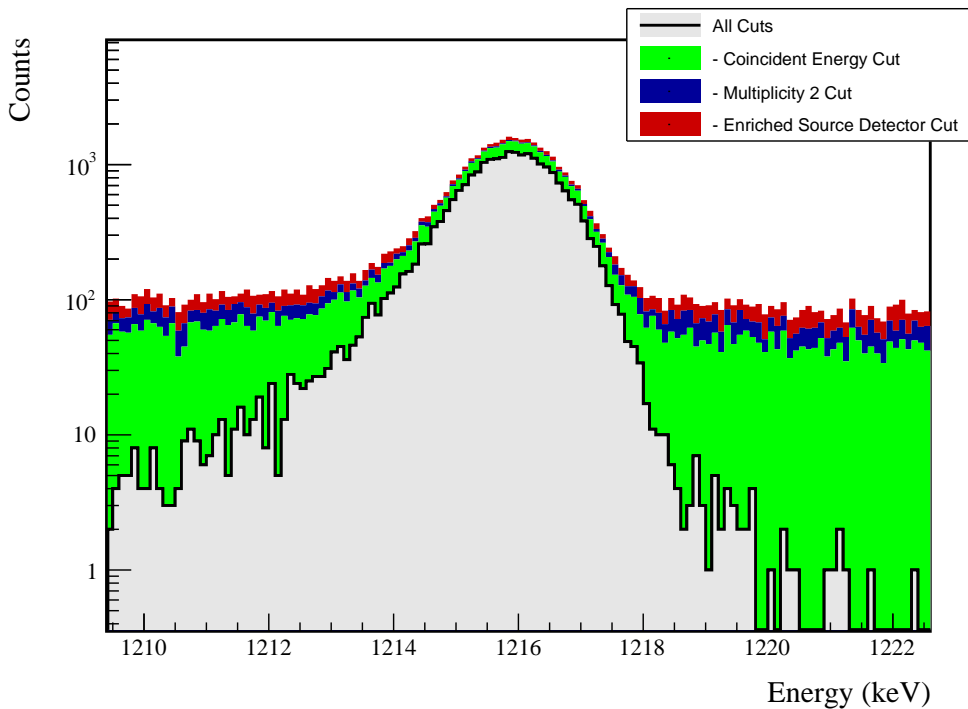


FIG. 100 Simulated (left) and measured (right) multiplicity 2 energy spectrum with sum and coincident energy cuts included for the 1216 keV peak.

FIG. 101 Effect of all cuts applied sequentially on ROI for 1216 keV peak of $0\nu\beta\beta$ to 2_2^+

Source	Module 1 efficiency	Module 2 efficiency
Multi-Detector with Full Energy γ	$0.8 \pm 0.2\%$	$0.4 \pm 0.5\%$
Region of Interest	$92.0 \pm 0.9\%$	$92.0 \pm 0.9\%$
Dead Layer	$68.8 \pm 5.3\%$	$61.2 \pm 6.8\%$
Detector Dead Times	$97.5 \pm 1.1\%$	$98.0 \pm 0.9\%$
Enriched Source Detector Cut	$96.1 \pm < 0.1\%$	$90.8 \pm < 0.1\%$
Multiplicity 2 Cut	$97.3 \pm < 0.1\%$	$98.2 \pm < 0.1\%$
Coincident Energy Cut	$76.9 \pm 0.3\%$	$75.7 \pm 0.3\%$
Final Efficiency	$0.44 \pm 0.12\%$	$0.19 \pm 0.22\%$

FIG. 102 Table of detection efficiencies for the 1216 keV peak.

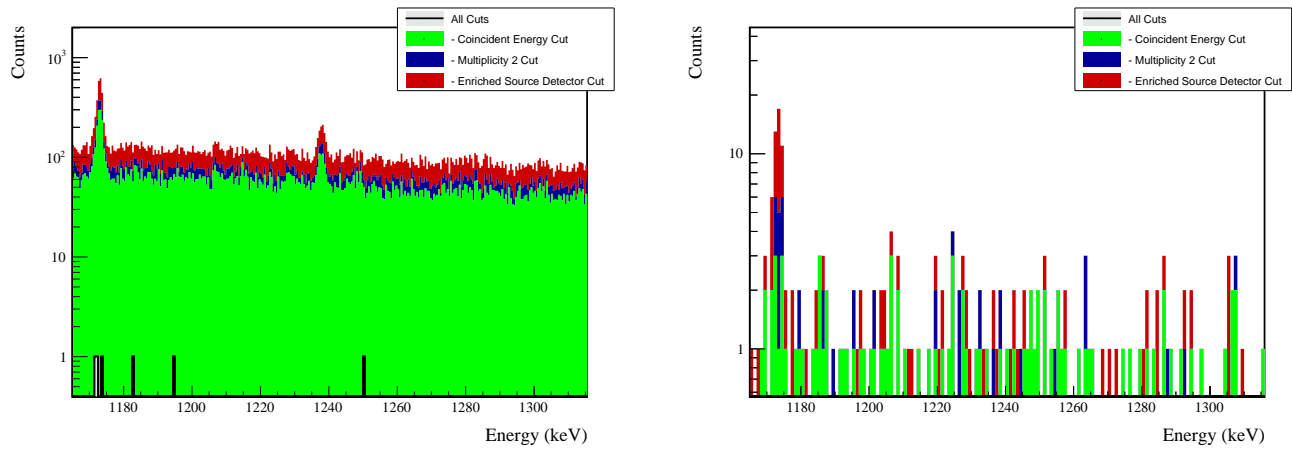
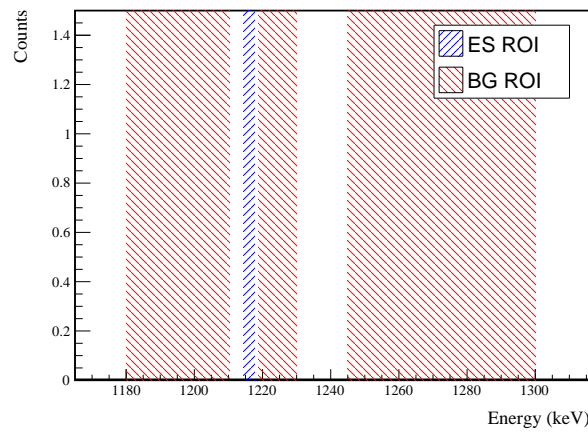


FIG. 103 Effect of all cuts applied to sequentially simulated (left) and measured (right) background data.

FIG. 104 All events after cuts in background (red) and signal (blue) ROIs for 1216 keV peak of $0\nu\beta\beta$ to 2_2^+



683 Appendix H: Sensitivity and Discovery Potential

684 When performing rare event searches in the presence of backgrounds, it is often useful to select regions of interest
685 and data cleaning cuts that optimize the experimental sensitivity. Median $n\sigma$ count sensitivity, $\hat{S}(\bar{B}, n_\sigma)$ is defined as
686 the median upper limit of an $n\sigma$ confidence interval on the number of observed signal counts, assuming the presence
687 of no signal and backgrounds sampled from a distribution based on measured background level \bar{B} . A similar quantity,
688 $n\sigma$ discovery sensitivity, is defined as the true strength of a signal that would produce a discovery with significance
689 $n\sigma$ 50% of the time. Unlike median sensitivity, discovery sensitivity accounts for the distribution in the number
690 of counts that would be seen based on the true rate. For this reason, discovery sensitivity is a slightly more useful
691 quantity when projecting or optimizing an experiment's sensitivity, even though median (or mean) sensitivity is the
692 quantity that is usually reported. For the purpose of this appendix, we will focus on discovery sensitivity.

693 The sensitivity of the experiment to the total rate of the process being searched for is

$$\hat{\Gamma}(\bar{B}, \epsilon, n_\sigma) \propto \frac{\hat{S}(\bar{B}, n_\sigma)}{\epsilon} \quad (H1)$$

694 where ϵ is the total detection efficiency of the signal being sought. Optimizing event selection for a search requires
695 balancing the tradeoff between reducing backgrounds, which will decrease $\hat{S}(\bar{B})$, and improving signal detection
696 efficiency.

697 When optimizing a search, it is useful to use certain approximations when calculating sensitivity. In the high
698 background limit, a common approximation is to assume the backgrounds measured will have a gaussian distribution
699 with standard deviation of $\sqrt{\bar{B}}$. In this case, the discovery (and median) sensitivity will be

$$\hat{S}(\bar{B}, n_\sigma) = n_\sigma * \sqrt{\bar{B}} \quad (H2)$$

700 This approximation fails, however, in the low background limit, where a better approximation is that the background
701 will instead be sampled from a Poisson distribution with mean counts \bar{B} . Because the Poisson distribution is a PDF
702 over a discrete variable, the resultant sensitivity will have step-like properties and must be solved for using a toy
703 Monte Carlo, properties that are not ideal for performing sensitivity optimizations. For this reason, when computing
704 the sensitivity we instead use the analytic continuation of the CDF of the poisson distribution, which is the lower
705 incomplete gamma function

$$\gamma(s, x) = \frac{1}{\Gamma(s)} \int_0^x t^{s-1} e^{-t} dt \quad (H3)$$

706 In this case, we can find the sensitivity, by first numerically solving for the number of counts required for an n -sigma
707 discovery, \hat{N} , with expected backgrounds \bar{B} , where

$$\gamma(\hat{N} + 1, \bar{B}) = \operatorname{erfc}\left(\frac{n_\sigma}{\sqrt{2}}\right) \quad (H4)$$

708 To get the median sensitivity, we then numerically solve

$$\gamma(\hat{N} + 1, \bar{B} + \hat{S}) = 0.5 \quad (H5)$$

709 We define the function found by solving these equations to be the discovery potential[15],

$$\hat{S}(\bar{B}, n_\sigma) = \operatorname{DP}(\bar{B}, n_\sigma) \quad (H6)$$

710 For the purposes of this dissertation, we always use the 3-sigma discovery potential

$$\operatorname{DP}(\bar{B}) = \operatorname{DP}(\bar{B}, 3) \quad (H7)$$

711 Figure 105 shows a comparison of the gaussian approximation for sensitivity to the discovery potential. This function is
712 implemented in `GATPeakShapeUtils.hh` as
713 `GATPeakShapeFunction::DiscoveryLimit`.

714 Next, we want to figure out how we will use these quantities to optimize our data selection. To determine whether
715 it is worth adding a cut or modifying a cut, consider the efficiency and expected background counts before and after
716 applying the cut (ϵ_i , \bar{B}_i and ϵ_f , \bar{B}_f , respectively). A cut represents an improvement if

$$\frac{\hat{S}(\bar{B}_f)}{\epsilon_f} < \frac{\hat{S}(\bar{B}_i)}{\epsilon_i} \quad (H8)$$

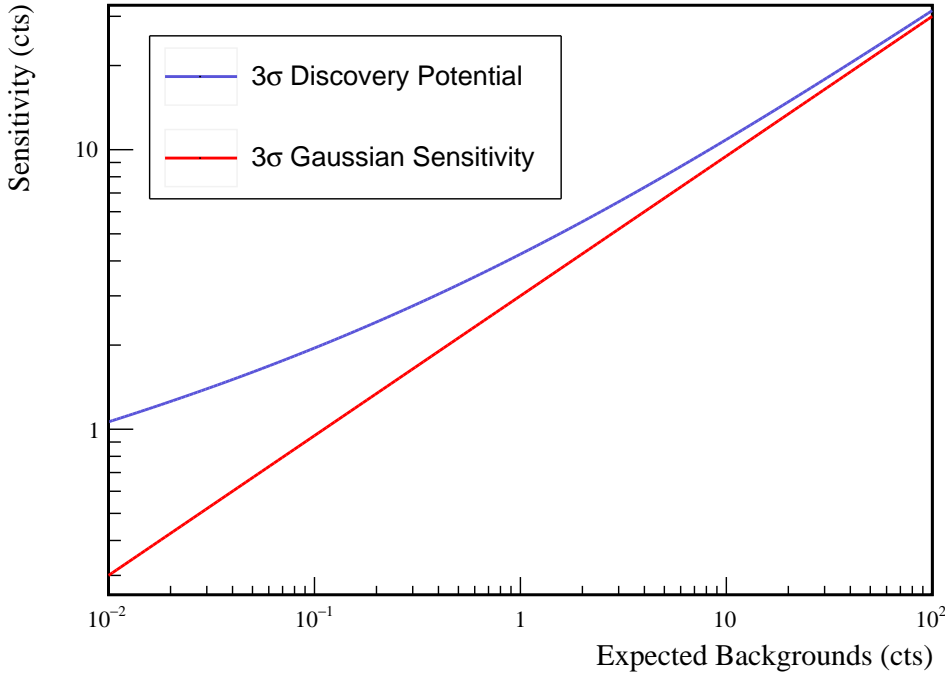


FIG. 105 A comparison of the Gaussian approximation for sensitivity and the discovery potential as a function of expected background level. Note that in the high background limit, both formulations for sensitivity converge, as expected.

717 Rearranging this, we get

$$\frac{\Delta \hat{S}(\bar{B})}{\hat{S}(\bar{B}_i)} < \frac{\Delta \epsilon}{\epsilon_i} \quad (\text{H9})$$

718 If we assume that a small number of events are cut, we can Taylor expand:

$$\frac{\partial \hat{S}}{\partial \bar{B}} \frac{\Delta \bar{B}}{\hat{S}(\bar{B})} < \frac{\Delta \epsilon}{\epsilon} \quad (\text{H10})$$

719

$$\frac{\partial \log(\hat{S})}{\partial \log(\bar{B})} > \frac{\text{False Positive Rate}}{\text{True Positive Rate}} \quad (\text{H11})$$

720 Looking at figure 105, we see that in the high background limit, using the Gaussian sensitivity approximation we will
 721 draw the same conclusion about whether or not a cut is worth applying regardless of the absolute background level. A
 722 cut is worth applying as long as the true positive rate of the cut is twice the true negative rate. On the other hand, in
 723 the low background limit, this is not the case; instead, as we approach zero background, we will be less aggressive in
 724 cutting events. For this reason, experiments approaching the background free limit will use wider regions of interest
 725 in peak searches.